AN EXPERIMENTAL STUDY OF ALUMINUM AT HIGH STRAIN RATES AND ELEVATED TEMPERATURES

Thesis for the Degree of Ph. D.

MICHIGAN STATE UNIVERSITY

Jerry L. Chiddister

1961

This is to certify that the

thesis entitled

AN EXPERIMENTAL STUDY OF ALUMINUM AT HIGH STRAIN RATES AND ELEVATED TEMPERATURES

presented by

JERRY L. CHIDDISTER

has been accepted towards fulfillment of the requirements for

DOCTOR OF PHILOSOPHY degree in APPLIED MECHANICS

Laurence E. Malvern
Major professor

Date December 22, 1961

O-169

LIBRARY
Michigan State
University

ABSTRACT

AN EXPERIMENTAL STUDY OF ALUMINUM AT HIGH STRAIN RATES AND ELEVATED TEMPERATURES

by

Jerry L. Chiddister

In this investigation short cylindrical specimens of aluminum were subjected to impact loads by means of a split Hopkinson pressure bar apparatus in which a third bar was used as a striker bar to produce a long flat-topped loading pulse. Tests were conducted at strain rates from 300 to 2000 inches per inch per second and at six temperatures from 30 to 550°C. True stress-true strain curves were obtained at nearly constant strain rates. The curves extended to approximately 5 percent strain for the lowest strain rates and to over 25 percent strain for the highest strain rates. Reliable data could not be obtained over the elastic portion of the stress-strain curves due to the nature of the loading pulse. Continuous records of stress and strain were obtained throughout the tests by means of strain gages mounted on the pressure bars. The area surrounding the specimen was heated by an electric resistance-type furnace.

Data was taken from the stress-strain curves to construct semi-logarithmic and log-log plots of stress versus strain rate. Both coordinate systems produced quite linear distributions of the data, which indicated that either the logarithmic flow law,

$$\sigma = \sigma_o + k \log \dot{\epsilon}$$

or the power law,

$$\sigma = \sigma_o \dot{\epsilon}^n$$

could be used to represent the data. In these laws σ_o, k and n are functions of strain and temperature and σ_o is the stress at

unit strain rate. Values of σ_o were determined for both laws by extrapolating back to the abscissa of unit strain rate. Values of k/σ_o and n, which characterize the strain-rate sensitivity of the material, are given for a strain of 5 percent at all test temperatures. The data was not sufficient for determining the variation of these parameters with the level of strain.

When the results were correlated with the data of Alder and Phillips, obtained from compression tests at lower strain rates, the power law was found to give a better fit to the plotted points.

Stress-temperature curves were plotted at several strain rates and for several levels of strain.

AN EXPERIMENTAL STUDY OF ALUMINUM AT HIGH STRAIN RATES AND ELEVATED TEMPERATURES

by

Jerry L. Chiddister

A THESIS

Submitted to
Michigan State University
in partial fulfillment of the requirements
for the degree of

DOCTOR OF PHILOSOPHY

Department of Applied Mechanics

1961

ACKNOWLEDGEMENTS

I wish to express my gratitude to Dr. L. E. Malvern who suggested the problem and gave valuable guidance and counsel throughout the project. Special thanks are also due to Dr. C.A. Tatro for assistance in solving the problems of instrumentation. Sincere thanks are due to the other members of my guidance committee, Dr. C. O. Harris, Dr. G. E. Mase and Dr. C. P. Wells.

I would also like to thank Mr. Donald Childs and Mr. R. Jenkins for assistance in constructing the apparatus and machining the specimens.

TABLE OF CONTENTS

LIST OF TABLES

LIST OF FIGURES

CHAPTER I
INTRODUCTION

1.1 General Discussion and Purpose

The mechanical behavior of engineering materials under conditions of dynamic loading is significantly different from that under conditions of static loading. Among the first indications of this was the fact that energy absorbed in the Charpy and Izod tests depended on the rate of impact. It is also well known that mechanical properties change markedly with temperature. The separate problems of determining these properties under dynamic loading conditions and of determining them at elevated temperatures have been investigated by a number of people. However, comparatively little has been reported on the combined problem of determining mechanical properties at impact rates of loading while the specimen is at an elevated temperature.

As might be expected, the problems involved in obtaining experimental data, especially stress-strain curves of metals under dynamic loading conditions were naturally directed toward increasing the speed of the quasi-static type testing machines. The range of loading speeds attainable by this method is quite limited because at higher speeds it becomes difficult to separate the inertia forces of the moving machine parts from the actual load on the specimen. This problem required new methods of measuring loads, and at the same time new methods were required for accurately determining the strains at these higher speeds. If loading rates are increased further into the impact range, stress wave propagation effects in the specimen must also be taken into consideration if an accurate stress-strain curve is to be obtained.

The problems involved in high temperature testing are not quite as formidable as those arising in impact testing, but they offer a considerable challenge when attempted in combination with impact testing.

The purpose of the present experiment is to obtain stress-strain curves of nearly pure aluminum at constant true strain rates of the order 1000 per second and at several temperatures from room temperature to near the melting point of the metal, the tests to be performed on short cylindrical specimens in compression impact. A desired objective is to obtain accuracy sufficient to determine the dependency of stress on the rate of strain for a particular value of strain at each test temperature.

1.2 Some Theories of Dynamic Plastic Deformation

A brief history of the development of the theory of plastic wave propagation will be given here, as it is a field which cannot rightfully be separated from the field of dynamic testing of materials in the anelastic range. Those who are interested in obtaining further information are referred to an extensive review of the literature in these associated fields completed recently by Hopkins (1961).*

The theory of one dimensional elastic wave propagation was developed in the early part of the last century, but the theory of plastic wave propagation is of more recent origin. It was Donnell (1930) who first devised a method of treating waves of propagation in a material which does not obey Hooke's law. He treated the stress wave in a long bar as a superposition of stress increments. Each increment was assumed to travel at a velocity which depended on the slope of

---

* Surnames followed by dates in parenthesis refer to Bibliography

the static stress-strain curve of the bar material at the stress level of the increment. These velocities were given by the relation

$$c = \sqrt{\frac{1}{\rho} \frac{d\sigma}{d\epsilon}} \tag{1.1}$$

where ρ is the mass density of the material, σ is nominal stress and ϵ is nominal strain. This of course reduces to the well known relation $c_o = \sqrt{E/\rho}$ for the case of elastic waves.

The problem of plastic wave propagation was not developed further until World War II when the details of the above method, including solutions for the problem of longitudinal impact of a semi-infinite bar, were worked out independently in this country by White and Griffis (1948) and von Karman and Duwez (1950), in England by Taylor (1958) and in Russia by Rakhmatulin (1945). The main assumptions of their theory, sometimes known as the von Karman-Taylor theory, are the following: There is one stress-strain curve for the bar material, independent of strain rate; the stress-strain curve is concave towards the strain axis, strain being a single valued function of stress; and radial inertia effects are negligible.

Soon after the development of the theory, experiments were carried out on long bars for the purpose of checking the principal results (Duwez and Clark, 1947). The results of these experiments agreed fairly well with the theory, but there were some discrepancies. For instance the measured strains near the impact ends of the bars varied from the predicted values. It was suggested that this variation was due to strain rate sensitivity of the bar material.

It had been proposed earlier by several investigators that stress at a constant temperature could be taken as a function of plastic strain ϵ_p and plastic strain rate $\dot{\epsilon}_p$, such that

$$\sigma = \phi(\epsilon_p, \dot{\epsilon}_p) \tag{1.2}$$

The problem now remained for someone to incorporate a function of this type into a solution of the plastic wave propagation problem. It was Malvern (1950, 1951) who first did this. Malvern assumed that for a particular level of plastic strain, the plastic strain rate $\dot{\epsilon}_p$ could be taken as a function of $\sigma - \sigma_o$ where σ is the stress under dynamic conditions and σ_o is the stress given by the usual quasi-static stress-strain curve. This function may be written in the form

$$\dot{\epsilon}_p = f(\sigma - \sigma_o) \tag{1.3}$$

or in the form

$$\sigma = \sigma_o + F(\dot{\epsilon} - \frac{\dot{\sigma}}{E}) \tag{1.4}$$

The theory was worked out for this quite general flow and an example was given in which a simplified version of the flow law was used. In the simplified law $\dot{\epsilon}_p$ was assumed to be linearly proportional to $\sigma - \sigma_o$, that is

$$\dot{\epsilon}_p = k(\sigma - \sigma_o) \tag{1.5}$$

which may also be written in the form

$$\sigma = \sigma_o + k_1 \dot{\epsilon} \tag{1.6}$$

In Equations (1.5) and (1.6) k and k_1 are coefficients which may depend on the material, the level of strain and the temperature.

Malvern's numerical calculations based on a linear dependence on strain rate did not appear to agree well with the kind of experimental data available at the time. They did, however, predict that a small dynamic increment superposed on a plastic strain distribution would travel at the elastic wave velocity and not at the appropriate plastic wave velocity as predicted by the von Karman-Taylor theory. This point was verified by Sternglass and Stuart (1953) who applied elastic

tensile pulses to copper bars which had been preloaded into the plastic region. Verification was also given by Alter and Curtis (1956) in experiments with lead bars in compression and by Riparbelli (1956) in experiments with copper wires loaded by tensile impact.

Malvern suggested that his theory might give better agreement with experimental results if stress is assumed to be a non-linear function of strain rate. One such functional relationship, derived on the basis of a mechanical model of a solid, has been proposed by Prandtl (1928). His relation may be written in the form

$$\sigma = \sigma_o + k_2 \ln \dot{\epsilon} \tag{1.7}$$

where σ_o is the stress corresponding to unit strain rate and k_2 is a coefficient which may depend on the material, the level of strain and the temperature. This relation was also proposed on empirical grounds by Ludwik (1909) and by Deutler (1932). Prandtl first arrived at the more general hyperbolic sine law

$$\dot{\epsilon} = C_1 \sinh a_1 \sigma \tag{1.8}$$

which reduces to the logarithmic law, equation (1.7) for large values of stress. Here C_1 and a_1 also depend on the level of strain, the temperature and the structure of the material. A hyperbolic sine law was also suggested by Nadai (Nadai and McVetty, 1943) on the basis of the results of creep tests performed at elevated temperatures.

Still another flow law which has received considerable support from experiments is the power law

$$\sigma = \sigma_o \dot{\epsilon}^n \tag{1.9}$$

where σ_o is the stress at unit strain rate and n depends on the material, the temperature and the level of strain. Alder and Phillips (1954) found that the power law provided a slightly better interpretation of their data from compression tests on copper, aluminum and steel

over a wide range of temperatures. Sokolov (1946-1950), who performed compression tests on tin, lead, aluminum, zinc, copper, nickel, brass and several steels at room and elevated temperatures, found the power law to give much better agreement with his plotted data than the logarithmic law. This was true except for high melting point steels whose behavior at room temperature could be described quite well with either relation. The power law has also been used to express yield stress as a function of strain rate (Hollomon and Jaffe, 1947) and to predict the critical stress at which creep initiates (Vitovec, 1957).

Several investigators have included the absolute temperature T in the plastic flow laws which they have proposed. Among these proposed relationships are the following in simplified form:

$$\dot{\epsilon} = C_2 \sinh \frac{a_2 \sigma}{T} \tag{1.10}$$

$$\dot{\epsilon} = C_3 e^{\frac{\beta}{T}} \sinh \frac{a_3 \sigma}{T} \tag{1.11}$$

$$\dot{\epsilon} = C_4 e^{\frac{-a_4 (s - \sigma)^2}{T}} \tag{1.12}$$

$$\sigma = C_5 + k_3 T \ln \lambda \dot{\epsilon} \tag{1.13}$$

$$\sigma = \left(\dot{\epsilon} e^{\frac{k_4}{T}} \right)^r \tag{1.14}$$

$$\sigma = \sigma_o \left(\frac{\dot{\epsilon}}{\dot{\epsilon}_o} \right)^{k_5 T} \tag{1.15}$$

where C_2, C_3, C_4, C_5, a_2, a_3, a_4, s, k_3, k_4, k_5, σ_o and ϵ_o may depend on the material and the level of strain. Equation (1.10) was derived by Eyring (1936) from his general equation developed from the theory of reaction rates. Equation (1.11) is a general equation of flow

developed by Freudenthal (1950), also from considerations of a rate process. The relations (1.12) and (1.13) were derived from theoretical studies of single crystals by Becker (1926) and Orowan (1934) and by Seeger (1954a, 1954b) respectively. Zener and Hollomon (1944) performed experiments on several steels over a wide range of strain rates and at temperatures between -190°C and + 20°C and their results gave good agreement with equation (1.14). This relationship indicates an equivalence between an increase in strain rate and a decrease in temperature. Sokolov (1949) arrived at (1.15) when he included the effects of temperature on his experiments. Equation (1.15), in another form, was derived earlier on a theoretical basis by Witman and Stepanoff (1939). It should be pointed out that for a particular temperature (1.10) and (1.11) reduce to the form of the hyperbolic sine law, equation (1.8). Also note that, when T is constant (1.14) and (1.15) reduce to the power law, equation (1.9).

Attempts to formulate theoretical flow laws are based on considerations of activation energy, the energy level a particle must attain in order to move across a potential barrier. If the energy distribution over the atoms can be expressed by the Boltzmann-Maxwell-Gibbs distribution function, then the rate of strain, which is proportional to the rate of activation, can be expressed by the relation

$$\dot{\epsilon} = f\left[e^{\frac{-U(\sigma)}{RT}}\right] \qquad (1.16)$$

where U is the activation energy and R is the universal gas constant (Freudenthal, 1950). It is seen that Equations (1.10), (1.11) and (1.12) are simply special cases of Equation (1.16) where some special form of $U(\sigma)$ has been used. Several examples of this type of function are considered in connection with yield stress, recovery in the annealing process and creep by Cottrell (1953).

MacGregor and Fisher (1946) suggested combining the effect

of strain rate and temperature so that the behavior of metals could be determined by a series of tensile tests involving only one variable. Their experiments on steel indicated that the true stress in a tension specimen depends only on the true strain and a "velocity-modified" temperature

$$T_m = T(1 - k \ln \frac{\dot{\epsilon}}{\dot{\epsilon}_o}) \tag{1.17}$$

where $\dot{\epsilon}_o$ is taken as $100 \cdot 10^{-5}$ per second and k is a constant.

A relation which includes strain as well as stress, strain rate and temperature was derived by Lubahn (1947). His proposed relation for plastic flow is

$$\sigma = C\, G^T \left(\frac{\dot{\epsilon}}{\dot{\epsilon}_o}\right)^{DT} \epsilon^{(E - FT \ln \frac{\dot{\epsilon}}{\dot{\epsilon}_o})} \tag{1.18}$$

where C, D, E, F, G and ϵ_o are constants of the material. The derivation is based on three empirically supported basic relations, one of which is the power law.

Noting the variety of the proposed plastic flow laws, one may doubt the usefulness of any of them. It can hardly be expected that one flow law would predict the behavior of every metal under all conceivable conditions. One reason for this is the change in structure which occurs in many metals with a change in temperature. Nevertheless, a relationship which predicts the behavior of a particular metal for a sufficiently wide range of strain rates and temperatures should be of considerable value.

1.3 History of Experimental Techniques

The experimental methods which have been used to study materials at loading speeds in the impact range may be placed in five categories: (a) Hopkinson pressure bar (b) compression impact

(c) tensile impact (d) plastic wave propagation and (e) torsion impact. The first four, with emphasis on the Hopkinson pressure bar and compression impact, will be discussed briefly here. For those who are interested in torsion testing, reference is given to Work and Dolan (1953) and to Goldsmith (1960) and the literature cited in these references.

1.3.1 Hopkinson Pressure Bar

B. Hopkinson (1914) was probably the first person to devise an effective method for measuring the forces involved in a high velocity impact situation. He determined the maximum pressures produced by the detonation of high explosives and by the impact of bullets. The bullets were fired against the end of a cylindrical steel bar producing an elastic pulse which proceeded along the bar and into another shorter bar of the same diameter. This second section of the bar was in effect a momentum trap since the compressive pulse due to the bullet was reflected as a tensile pulse from the free end of this short section and when the amplitude of this tensile wave, arriving again at the intersection of the bars, became greater than the amplitude of the compressive pulse continuing toward the free end, the short end piece would separate from the longer section and continue moving with the momentum of the trapped portion of the pulse. By taking end pieces of different lengths and measuring the momentum trapped in each, the area under the pressure-time curve over corresponding intervals could be obtained, the time interval being determined from the length of the end piece and the known elastic wave velocity. In general the exact shape of the pressure-time curve could not be obtained by this method since the starting points of these intervals could not be located in time, but the important values of maximum pressure and total duration of impact could always be obtained. The momentum in the end pieces was measured by catching the pieces in

a box supported as a pendulum from the ceiling, the angle of swing through which the box traveled being the measured quantity The longer incident bar was also supported in pendulum fashion and the smaller end pieces were held in place before impact by a magnetic force

The Hopkinson pressure bar testing method was not improved considerably until the development of modern electronic equipment. Davies (1948) made a critical study of the method and devised an electrical means to obtain a continuous record of the particle displacements due to an elastic pulse. The plane surface at the free end of the pressure bar served as one side of a parallel plate capacitor which was connected to a cathode ray oscilloscope. This gave a direct measurement of the displacement of the end of the bar. The pressure-time curve could be obtained from a photographic record of these displacements. If a pressure wave is assumed to travel at the elastic wave velocity $c_o = \sqrt{E/\rho}$ in an uninterrupted portion of a bar, then the pressure or stress σ may be calculated from

$$\sigma = \rho c_o \frac{du}{dt} \qquad (1.19)$$

where u is the particle displacement at a point in the bar as the wave passes that point, and t is time. Now the displacements of the free end of a bar will be twice as large as those due to the original pulse because the displacements of the reflected pulse are superposed upon those of the original pulse. Therefore, the stress in Davies method is calculated from the relation

$$\sigma = \frac{1}{2} \rho c_o \frac{du_1}{dt} \qquad (1.20)$$

where u_1 is the measured particle displacement at the end of the bar.

Using the Pochhammer-Chree equations for dispersion in an infinitely long cylindrical bar, (see Pochhammer, 1876 and Chree, 1889),

Davies showed that the stress pulses are propagated without distortion only if the wavelengths of the elastic waves involved in the propagation of the pulse are large when compared with the diameter of the bar. He showed that this condition is also necessary for an even distribution of longitudinal displacements and stress at a cross section of the bar.

In Davies's study of the pressure bar technique an experiment was performed which adds still more to the validity of the method. It was shown that the stress in a pulse is practically uniformly distributed over a cross-section of the bar at a distance of about four diameters from the impact end even when the force applied is concentrated near the center of the end. This experiment was performed by replacing the original momentum trap piece with a distribution of small steel balls. This dynamic case of Saint Venant's principle has also been verified to some extent by Flynn and Frocht (1961) with preliminary photoelastic studies of elastic waves.

Kolsky (1949) investigated the mechanical properties of several materials using a pressure bar technique which incorporated the capacitor measuring device of Davies. A diagram of Kolsky's apparatus is shown in Figure 1. The specimen, a thin disc, was mounted between two steel pressure bars and the force was applied by means of a small explosive charge. An attempt was made to use a cylindrical capacitor to obtain the longitudinal displacements of the incident bar, but this did not prove reliable due to distortions introduced by the bar. Without the use of this cylindrical capacitor, it was necessary to obtain the displacement-time records of two pulses in order to calculate the strain in each specimen. One pulse was fired without a specimen in place. The stress-time record was obtained by taking the gradient of the displacement-time curve for the specimen in place.

Some other disadvantages of Kolsky's method should be pointed

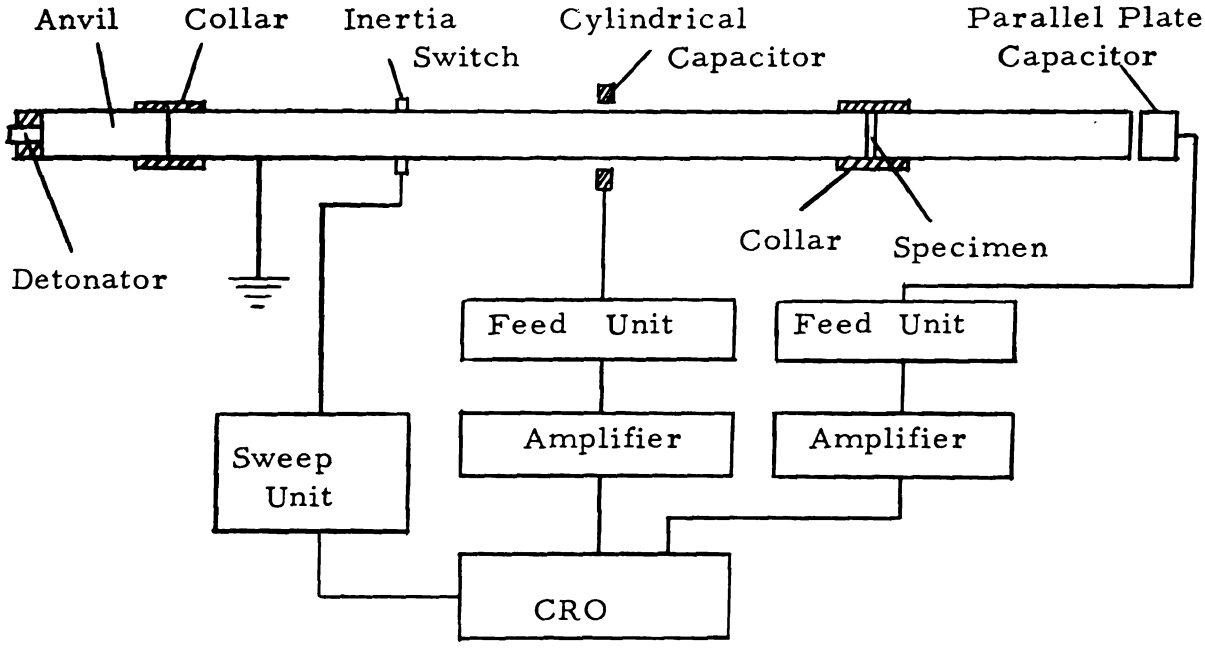

Figure 1. Schematic Diagram of Kolsky Apparatus

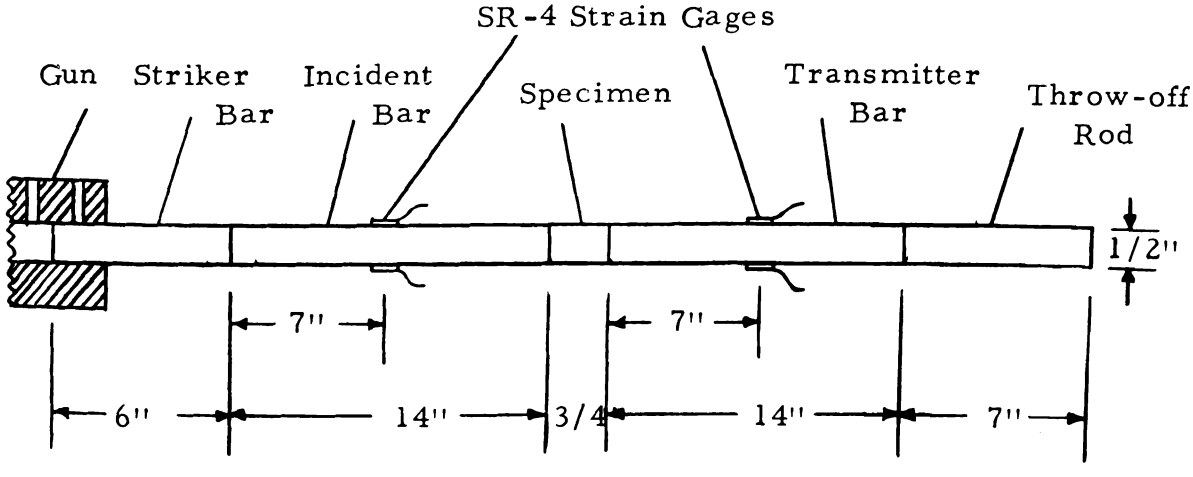

Figure 2. Schematic Diagram of the Pressure Bar System of Krafft, Sullivan and Tipper

out. For example, the nature of the loading pulse was such that the strain rate in the specimen varied throughout the test. Also, the effect of friction on the thin specimens used, 0.05 and 0.10 cm. thick by 1.0 inch in diameter for lead and copper, is an unknown quantity even though it was minimized by applying a thin coat of lubricant to each side of the specimen.

Krafft, Sullivan and Tipper (1954) used a pressure bar technique which is quite similar to the one used in the present investigation. A diagram of their bar arrangement is shown in Figure 2. Tests were conducted on high purity iron and a mild steel at temperatures from $-195^{\circ}C$ to $+100^{\circ}C$. The temperature was maintained by surrounding the specimen with a container through which a heating or cooling fluid was circulated. Stress-strain curves were plotted for several temperatures. Quite serious oscillations occurred in the strain records obtained from the SR-4 strain gages mounted on the pressure bars. The reasons for such oscillations and furthers details of this method will be given in the next chapter.

1.3.2 Compression Impact

Habib (1948) obtained energy-deformation curves for copper at average strain rates from 100 per second to 3000 per second by compressing small copper cylinders (0.5 inches long by 0.3255 inches in diameter) with a high velocity projectile as shown in Figure 3. In this apparatus the hardened steel piston is accelerated in a gun barrel with compressed air. The strain rate was varied by changing the velocity of the piston, and the total strain of the specimen for a particular strain rate was varied by changing the size of the piston. Several hundred specimens were tested. The energy absorbed by each was calculated from the piston velocity which was measured before and after impact by means of pulses produced on an oscilloscope trace by photocells. The energy absorbed by the anvil behind the

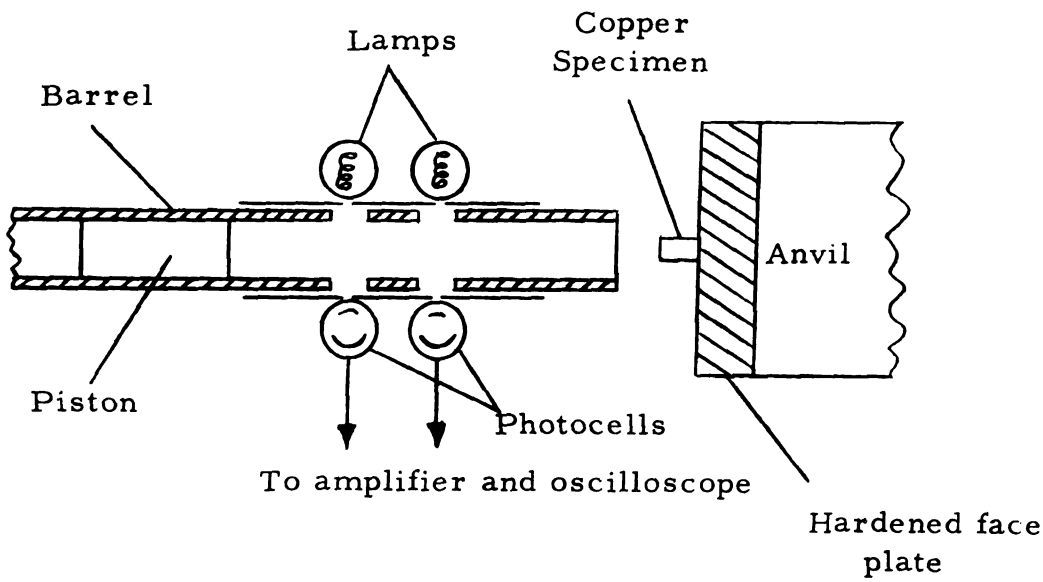

Figure 3. General Arrangement of Habib Apparatus

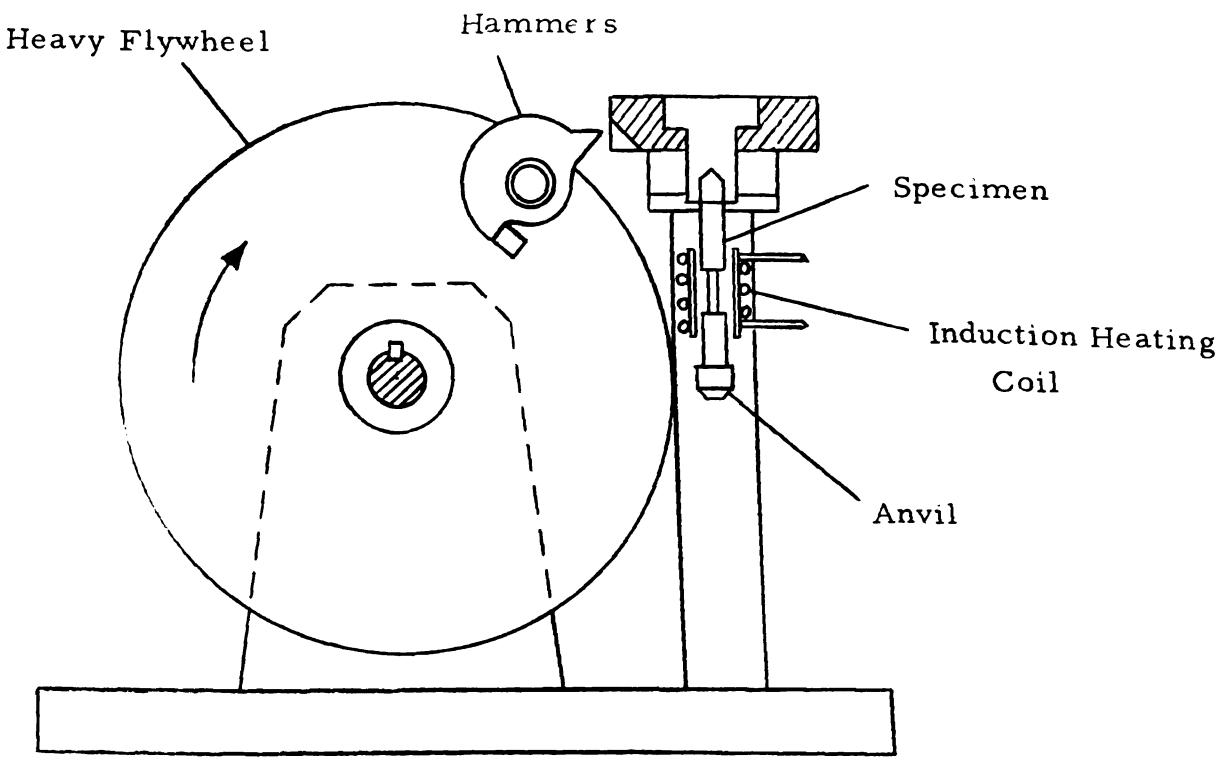

Figure 4 Mechanical Arrangement of Manjoine-Nadai Apparatus

specimen was assumed to be negligible. Stress-strain curves were plotted for several strain rates, the stresses being determined from the slope of the energy-deformation curves. The strain rate was taken directly from the average piston velocity during contact with the specimen. This velocity was assumed to be one-half the initial velocity. Habib's results showed that the energy absorbed at a particular level of deformation increased with an increase in strain rate and that stress is a function of strain rate which changes with the level of strain. It should be pointed out that plastic wave propagation effects in the specimens may have had considerable effect on Habib's data. Habib's calculations based on the von Karman-Taylor strain rate independent theory indicated that the plastic wave did not have time to traverse the specimen in both directions during the time of impact, when the lightest piston was used. This indicates a non-uniform strain distribution in the specimen which could produce an apparent rise in stress. That is a rise in stress which is not due to an actual material strain rate effect.

Lee and Wolf (1951) made a detailed analysis of the wave propagation in Habib's impact tests and concluded that the strain distribution effects were negligible for most of Habib's tests but an error of up to 10 percent was possible when the lightest piston was used. It was pointed out that a non-uniform strain distribution causes an increase in energy absorption for a fixed reduction in length. They concluded in general that if several traverses of the plastic wave up and down the specimen occur during straining, then essentially uniform strain conditions will occur and the effects of specimen inertia may be neglected when considering the use of an average strain rate.

Several investigators at the University of Texas have used an apparatus similar to Habib's for studying metallic cylinders under impact conditions. The basic apparatus consisted of an air gun

which fired a steel piston directly against the specimens and a Hopkinson type pressure bar to measure the force transmitted by the specimen. The pressure bar was instrumented with resistance strain gages. Ripperger (1960b) used the apparatus to study the effects of strain rate and specimen configuration on the yield stress of copper and tellurium lead. He used specimens from 0.0625 to 1.0 inches in diameter and from 0.5 to 2.0 inches long with piston velocities from 35 to 110 feet per second. The dynamic yield stresses measured varied considerably under supposedly identical conditions, but the results were sufficiently accurate to conclude that specimen configuration has an important influence on the measured stresses. He also concluded that lead is relatively insensitive to changes in strain rate, a conclusion which was not supported by Kolsky (1949).

Karnes (1960) used the apparatus at the University of Texas for experiments in which he mounted resistance strain gages directly on the specimens. Copper specimens of 0.5 inch diameter and lengths of 0.5 , 1.0 and 2.0 inches were used. The gages were mounted longitudinally at both ends of the specimen in order to determine the plastic wave propagation effects. These gages were inherently limited to measuring strains of up to about 1.5 percent. Karnes' experimental results, as given for the three specimen sizes in Figures 46, 48 and 49 of his report, indicate that at a piston velocity of 65 feet per second the wave propagation effects become negligible, at least in the case of the 0.5 inch long specimen, after the elastic wave has traveled twice the length of the specimen. These results show the reduction of wave propagation effects with a reduction in specimen length. His Figure 48 shows that the strain rate at either end of the 0.5 inch long specimen is approximately the same after two traverses of the wave even though the level of strain is higher at the impact end. This result supports the use of an average specimen strain in tests of very

short specimens at high strain rates. It might be of interest to point out here that the impact velocities and specimen lengths used in the present investigation are less than those used by Karnes.

Tapley (1960) made a theoretical analysis of the plastic wave propagation in the 0.5 and 1.0 inch long copper specimens used by Karnes. The analysis was based on an impact velocity of 65 feet per second in order to compare results. He used the Malvern strain rate theory and a modification if it which included the effects of radial motion The results gave good agreement with experiment for the 0.5 inch long specimen but only fair agreement for the longer specimen. An important result is that the theory predicts an essentially uniform longitudinal stress distribution for the 0.5 inch specimen after the elastic wave travels twice the length of the specimen.

The University of Texas apparatus was also used by Guyton (1960, for experiments on the effects of radial friction on the specimen faces, variations in the material, and specimen configuration on the results of impact tests. His experiments were carried out with copper specimens. He concluded that radial friction definitely affects the dynamic yield stress for length-to-radius ratios as small as one-half but is unnoticeable for ratios as high as four. The experments consistently indicated that dynamic yield stress increases for an increase in specimen radius and that the effects of cold working in the machining of specimens were negligible

Additional information on recent plastic wave propagation research at the University of Texas may be found in reports by Plass (1960) and Ripperger (1960a). In the former report Plass developed a theory of plastic wave propagation including the effects of strain rate, radial inertia and shear.

Alder and Phillips (1954) used a compression machine in which the load platform at one end of the specimen was driven by a logarithmic

shaped cam. The load was measured by the birefringence created in two glass blocks, the change in birefringence being recorded photographically on a rotating drum. Tests in which copper, aluminum and steel specimens were compressed to 50 percent in height at strain rates from 1.34 per second to 39.3 per second were performed. These tests were also conducted over a wide range of temperatures. This was accomplished by enclosing the specimen in a guard ring box which was heated in an electric furnace or cooled by immersion in a low boiling point liquid and then transferred to the compression machine just before the test. The specimen remained in the box during the test, being compressed by two platens which were free to move longitudinally in the box while being in direct contact with both the specimen and the load platforms of the machine. The results of these tests, as stated earlier, agreed quite well with both the logarithmic and the power law, the latter giving a slightly better fit to the plotted data. Strain rate sensitivity was found to increase with temperature for all three metals.

Sokolov (1946-1950) used a modified Charpy impact machine for the high strain rate compression tests discussed in section 1.2. A striker tip was mounted on the pendulum of the machine and an anvil was added to take the force transmitted by the specimen. His impact tests were performed at average strain rates up to 120 per second. The specimens were 20 millimeters long and 10 millimeters in diameter and the stress-strain curves were obtained from energy-deformation curves as in Habib's experiment.

1.3.3 Tension Impact

Tensile impact tests have been performed by many investigators, most of the tests being performed to determine the effects of loading rate on such properties as yield strength, energy absorption, reduction in area and elongation. Few investigators have actually determined

force-elongation or stress-strain curves during high impact tensile loadings. Manjoine and Nadai (1940) (see also Nadai and Manjoine, 1941 and Manjoine, 1944) were probably the first to effectively measure the load and extension during these short time tests. They developed a high speed rotary impact machine whose mechanical parts were much like those of a machine designed earlier by Mann (1936). A diagram of the Manjoine and Nadai machine is shown in Figure 4. The impact was applied by two hammers mounted on a heavy flywheel which was rotated by a variable speed direct current motor. At a predetermined speed the hammers were allowed, by means of a trigger mechanism, to engage an anvil fastened to the bottom of the specimen. The load-extension curve was obtained directly from an oscilloscope by an ingenious photoelectric cell arrangement. The apparatus also included an induction heating coil around the specimen which could produce temperatures up to 1200°C.

By using another machine for the slower strain rates, extensive data was collected on copper, aluminum and steel at strain rates from 10^{-6} per second to 10^{3} per second and at a series of temperatures. When ultimate stress was plotted versus the logarithm of strain rate the curves for copper and aluminum showed a marked non-linearity in the region of high strain rates, the stress increasing in this region. This effect was more pronounced as the temperature was increased. These results in the region of high strain rates must be taken with caution since they may have been affected by plastic wave propagation in the specimens. This problem was discussed by Clark and Duwez (1948). It should also be mentioned that large oscillations, which seemed to be due to the inertia of the specimen supports, appeared in the records at extremely high strain rates.

More recently, Austin and Steidel (1959) developed an ex-

plosive impact tensile tester capable of producing strain rates up to 17,000 per second. The load was measured with SR-4 strain gages near the stationary end of the specimen and the strain and deformation were recorded by means of a high speed movie camera. Stress-strain curves for an aluminum alloy and cold rolled steel at room temperature were obtained. Here again, the plastic wave propagation effects in the specimens could introduce error in the load measurements.

Clark and Duwez (1950) devised a method for obtaining impact rates of strain in tension which virtually eliminated plastic wave propagation effects in the specimen. In this method circumferential strain is induced in a thin-wall hollow cylindrical specimen by an internal fluid pressure. A nearly constant strain rate is produced by compressing the liquid (mercury) with a piston moving at constant velocity. Tests were made on steel specimens at strain rates up to 200 persecond, but unfortunately the data has limited usefulness since only stress-time records were obtained.

1.3.4 Plastic Wave Propagation

Stress-time curves have also been obtained indirectly from the strain-time records of plastic waves in longitudinal bars. If the propagation velocities at successively increasing levels of strain are determined for a plastic wave then the tangent moduli $\frac{d\sigma}{d\epsilon}$ of the stress-strain curve can be calculated from

$$c = \sqrt{\frac{1}{\rho}\,\frac{d\sigma}{d\epsilon}} \qquad (1.2)$$

the relationship proposed in the von Karman-Taylor theory. If the tangent moduli are plotted against strain and the resulting curve is integrated, a dynamic stress-strain curve is obtained.

Campbell (1952) used this method to determine dynamic stress-strain curves for hard and soft copper. He performed experiments

on long bars impacted in tension by a freely falling weight. The strain-time records were determined at two points near the impact ends by means of resistance strain gages. The propagation velocities at successive levels of strain were then obtained by plotting these strain-time curves on the same time axis and measuring the time required for each level of strain to be propagated from one gage station to the other. The dynamic stress strain curves from these experiments showed stress values much lower than those of the static curves. However, Campbell suggested that the calculated stresses were in error by as much as 25 percent due to the lack of refinement in experimental technique.

Johnson, Wood and Clark (1953) and Bell (1959, 1960) also determined dynamic stress-strain curves by the tangent modulus method. Their experiments were performed on soft aluminum under compression impact. Bell measured strains with a diffraction grating method in which light is reflected by a fine grating ruled directly on the surface of the specimen. The method utilizes the fact that the angle of diffraction is dependent upon the number of lines per inch of the grating. Bell's experiments have also given support to the von Karman-Taylor strain rate independent theory.

The plastic wave propagation method of determining dynamic stress-strain curves discussed above can be used only under conditions where the variations in strain rate during the test are known not to influence the wave propagation, because the use of $c = \sqrt{\frac{1}{\rho}\frac{d\sigma}{d\epsilon}}$ is based on the existence of a single dynamic stress-strain relation applying throughout the test.

CHAPTER II
EXPERIMENTAL METHOD

2.1 General Description and Objectives

The basic apparatus of the present investigation was developed and used by Lindholm (1960) for high strain rate experiments on copper, lead and aluminum at room temperature. A few minor changes have been made in the basic apparatus and a furnace has been added for heating the specimens Lindholm's objectives in developing the apparatus were to: (a) obtain stress-strain curves at as nearly constant strain rate as possible, (b) obtain each complete curve from a single specimen, recording stress and strain continuously during the test, (c) obtain stress and strain records well into the plastic range, (d) obtain dynamic curves up to 1000 in./in./sec., and (e) minimize wave propagation effects in the specimen. His apparatus, which was an adaptation of the split Hopkinson pressure bar method used by Kolsky, met all of these objectives. In Lindholm's apparatus, the loading pulse was obtained by longitudinal impact with a steel striker bar which had been accelerated by means of a commercial impact testing machine The strain pulse was monitored by means of strain gages mounted on the pressure bars as in the Krafft, Sullivan and Tipper experiment discussed in Section 1.3.1.

For the present study changes in the apparatus were made to: (a) obtain dynamic stress-strain curves at a series of temperatures from room temperature to near the melting point of aluminum, (b) develop accuracy sufficient to determine changes in stress with changes in strain rate at each test temperature, and (c) accurately determine specimen temperature at the time of the test. An electric furnace was placed around the pressure bars, covering the section containing the

specimen. A thermocouple placed near the specimen was used to monitor the temperature at the time of the test. The accuracy of the apparatus was improved by using foil strain gages with a higher output than those used by Lindholm. A schematic drawing of the apparatus is shown in Figure 5 and a general view of the test setup is shown in Figure 6.

2.2 Pressure Bar System.

The arrangement and dimensions of the pressure bar system are shown in Figures 7 and 8. The striker bar and the pressure bars were made of 3/4 inch diameter centerless ground, type 303, stainless steel rod, stainless steel being used to reduce oxidation at the higher temperatures. This 18-8 stainless steel also has good impact properties at all temperatures. The pressure bars were supported in rubber "O" rings, which were in turn supported in steel pillow blocks constructed for this purpose (see Figure 9). The "O" rings allowed sufficiently free lateral expansion of the bars, so that no reflections of the strain waves from the supports were observed in the strain records.

The length of the bars and the locations of the gage stations were calculated to permit the recording of complete strain pulses without interference from reflected pulses returning from the bar ends. The problem of reflected pulses due to temperature gradients in the bars was also considered; this is discussed in Appendix A.

It was also necessary to consider the effect of temperature on the performance of the strain gages. The gages were located so that the operating temperatures were well within the safe operating temperature listed by the manufacturer.

The ends of the bars which were to be in contact with the specimen were carefully turned in a lathe and finished with a fine emery paper in order to reduce the effects of radial friction during compression of the specimen. The bars were aligned longitudinally

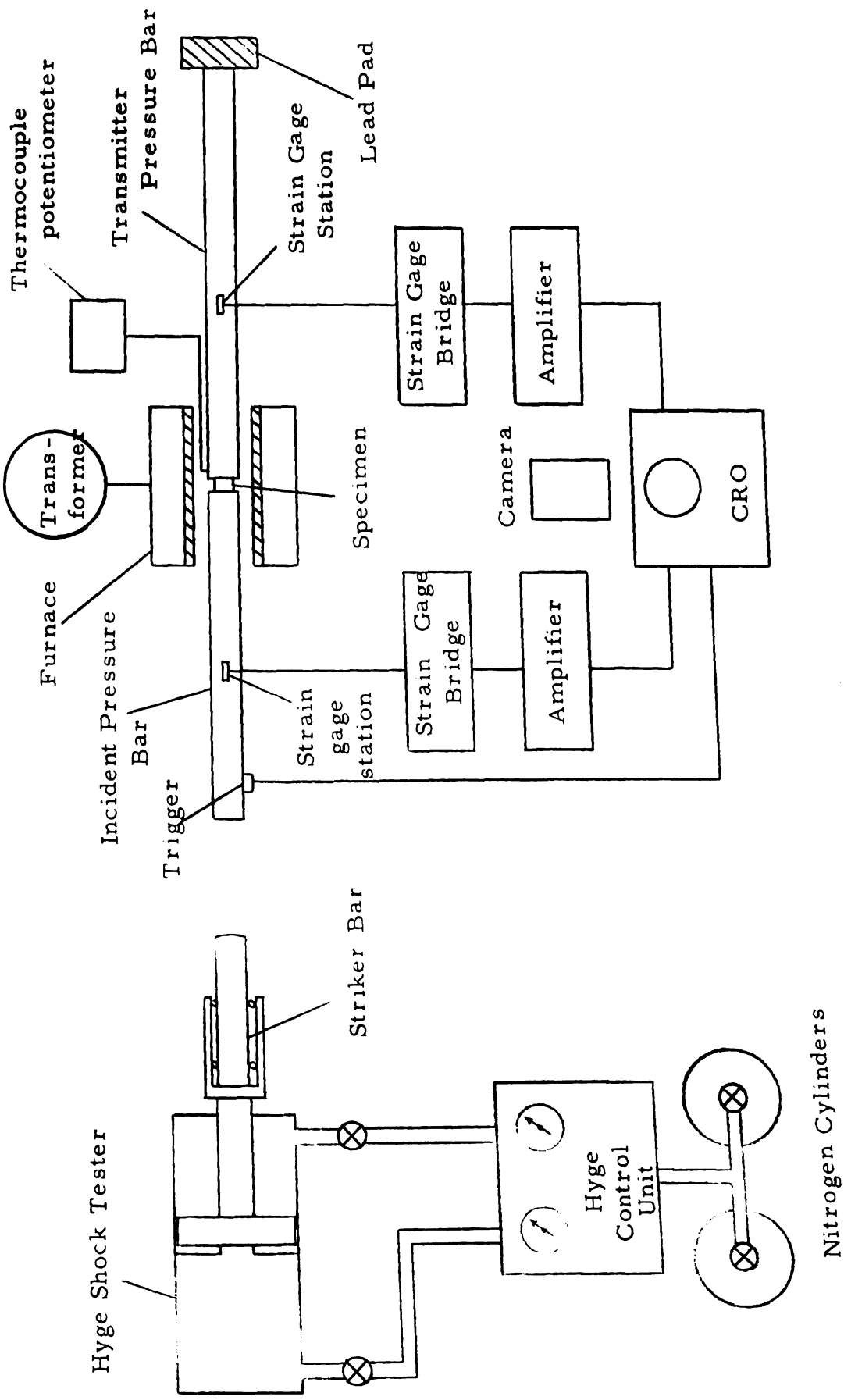

Figure 5. Experimental Test Setup

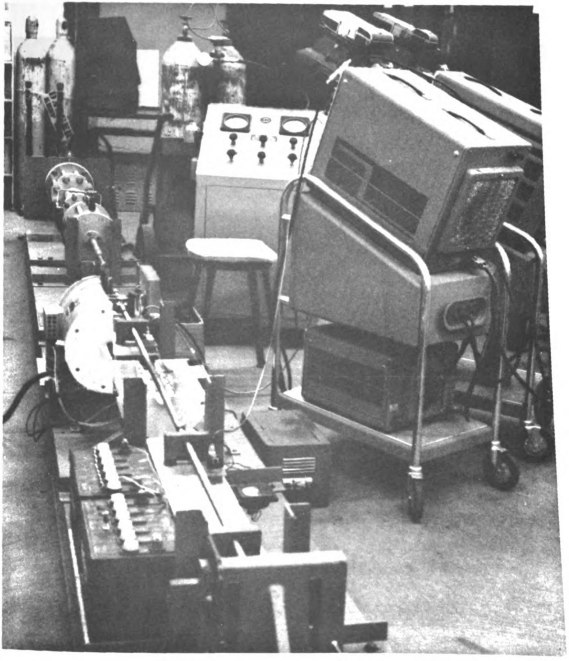

Figure 6. General View of Test Setup

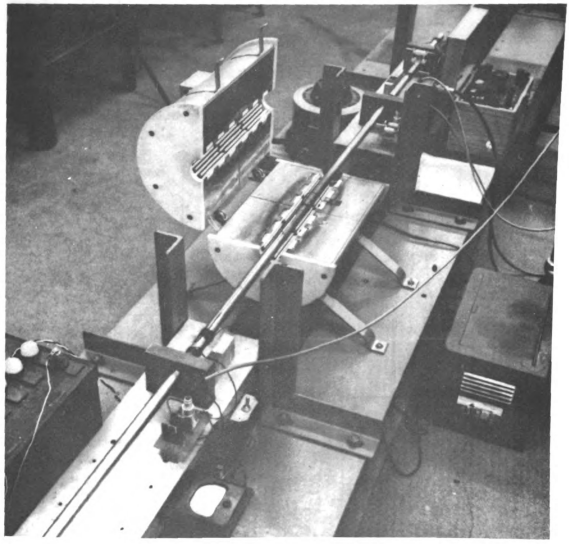

Figure 7. Close-Up of Pressure Bars and Furnace

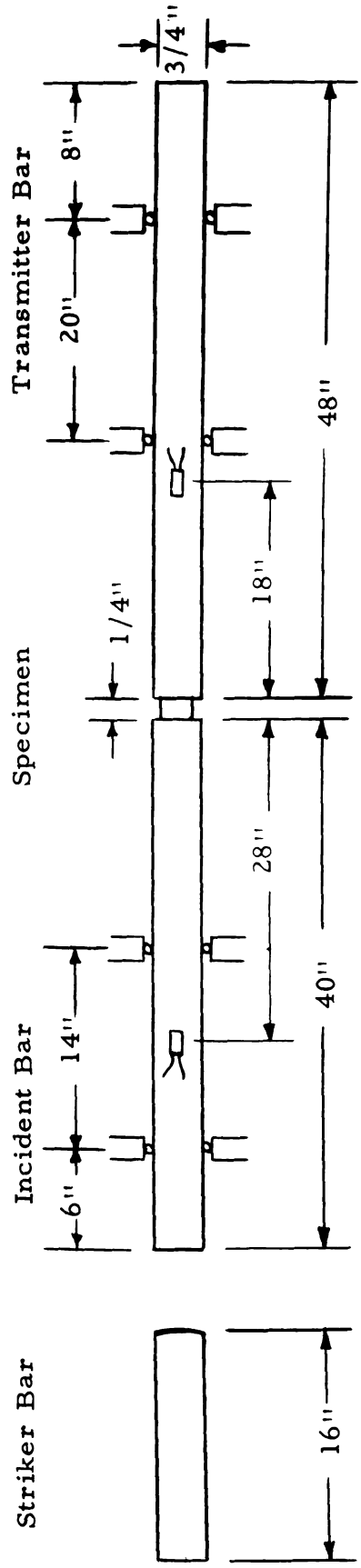

Figure 8. Dimensions of Striker and Pressure Bars

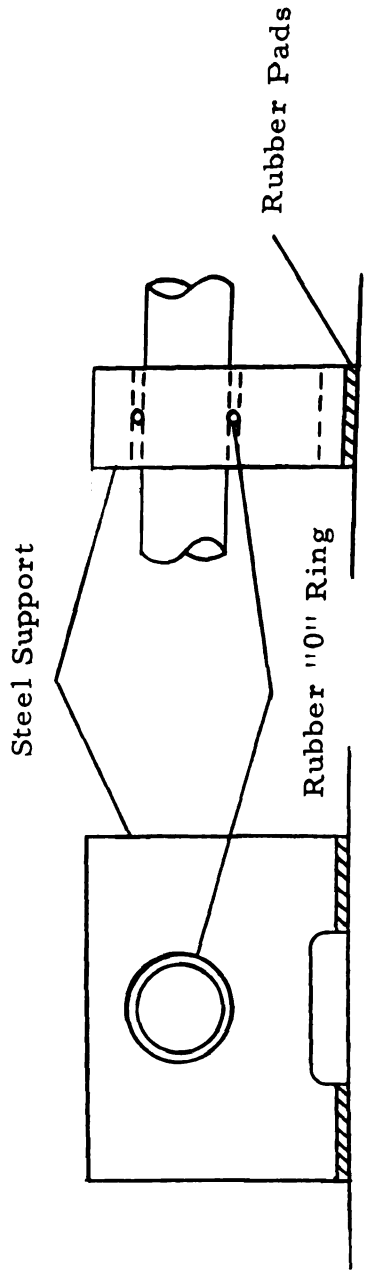

Figure 9. Pressure Bar Supports

by measuring from the "I" beam shock tester supports and then more carefully by placing a light behind the specimen opening with the pressure bars in contact. A lead pad was placed at the far end of the transmitter bar to absorb the energy of the pulse.

The 16-inch long striker bar produced a 32-inch long flat-topped pulse in the incident pressure bar, since the striker bar remained in contact with the pressure bar until the compression pulse was reflected from the free end of the striker bar and returned to the interface as a tensile pulse. The impact end of the striker bar was rounded slightly to assure axial impact and to reduce the effects of dispersion on the strain record of the pulse by lengthening the rise time of the pulse. Figure 10 shows strain records obtained at two stations on a solid steel pressure bar. Each photograph records a single pulse; the upper trace is from the first gage station at a point 22 inches from the impact end, while the lower trace shows the same pulse when it reaches the second station 58 inches from the impact end. Figure 10a is for the rounded striker bar, the arrangement actually used in the study, while Figure 10b is for a nearly flat-ended striker bar. The oscillations at the leading edge of the record from the second station are dispersion effects of the high-frequency components in the rise portion of the main pulse. The flat-ended striker bar produced a pulse with a shorter rise time so that the shorter wave length components are more significant and therefore, according to the Pochhammer-Chree theory (see Davies, 1948), the dispersive effects are greater. This explains the greater oscillation in Figure 10b.

The problem of dispersion in elastic bars has been studied by many investigators. One of the more recent studies was made by Curtis (1960). Suggestions for eliminating strain record disturbances caused by dispersion and other factors were given by Krafft (1955) who

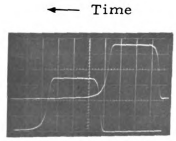

(a) Rounded Striker Bar

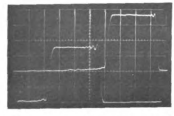

(b) Nearly Flat-ended Striker Bar

Figure 10. Strain-Time Records Showing Effect of Dispersion The impact velocity is approximately 25 feet per second.

also observed that slight deviations from parallelism between the impact surfaces of the bars have little effect upon the oscillations.

2.3 Impact Loading Machine

The striker bar was accelerated by means of a commercial Hyge Shock Tester, type HY-3422, manufactured by Consolidated Electrodynamics Corporation. The tester is shown in Figure 6 and a schematic sketch is shown in Figure 11. The piston diameter is 3 inches and the full stroke is 16.75 inches.

The acceleration of the piston is achieved in the following manner: A given set pressure is applied to chamber B by means of compressed nitrogen. This pressure acts over the full area of the piston, pushing it against a ring seal at C. A load pressure is then applied to chamber A, this pressure being restricted to a smaller area of the piston by the ring seal thus causing a smaller force to act on this side of the piston. When the load pressure reaches a magnitude of 4.2 times that of the set pressure, the forces acting on the piston become equal. If additional load pressure is applied, the seal at C is broken and the load pressure expands over the entire face of the piston causing a large acceleration.

The acceleration is regulated by a conical pin which regulates the amount of gas supplied to the piston face during the initial part of the acceleration. The deceleration is aided by a hydraulic fluid which occupies approximately one-half of the volume of chamber B. The deceleration is accomplished by a pin which gradually closes the area of the escape orifice D through which the hydraulic fluid is forced. The system is controlled from a separate control panel which contains pressure gages and control valves.

A "barrel" was designed and threaded onto the end of the piston shaft to support the striker bar. A diagram of this barrel is

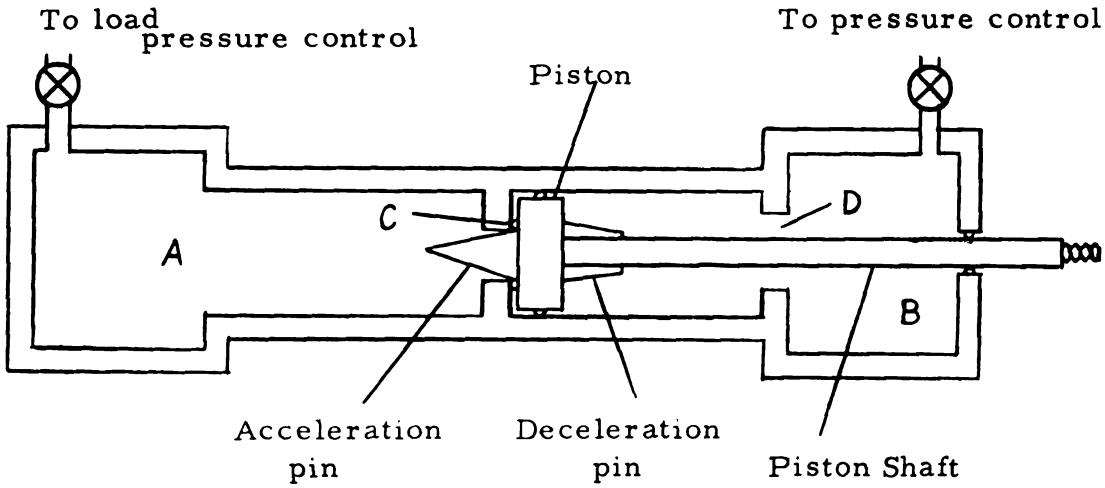

Figure 11. Schematic of Hyge Shock Tester

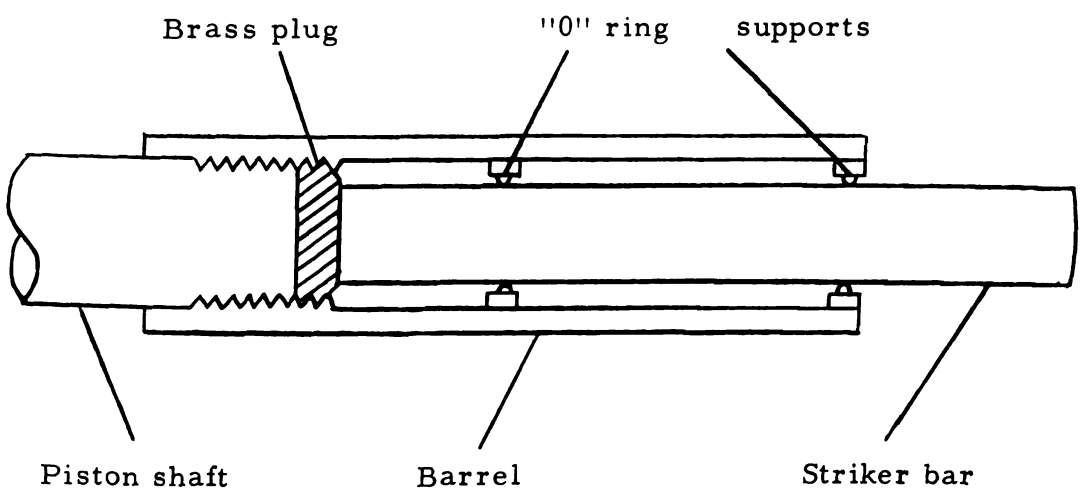

Figure 12. Barrel with Striker Bar

shown in Figure 12. The striker was supported within the barrel by rubber "O" rings which were lightly lubricated with petroleum jelly to allow free sliding of the bar at the end of the piston stroke. The spacing between the shock tester and the incident bar was such that the striker bar was in free motion within the "O" rings just prior to impact.

2.4 Furnace and Temperature Control

A Type M-1012 electric resistance combustion tube furnace manufactured by Hevi-Duty Electric Company was used to heat the area around the specimen. The furnace had an internal diameter of 1.75 inches and the heating element was 12 inches long. A hinged cover was provided for free access to the specimen (see Figure 7). The furnace was capable of producing temperatures to 1950°F for intermittent operation and to 1850°F for continuous operation. The temperature within the furnace was monitored by means of a Chromel-Alumel thermocouple which was welded directly to the transmitter bar at a distance of 3/8 inches from the specimen. A variable transformer was connected to the furnace to maintain specimen temperature at the desired level. The furnace was capable of reaching the maximum temperature used in the experiment in approximately 15 minutes and essentially steady state conditions were attained in the pressure bars within 30 minutes.

2.5 Strain Measuring and Recording Equipment

The pressure bars were instrumented with SR-4 Type FAP-25-35 foil strain gages with a gage length of 1/4 inch. The distortion of the pulse introduced by the 1/4 inch gage length was considered negligible since the gage length was small in comparison with the rise portion of the pulse. The resistance of these gages as given by the manufacturer was 350 ohms $\pm$ 2.5 ohms and the gage

factor was 2.16 $\pm$ 1 percent. Two gages were mounted at each gage station. They were placed diametrically opposite one another and longitudinally along the bar. This effectively eliminated the measurement of bending strains when the two gages at a station were placed in opposite arms of a Wheatstone bridge as shown in Figure 13. The dummy gages in the other two arms of each bridge were 350 ohm precision resistors. The bridge voltage was supplied by two 12 volt wet cell batteries connected in series, and voltage was recorded by means of a voltmeter which could be read to the nearest 0.05 volt.

Two Tektronix Type 53/54 E plug-in preamplifiers were used to amplify the signals from the bridges. These are high gain differential preamplifiers with a vertical sensitivity to 50 microvolts per centimeter and a frequency response from 0.06 to 60,000 cycles per second. The differential feature permits attenuation of any undesired signal by means of outphasing.

The preamplifiers were mounted in a Tektronix Type 551 dual beam oscilloscope which permitted the signals from the two gage stations to be displayed at the same time with one horizontal sweep of the beams. The amplifier of this scope has a vertical rise time of 0.012 microseconds. The sweep speed could be varied continuously from 1 microsecond per centimeter to 5 seconds per centimeter The scope was triggered by means of a piezoelectric crystal which was mounted on the incident bar about 4 inches ahead of the first gage station.

The strain pulses were permanently recorded with a Dumont Type 302 oscilloscope record camera using Polaroid Pola Pan 400, type 44, film. An open shutter with an aperture setting of f/2.8 was used.

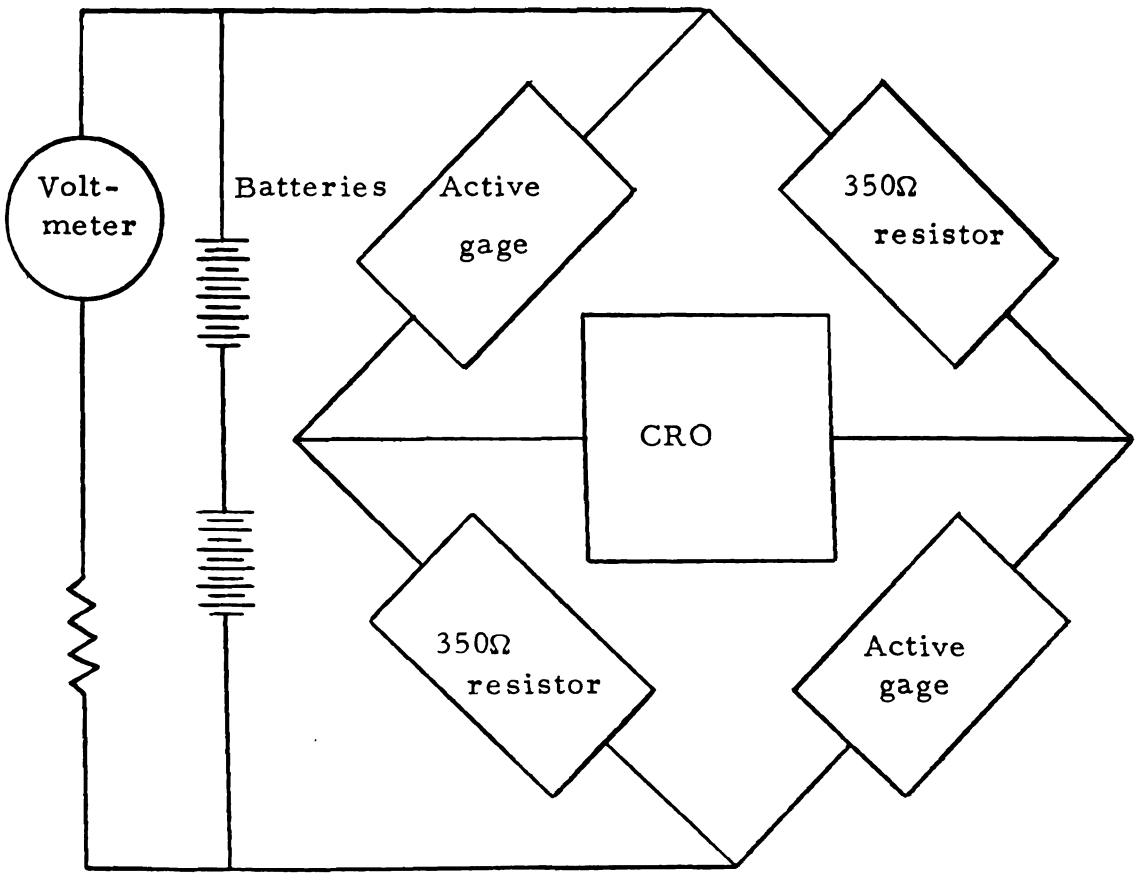

Figure 13. Strain Gage Bridge

2.6 Specimens

The specimens were all machined from the same 1/2 inch diameter bar of extruded aluminum. This was number 1100 F aluminum (2S aluminum) with the following composition as certified by the distributor:

Element	Percent by Weight
Aluminum	99.00 max.
Copper	0.20 max.
Silicon and Iron	1.00 max.
Manganese	0.05 max.
Zinc	0.10 max.

The specimens were carefully turned to 0.495 inches $\pm$ 0.002 inches in diameter and 0.250 inches $\pm$ 0.005 inches in length on a high speed collet lathe. Special care was taken to assure parallelism between the end faces of the specimens, nonparallelism being limited to less than 0.001 inch in all cases and usually less than half of this value. Annealing was at 400°C for one hour in an electric furnace.

The diameter of the specimens was sufficiently smaller than the 3/4 inch diameter pressure bars to insure full contact of the specimen faces with the parallel faces of the pressure bars during compression.

2.7 Derivation of Stress and Strain in the Specimen

The average specimen strain is determined from the displacement-time records of the pressure bar faces in contact with the specimen. These displacement-time records are in turn obtained from the strain-time records of the incident and transmitted pulses as obtained from the two gage stations. From the theory of elastic wave propagation in a longitudinal bar we have

$$\epsilon = \frac{v}{c_o} = \frac{1}{c_o}\frac{du}{dt} \qquad (2.1)$$

where v is the particle velocity and c_o is the elastic wave velocity which is constant for a particular temperature. Solving this equation for u, the particle displacement, we have

$$u = c_o \int_o^t \epsilon \, dt \tag{2.2}$$

which shows that the particle displacements in a bar which is originally at rest can be obtained by integrating the strain-time history curve at the point under consideration.

In order to determine the strain-time histories at the faces of the bars from the strain-time records taken from the remote gage stations we must consider the reflections of the incident and transmitted pulses from the specimen interfaces and from the temperature gradients in the pressure bars on either side of the specimen. It should also be pointed out that the magnitude of the strain in a pulse changes as the pulse proceeds into a section of bar having a different temperature, and consequently, a different Young's modulus. This means that the amplitude of the incident pulse as measured at the first gage station must be multiplied by a correction factor in order to obtain the strains occurring at the end face of the bar within the furnace. If a strain wave is propagated into a region where the temperature is above room temperature, we can determine the transmitted strain ϵ_t from the relation

$$\frac{\epsilon_t}{\epsilon_i} = \frac{2E}{E_1 + \sqrt{E E_1}} \tag{2.3}$$

where ϵ_i is the incident strain and E_1 is Young's modulus at the higher temperature T_1. Similarly, the reflected strain ϵ_r can be determined from

$$\frac{\epsilon_r}{\epsilon_i} = \frac{\sqrt{E_1} - \sqrt{E}}{\sqrt{E_1} + \sqrt{E}} \tag{2.4}$$

These relations are derived on the basis of a single discontinuous jump in temperature but experimental evidence indicates that they are also valid for a continuous temperature distribution in which the total change occurs in a section of bar which is long in comparison with the bar diameter. The derivation of Equations (2.3) and (2.4) and experimental evidence of their validity is presented in Appendix A. In the present investigation the transmitted strain pulse is a maximum 20 percent higher than the incident pulse, and the maximum reflected strain pulse is 6 percent of the incident pulse.

In order to reduce the amount of writing in the following derivation of the displacements at the faces of the specimen let us denote the interfaces of the specimen and the pressure bars as α and β, α being the interface with the incident bar. Let us also denote the temperature distributions in the bars as λ and ζ, λ being the distribution in the incident bar as shown in Figure 14. In this figure, compressive strain pulses are plotted above the axes and the arrows indicate the direction of propagation but not necessarily the direction of particle velocity. The pulses propagated past the gage stations are listed below their respective stations. If we correct the pulse records obtained from the gage stations by a temperature factor which can be calculated from Equation (2.3) we will have the strains these pulses cause at α and β. Let these strains at α and β be identified by the subscripts α and β. For instance, let $\epsilon_{I\alpha}$ be the strain at a later time at α due to the incident gage station pulse ϵ_I. Only first-order temperature reflections are considered, as the reflection of a reflection is assumed to be a negligible quantity.

The incident pulse ϵ_I is partially reflected at λ, at $\alpha + \beta$

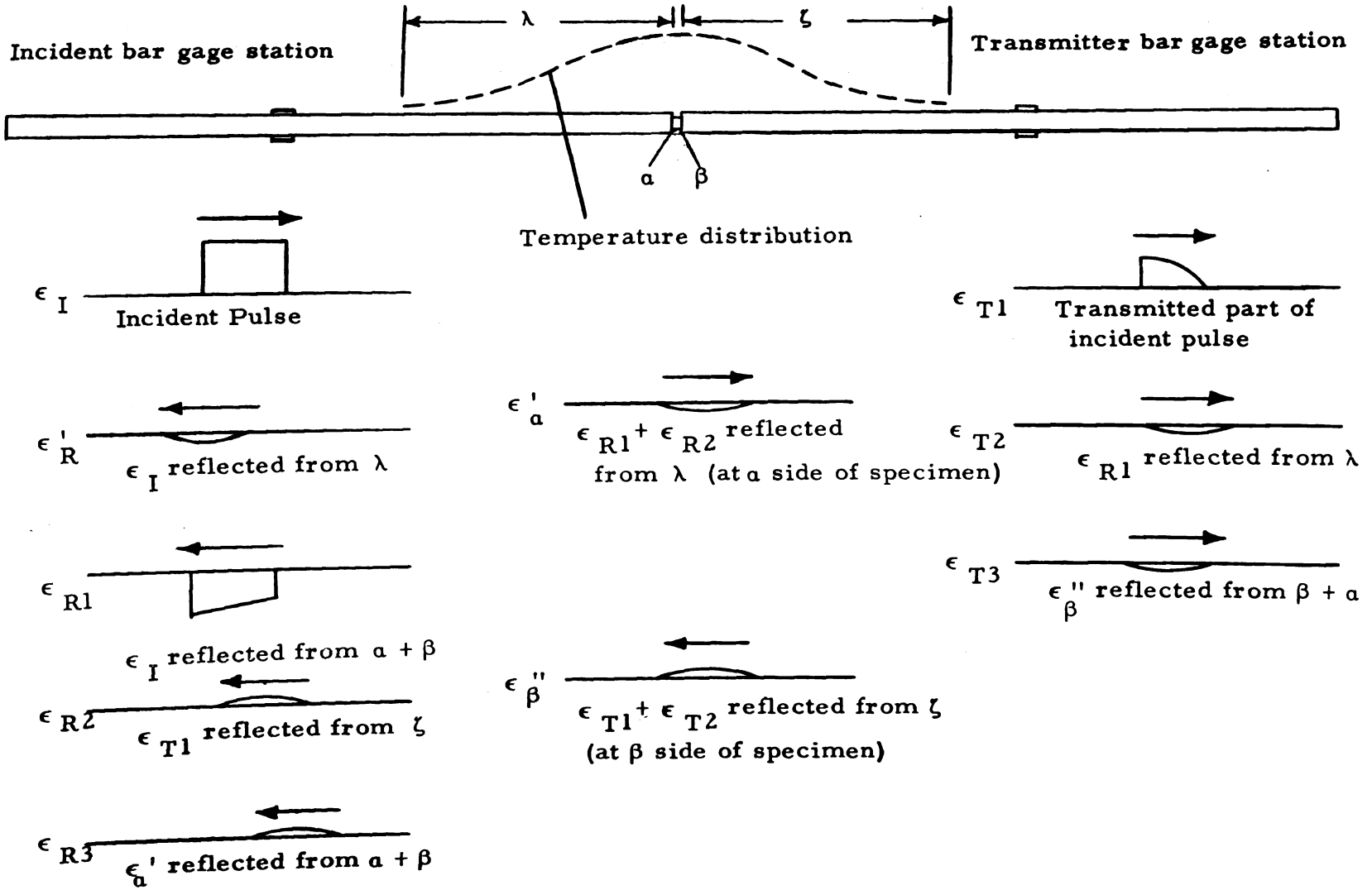

Figure 14. Breakdown of the Strain-Time Records

and at ζ . These three reflected pulses are denoted by ϵ_{R}', ϵ_{R1} and ϵ_{R2} respectively. At the transmitter bar gage station we have ϵ_{T1}, the transmitted part of the incident pulse and superposed on this is ϵ_{T2}, the part of ϵ_{R1} which was reflected from λ and transmitted back through the specimen. We also have ϵ_{T3} which is the double reflection of $\epsilon_{T1} + \epsilon_{T2}$ from ζ and from $\beta + \alpha$. The total reflected pulse as seen at the incident gage station is the sum of $\epsilon_{R}' + \epsilon_{R1} + \epsilon_{R2}$ and ϵ_{R3}, ϵ_{R3} being a double reflection of $\epsilon_{R1} + \epsilon_{R2}$ from λ and from $\alpha + \beta$. The pulses ϵ_{α}' and ϵ_{β}'' which are the reflections of $\epsilon_{R1\alpha} + \epsilon_{R2\alpha}$ from λ and $\epsilon_{T1\beta} + \epsilon_{T2\beta}$ from ζ respectively, act at the pressure bar faces but do not appear in the strain-time records taken from the gage stations since they are traveling away from their respective stations.

If ϵ_{α}' is determined and is added to the incident and reflected strain pulses acting at α which can be obtained from the incident gage station record and if ϵ_{β}'' is determined and is added to the superposed transmitted pulses acting at β, we will be able to calculate the strain-time histories of points α and β and the displacements can then be determined from Equation (2.2). If the temperature distribution is assumed to be a step function with several discontinuous jumps in temperature (λ and ζ were each divided into 5 increments in the present case), then the reflection pulses ϵ_{α}' and ϵ_{β}'' can be obtained by superposing the reflections from each jump in temperature. The time axis for each of these increments of reflection is shifted by an amount equal to the time of travel between the temperature jumps. This time is easily determined since the elastic wave velocity is known at every point along the bar. The origin of the total reflected pulse is determined from the distance between the specimen and the first temperature jump.

If we let $\epsilon_{R\alpha}$ be the sum of the reflected strains occuring at α then we see from Figure 14 that

$$\epsilon_{R\alpha} = \epsilon_{R1\alpha} - \epsilon_{R2\alpha} - \epsilon_{R3\alpha} \tag{2.5}$$

where the strains are taken as absolute values.

If $\epsilon_{T\beta}$ is the sum of the transmitted strains at the interface β then

$$\epsilon_{T\beta} = \epsilon_{T1\beta} - \epsilon_{T2\beta} - \epsilon_{T3\beta} \tag{2.6}$$

Now let us denote the longitudinal displacements of the pressure bars at α and β as u_α and u_β respectively as shown in Figure 15, then we have

$$u_\alpha = c_\alpha \int_0^t (\epsilon_{I\alpha} + \epsilon_{R\alpha} - \epsilon'_\alpha)\, dt \tag{2.7}$$

where c_α is the elastic wave velocity at α. Here $\epsilon_{I\alpha}$ and $\epsilon_{R\alpha}$ are positive since a compressive wave traveling in the positive direction, that is away from the impact end, and a tensile wave traveling in the negative direction cause a positive displacement. The strain ϵ'_α has a minus sign before it since a tensile wave traveling in the positive direction causes a negative displacement. Using this same reasoning we have

$$u_\beta = c_\beta \int_0^t (\epsilon_{T\beta} - \epsilon''_\beta)\, dt \tag{2.8}$$

where c_β is equal to c_α since the temperature is the same on both sides of the specimen.

If the stresses corresponding to the previously considered strains are denoted by like subscripts, and if we assume that the total stress on either side of the specimen is the same then we

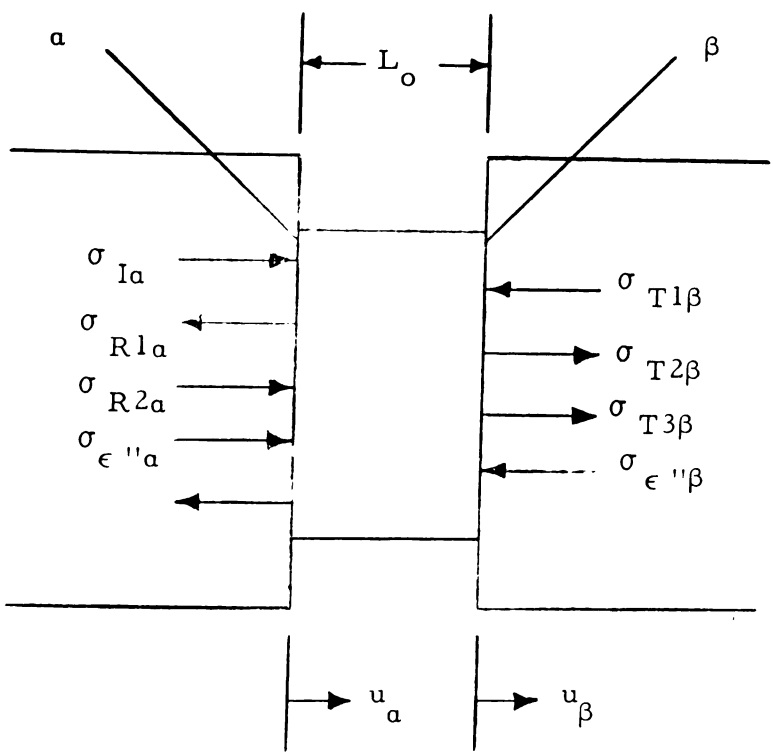

Figure 15. Schematic of Specimen Showing Stresses and Displacements

have

$$\sigma_{I\alpha} - \sigma_{R1\alpha} + \sigma_{R2\alpha} + \sigma_{R3\alpha} - \sigma_{\epsilon'\alpha} = \sigma_{T1\beta} - \sigma_{T2\beta} - \sigma_{T3\beta} + \sigma_{\epsilon'\beta} \quad (2.9)$$

or by substituting from Equations (2.5) and (2.6),

$$\sigma_{I\alpha} - \sigma_{R\alpha} - \sigma_{\epsilon'\alpha} = \sigma_{T\beta} + \sigma_{\epsilon''\beta} \quad (2.10)$$

Dividing Equation (2.10) by E_a, Young's modulus at α and β, we have

$$\epsilon_{I\alpha} - \epsilon_{R\alpha} - \epsilon'_{\alpha} = \epsilon_{T\beta} + \epsilon''_{\beta} \quad (2.11)$$

Solving this for $\epsilon_{R\alpha}$ and substituting into Equation (2.7) we have

$$u_a = c_a \int_0^t (2\epsilon_{I\alpha} - \epsilon_{T\beta} - 2\epsilon'_{\alpha} - \epsilon''_{\beta})dt \quad (2.12)$$

If the length of the specimen is taken as L_o then the nominal strain in the specimen is

$$\epsilon_s = \frac{u_\alpha - u_\beta}{L_o} \quad (2.13)$$

or by substituting from Equations (2.8) and (2.12),

$$\epsilon_s = \frac{2c_a}{L_o} \int_0^t (\epsilon_{I\alpha} - \epsilon_{T\beta} - \epsilon'_{\alpha})dt \quad (2.14)$$

where $\epsilon_{I\alpha}$ and $\epsilon_{T\beta}$ are obtained from the strain pulses ϵ_I and ϵ_T recorded at the incident and transmitter bar gage stations, but corrected in amplitude as in Equation (2.3) because of the transmission through the thermal gradient and ϵ'_{α} is a reflection pulse which can be determined from $\epsilon_{I\alpha}$ and $\epsilon_{T\beta}$. Equation (2.14) is used to calculate all specimen strains in the present study. This equation shows that it is not necessary to obtain a record of the reflected pulses at the incident gage station in order to determine the specimen strain. Time in Equation (2.14) is measured from the instant the incident strain pulse reaches the specimen. This is measured on the photographic records beginning with the initial rises of the incident

and transmitted pulses.

The stress in the specimen is obtained from the strain at the face of the transmitter bar in contact with the specimen, that is $\epsilon_{T\beta} + \epsilon''_{\beta}$. Since this bar remains elastic we have

$$\sigma_s = E_\beta(\epsilon_{T\beta} + \epsilon''_\beta) \tag{2.15}$$

where ϵ''_β is a pulse which can be determined from ϵ_I and ϵ_T.

Note that if the temperature is uniform over the pressure bars, which is the case for the room temperature tests, then ϵ'_α and ϵ''_β do not exist and Equations (2.13) and (2.14) become

$$\epsilon_s = \frac{2c_o}{L_o}\int_o^t (\epsilon_I - \epsilon_T)dt \tag{2.16}$$

and

$$\sigma_s = E\ \epsilon_T \tag{2.17}$$

where ϵ_I and ϵ_T are the actual strains occuring at the gage stations.

The applicability of Equation (2.16) to the pressure bar method used in this investigation was verified experimentally. A description and the results of this work is given in Appendix B. A comparison of $\epsilon_I - \epsilon_R$ against ϵ_T for room temperature is also given in this appendix.

CHAPTER III
EXPERIMENTAL PROCEDURE

3.1 Determination of the Elastic Wave Velocity

In order to determine the stress and strain in the specimen it was necessary to determine the elastic wave velocity in the pressure bars. The elastic wave velocity at room temperature (26°C) was determined by measuring the time required for a pulse to travel twice the length of the incident bar. The time was measured with a Model 226 B Universal Counter-Timer manufactured by Computer Measurements Company. This electronic counter was triggered with the signal from the strain pulse in the bar. The signal from the strain gage bridge was fed into a Tektronix Type 122 Low Level Preamplifier to provide the necessary voltage to trigger the counter. The counter was started when the initial compressive pulse reached the gage station and was stopped when it returned to the station again as a compressive pulse after being reflected from both ends of the bar. The counter was operated with the start and stop triggers connected in common to insure a time measurement from the same amplitude level of the pulse. A time of 407 microseconds was consistently recorded for the 80 inch wave travel which gives a wave velocity of 196,600 inches per second.

It was also necessary to know Young's modulus of the bar material. This was obtained from the relation $c_o = \sqrt{E / \rho}$ where ρ was determined by weighing a 10 foot section of the stainless steel bar. The value for E turned out to be 28.56×10^6 pounds per square inch which compares favorably with 28×10^6 pounds per square inch given by the Metals Handbook published by the American Society for Metals.

The electronic counter was also used to check the sweep speed of the dual beam oscilloscope. There was less than one percent error in the speed.

3.2 Dynamic Calibration of Strain Gages

The strain gages were dynamically calibrated by comparing the measured strain with the strain calculated from an equation expressing the strain as a function of impact velocity. The impact velocity equation may be derived by considering the impulse and momentum of the collision between the striker bar and the incident bar. If at the moment of impact the incident bar is stationary and the striker bar is moving with velocity v_s, then a compression wave will proceed from the interface into both bars at a velocity c_o as shown in Figure 16. The strain behind the wave fronts remains constant and uniformly distributed over the bars until the pulse is reflected from the free end of the shorter striker bar.

The wave front in the incident bar will have traveled a distance $c_o t$ in time t and the mass of the bar behind the wave front will be moving with the velocity v_i which is the particle velocity at every point behind the wave front. Equating the impulse with the momentum in the bar we have

$$Ft = (\rho A c_o t) v_i \tag{3.1}$$

where F is the force acting at the interface, and A is the cross-sectional area of the bar. Similarly, we have for the striker bar

$$Ft = (\rho A c_o t)(v_i - v_s) \tag{3.2}$$

where v_s is the velocity of the striker bar. By equating the impulses we get

$$v_i = \frac{v_s}{2} \tag{3.3}$$

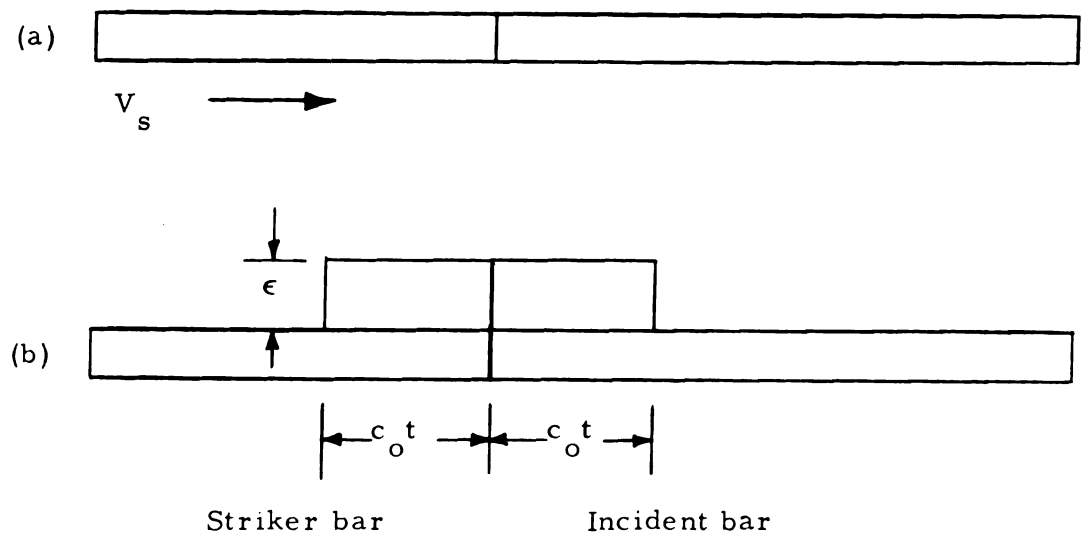

Figure 16. Striker and Incident Bar (a) at moment of impact (b) after time t.

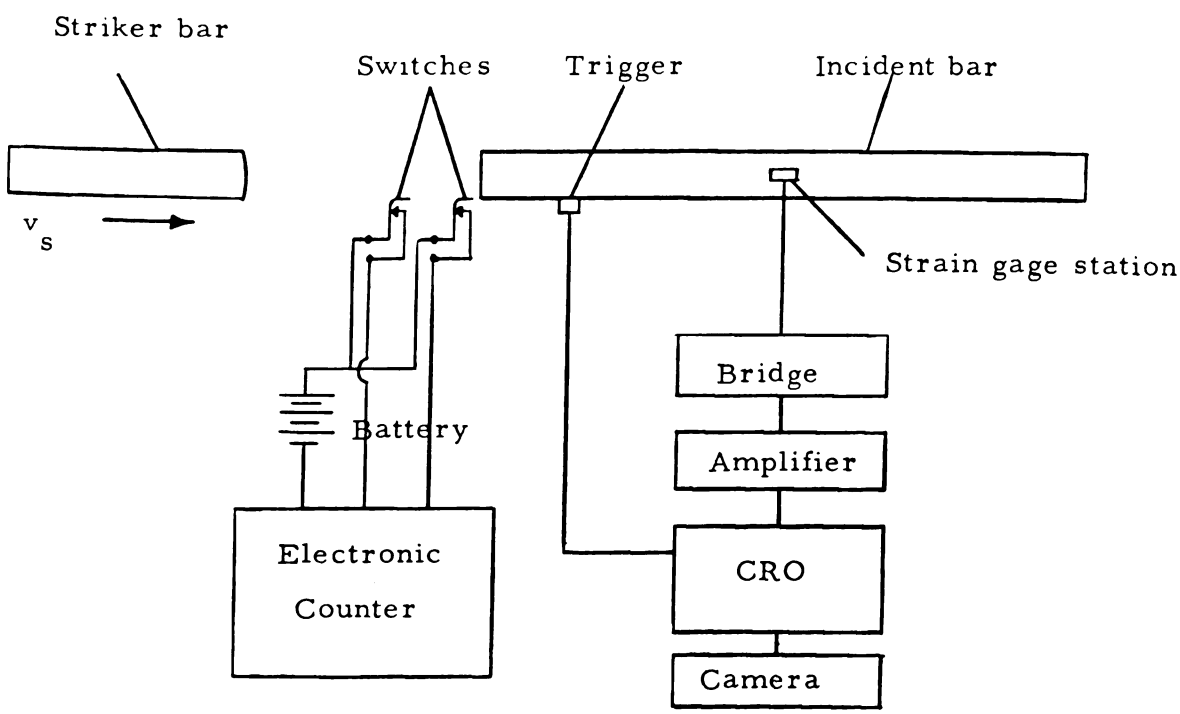

Figure 17. Schematic Diagram of Calibration Apparatus

since the bars are of the same diameter and material. The strain is uniformly distributed behind the wave front, therefore, the strain in the incident bar is simply the particle displacement at the interface divided by the distance traveled by the wave front or

$$\epsilon = \frac{v_i t}{c_o t} = \frac{v_i}{c_o} \tag{3.4}$$

If Equation (3.3) is substituted into Equation (3.4) we have strain as a function of impact velocity, that is

$$\epsilon = \frac{v_s}{2c_o} \tag{3.5}$$

The amplitudes of the pulses measured by the strain gages were calculated from the strain gage bridge equation

$$\epsilon = \frac{2\Delta v}{V_o F} \tag{3.6}$$

where Δv is the bridge output produced by the strain ϵ, V_o is the voltage supplied to the bridge and F is the gage factor of the strain gages.

Several tests were performed in which the striker bar velocity was determined by means of an electronic counter. The counter was used to measure the time required for the striker bar to travel a fixed distance. It was triggered to start and to stop by two mechanical switches which were placed near the end of the striker bar travel as shown in Figure 17. The switches were constructed of spring brass and their performance was checked during several tests by comparing their signals with the timing marks from the counter on an oscilloscope photograph.

A comparison of the strains calculated from Equations

(3.5) and (3.6) is given in Figure 18. The straight line is from Equation (3.5) and the points represent the strains calculated from the photographic records by means of Equation (3.6). The abscissas of these points are the measured impact velocities. The velocities were measured over distances of 1.5, 2 and 2.5 inches. The results show that the differences in the strains from the two equations were less when the measuring distance was decreased and that the measured strains in nearly every case were less than those calculated from impact velocity. This was probably due to a decreasing striker bar velocity near the end of the stroke caused by the friction drag of the "0" ring supports. If the striker bar was slowing down, the longer measuring distance over which an average velocity was obtained would result in a measured velocity higher than the actual velocity. Therefore it is believed that the velocities measured over the 1.5 inch distance were approaching the actual velocity of the bar. With the 1.5 inch gage length, the difference between the strains from the two equations was less than 2 percent for impact velocities from 25 to 45 feet per second. The Strain Gage Equation (3.6) was used to calculate pressure bar strain in the following tests.

3.3 Specimen Size and Material Effects

Some specimen size and material effects were observed when an attempt was made to increase strain rate by reducing the size of the specimen. The highest strain rate obtainable with the apparatus used in this investigation was dependent upon the yield point of the pressure bar material and the length of the specimen. The yield point of the bar material limited the elastic strain obtainable in the bars and therefore limited the specimen strain rate. This can be seen by differentiating both sides of Equation (2.13) with respect to time to obtain

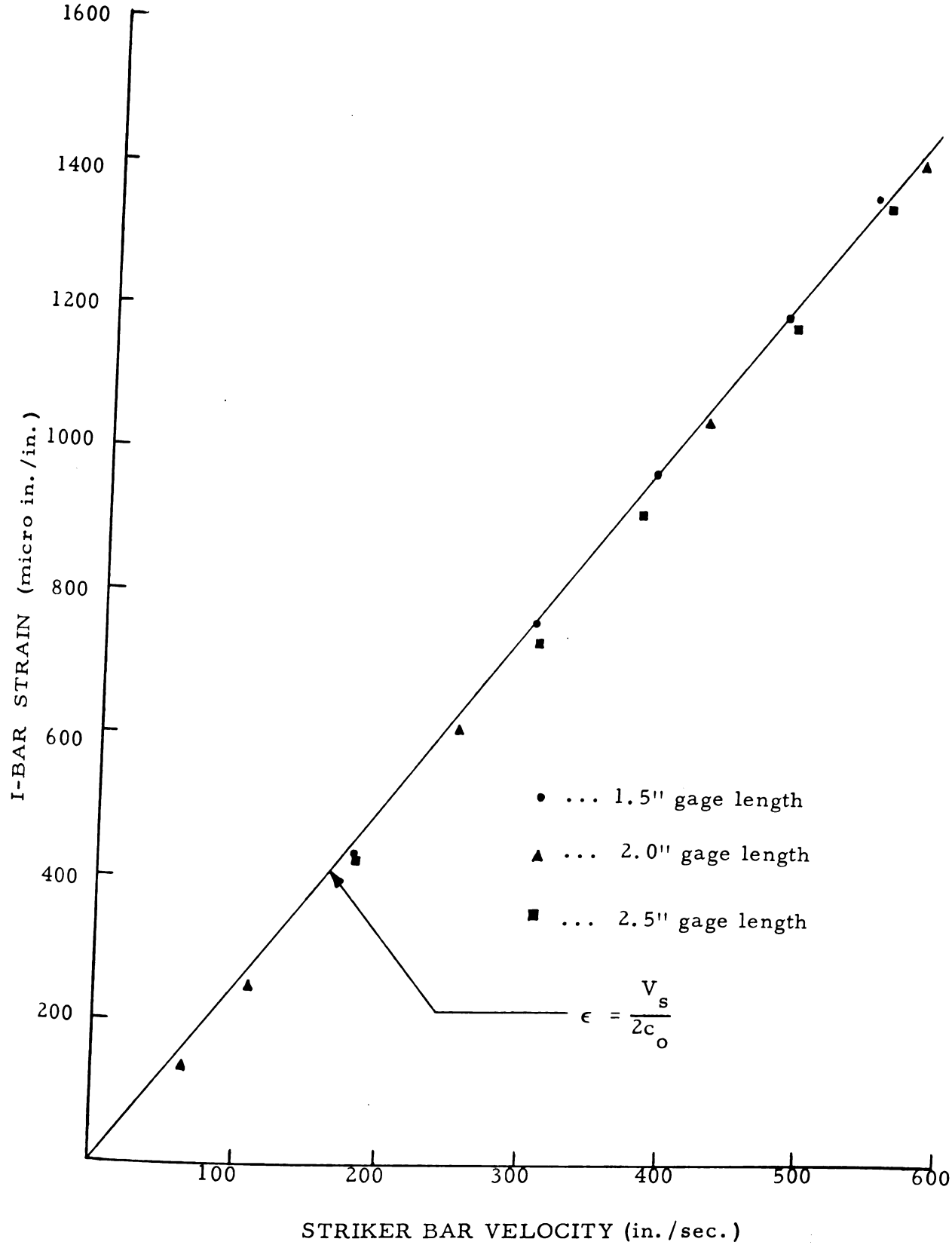

Figure 18. Comparison of Strains Determined from Impact Velocity and the Incident Strain Gage Station

$$\dot{\epsilon}_s = \frac{2c_a}{L_o} \quad (\epsilon_{I\alpha} - \epsilon_{T\beta} - \epsilon'_\alpha) \tag{3.7}$$

Here $2c_a/L_o$ is a constant for a particular temperature and $\epsilon_{I\alpha}$ is greater than $\epsilon_{T\beta}$ or ϵ'_α. Thus an upper limit is placed on $\dot{\epsilon}_s$ by the permissible magnitude of $\epsilon_{I\alpha}$. The diameter of the pressure bars was measured at several points, including points within the furnace, after each temperature run and no evidence of yielding was found. It is also seen from Equation (2.13) that a decrease in specimen length also increased the strain rate. Some specimens were made with a 25 percent reduction in length with intentions of making use of this fact. It was also necessary to reduce the diameter by 25 percent since tests performed by Lindholm (1960) showed that a reduction in the length to radius ratio from the standard ratio of one, used in his experiment and in the present investigation, introduced noticeable radial friction effects. Guyton (1960) also found that friction effects were significant for length to radius ratios as small as one-half. The smaller specimen is shown in Figure 19a along with a standard size specimen.

This attempt to extend the range of strain rates did not give results which could be correlated with the data from the standard size specimens. Five of the smaller specimens were tested at various strain rates at room temperature and the stress-strain curve from each one showed stresses which were approximately 5 percent higher than those obtained from standard specimens. The smaller specimens were machined from the same 1/2 inch diameter bar of aluminum that the standard specimens were machined from and were annealed under the same conditions. A possible explanation for the difference in stresses is that the bar material varied across the cross-section

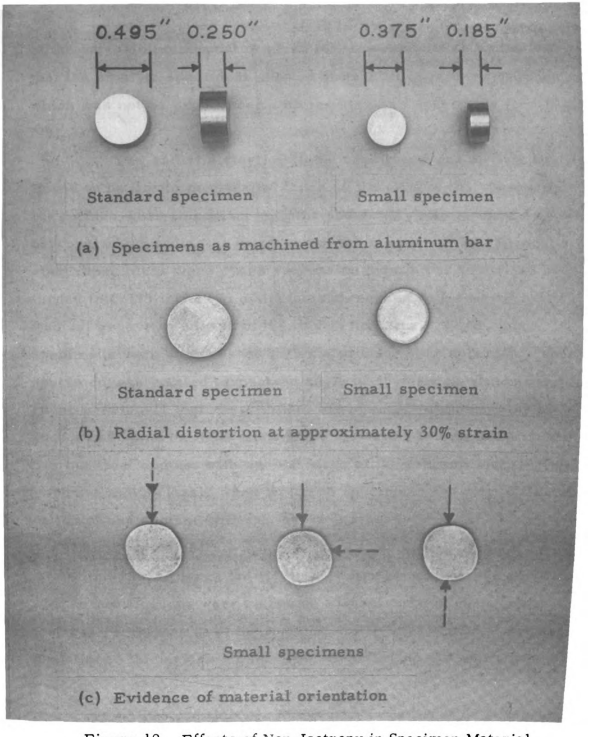

Figure 19. Effects of Non-Isotropy in Specimen Material
The solid arrows in part (c) indicate locations at mark placed on the bar before the specimens were cut off and the dotted arrows indicate the alignment of the specimens with the pressure bar surfaces.

of the

that t

which

[96].

lieve

bars

obtai

small

turne

studi

speci

speci

to the

show

bar r

is sh

on to

3.4

and t

test

cond

used

per c

in or

oscil

of the bar. Some support is given for this explanation by the fact that the smaller specimens showed quite a bit of radial distortion which was not as pronounced with the standard specimens (see Figure 19b).

The radial distortion in the specimens was at first believed to be due to nonparallel faces on the ends of the pressure bars which were in contact with the specimen, but evidence was obtained which indicates this was not the reason for it. Three small specimens were cut in succession from a bar which had been turned to 0.185 inches in diameter and marked with a small longitudinal groove by means of the tool in the lathe. When these specimens were compressed with the pressure bar apparatus, each specimen was rotated through an angle of 45 degrees with respect to the previously tested specimen. The results of these tests as shown in Figure 19c indicate that the distortion is oriented with the bar material and not with the end faces of the pressure bars. This is shown more clearly when the three specimens are placed directly on top of one another with the marks in line.

3.4 Test Procedure

The furnace, the strain gage bridge voltage, the amplifiers and the oscilloscope were turned on at least one-half hour before a test was performed in order to obtain nearly steady state operating conditions. In performing the tests the following procedure was used:

1. The oscilloscope sweep speed was set at 50 micro-seconds per centimeter and the trigger was placed on single sweep lockout in order to obtain a complete record of the test with one sweep of the oscilloscope trace.

2. The vertical gain adjustments of the amplifiers were set

in accordance with the impact tester set pressure used for the test.

3. The length and diameter of the specimen were measured to the nearest 0.0002 inch with a micrometer and the measurements were recorded.

4. The parallel faces of the specimen were covered with a light coat of lubricant and the specimen was centered between the two pressure bars. The specimen was held in place by a small longitudinal force applied to the incident bar by means of rubber bands.

5. A set pressure was applied to the forward chamber of the Hyge unit and locked in.

6. The specimen temperature was checked and adjusted. The specimen was held at the test temperature at least 5 minutes to obtain a uniform temperature distribution.

7. The load pressure was increased to near the firing pressure.

8. The camera shutter was opened and held open until after the Hyge unit fired.

9. The load pressure was released and the Hyge piston was retracted to be ready for the next test.

10. The strain gage bridge voltage was read and recorded.

11. The specimen was removed and the end faces of the pressure bars were wiped clean for the next test.

Specimens were tested at 30^{o}, 150^{o}, 250^{o}, 350^{o}, 450^{o} and 550^{o}C. At each test temperature, a series of tests was performed in which the Hyge set pressure was varied to obtain an evenly distributed range of strain rates from approximately 300 to approximately 2000 inches per inch per second. The number of specimens tested at each temperature depended on the results obtained at that temper-

erature. All tests at a particular temperature were completed and the stress-strain curves were plotted before starting tests at the next test temperature.

In order to maintain control over specimen temperature during the room temperature tests, the furnace was used to heat the specimens slightly. The specimen temperature was held at 30°C while the actual room temperature varied from 25° to 28°C. Temperature reflections in the bars were neglected for these small temperature increases.

Molykote (commercial molybdenum disulfide) was used for specimen lubrication at test temperatures of 30°, 150°, 350° and 450° C. It was necessary to use powdered graphite at 250° C because at this temperature the Molykote formed a hard coating on the faces of the specimen and the pressure bars which was difficult to remove between tests. A powdered glass with a low softening point was used as a lubricant at 550°C. The glass powder was mixed with alcohol to form a paste which was easily applied to the faces of the specimen. The glass was composed of 80 percent PbO and 20 percent B_2O_3 by weight. It was prepared by melting the constituents together and then powdering the resultant pieces of glass with a mortar and pestle.

3.5 Reduction of Data

Measurements were taken from the photographic records using a Pye two-dimensional traveling microscope accurate to 0.01 millimeter. Slight corrections were made for photographic and oscilloscope screen distortions. Amplitudes of the incident and transmitted pulses were measured at a series of points along the time axis. The spacing of the points was determined according to the need for accuracy at the particular section of the curve. The time axes for the two pulses were made to coincide by aligning the initial rise portions of the curves.

The strain pulses ϵ'_a and ϵ''_β were determined by the method described in Appendix A. The pulse ϵ''_β was obtained by calculating the reflection of the transmitted pulse $\epsilon_{T\beta}$ from the temperature gradient in the transmitter bar as shown in Figure 14. In order to obtain ϵ'_a it was necessary to find the reflected pulse ϵ_{Ra}. The pulse ϵ_{Ra} was approximated by the sum of the pulses ϵ_{Ra}, ϵ'_a and ϵ''_β which was obtained by adding ϵ''_β to both sides of Equation (2.11), transposing ϵ_{Ia} and changing signs. Let ϵ''_{Ra} be the assumed value for ϵ_R then

$$\epsilon''_{Ra} = \epsilon_{Ra} + \epsilon'_a - \epsilon''_\beta = \epsilon_{Ia} - \epsilon_{T\beta} - 2\epsilon''_\beta \qquad (3.8)$$

The strain ϵ'_a was calculated from ϵ''_{Ra} and then substituted back into Equation (2.11). This showed that the error in ϵ'_a as determined by this procedure was insignificant for the range of temperatures used in this investigation.

Nominal specimen strain was calculated from Equation (2.14) by plotting $\epsilon_{Ia} - \epsilon_{T\beta} - \epsilon'_a$ versus time and then numerically integrating this curve with a planimeter. True or logarithmic strain ϵ_n was determined from

$$\epsilon_n = \ln \frac{1}{1 - |\epsilon_s|} \qquad (3.9)$$

Taking into account the change in diameter between the specimen and the pressure bars and assuming there is no volume change in the specimen during compression, the true stress σ_n in the specimen is

$$\sigma_n = \frac{D^2}{d^2} E_\beta (\epsilon_{T\beta} + \epsilon''_\beta)(1 - |\epsilon_s|) \qquad (3.10)$$

where D and d are the initial diameters of the pressure bars and the specimen respectively. All stress-strain curves plotted are for

true stress and true strain.

The assumption of no volume change in the specimen was checked by measuring specimens before and after compression at several test temperatures. The error in all cases was less than one percent.

CHAPTER IV
RESULTS

4.1 Oscilloscope Records

Typical records of oscilloscope traces for the six test temperatures are given in Figure 20. The time scale reads from right to left in these photographs. The upper trace on each record is the output from the gage station on the incident bar and the lower trace is from the transmitter bar station. The reflected pulses at the incident gage station are not shown. They were adjusted out of the range of the upper beam in order to utilize higher gain settings on the preamplifier.

It is seen from Equation (2.15), which gives specimen stress in terms of the transmitter bar strain, that the shape of the stress-time curve for each specimen is represented approximately by the shape of the transmitted pulse record, since ϵ'_β is small in comparison with $\epsilon_{T\beta}$. A direct comparison of the shapes of the stress-time curves and their amplitudes at the different temperatures cannot be made on a common basis from the photographs in Figure 20 since the gain settings and the amplitudes of the incident pulses are not the same, although Figures 20a and 20e show the effect of temperature on the curve quite well. It is seen that aluminum has a more clearly defined yield stress at the higher temperatures.

The oscillations which occur in the leading portions of the transmitted pulses are apparently due to dispersion of the pulse components as discussed in Chapter II, since the period of these oscillations is approximately the same as those observed for the incident pulse in the long one-piece pressure bar. The amplitude of these oscillations increases with temperature. This may be due

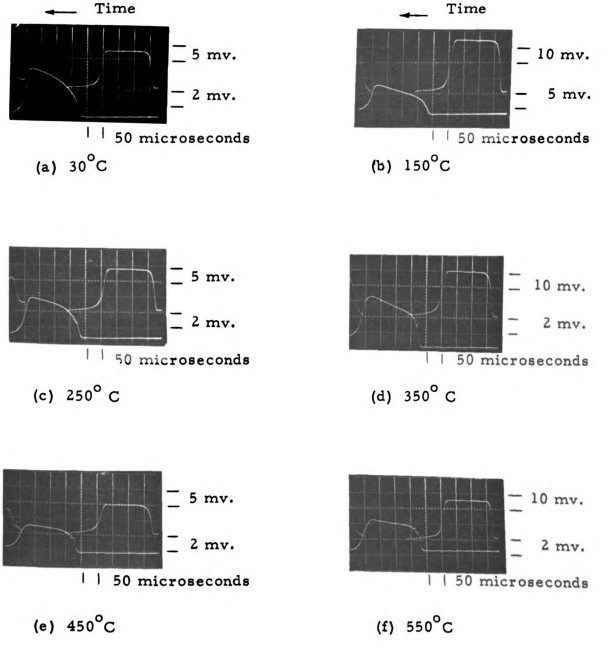

Figure 20. Typical Oscilloscope Records for 1/2 Inch Diameter by 1/4 Inch Long Aluminum Specimens Incident and transmitted pulses are shown on the upper and lower traces respectively.

to the shape of the transmitted pulses at the higher temperatures (more high frequency components) or it may be due to effects in the heated pressure bars. Attempts to reduce the amplitude of these oscillations at the higher temperatures by further rounding of the end of the striker bar failed.

The oscilloscope records also show that the transmitted pulses are longer than the incident pulses. This is due to the fact that the incident pulse continues to exert a force on the specimen after its amplitude begins to decrease. This may be seen from a graph of the incident, reflected and transmitted pulses where the transmitted pulse is shown to be the result of taking the difference of the magnitudes of the incident and reflected pulses. Such a graph is given in Appendix B.

4.2 Deformation in the Specimens

A photograph of specimens tested at each temperature is shown in Figure 21. The dark surface and ridges at the edges of the 550°C specimens are due to the glass lubricant which bonded to them. The specimens tested at the higher temperatures were slightly barreled but there was almost no evidence of barreling at room temperature. The small amount of barreling at the higher temperatures was believed to have little effect on the amount of longitudinal strain in the specimens. The circumferential surface did not fold under on any of the specimens used in this experiment. The barreling at the higher temperatures was probably due to a reduction in the effectiveness of the lubricants at these temperatures. No irregularities appeared on the parallel surfaces of the specimens.

4.3 Strain-Time Curves

Strain-time curves for four typical specimens at 30°C and for four others at 550°C are given in Figures 22 and 23 respectively.

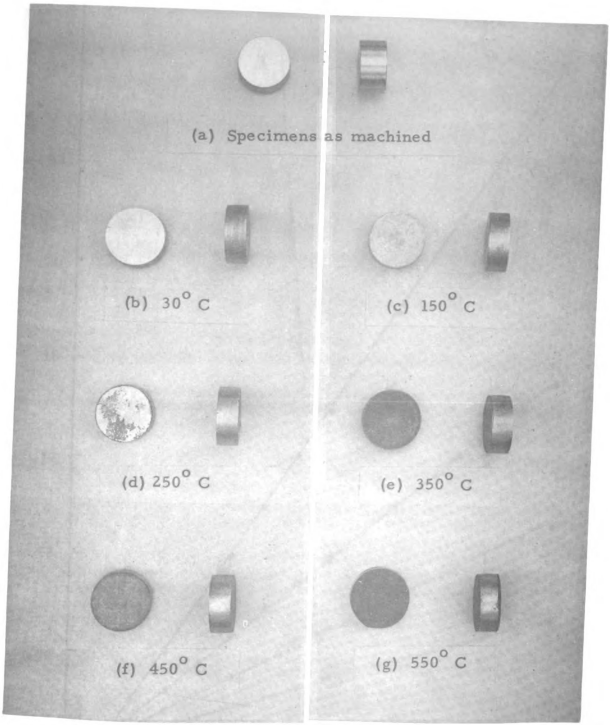

Figure 21 Typical Deformed Specimens at each Test Temperature
The strains are from 20 to 25 percent true strain.

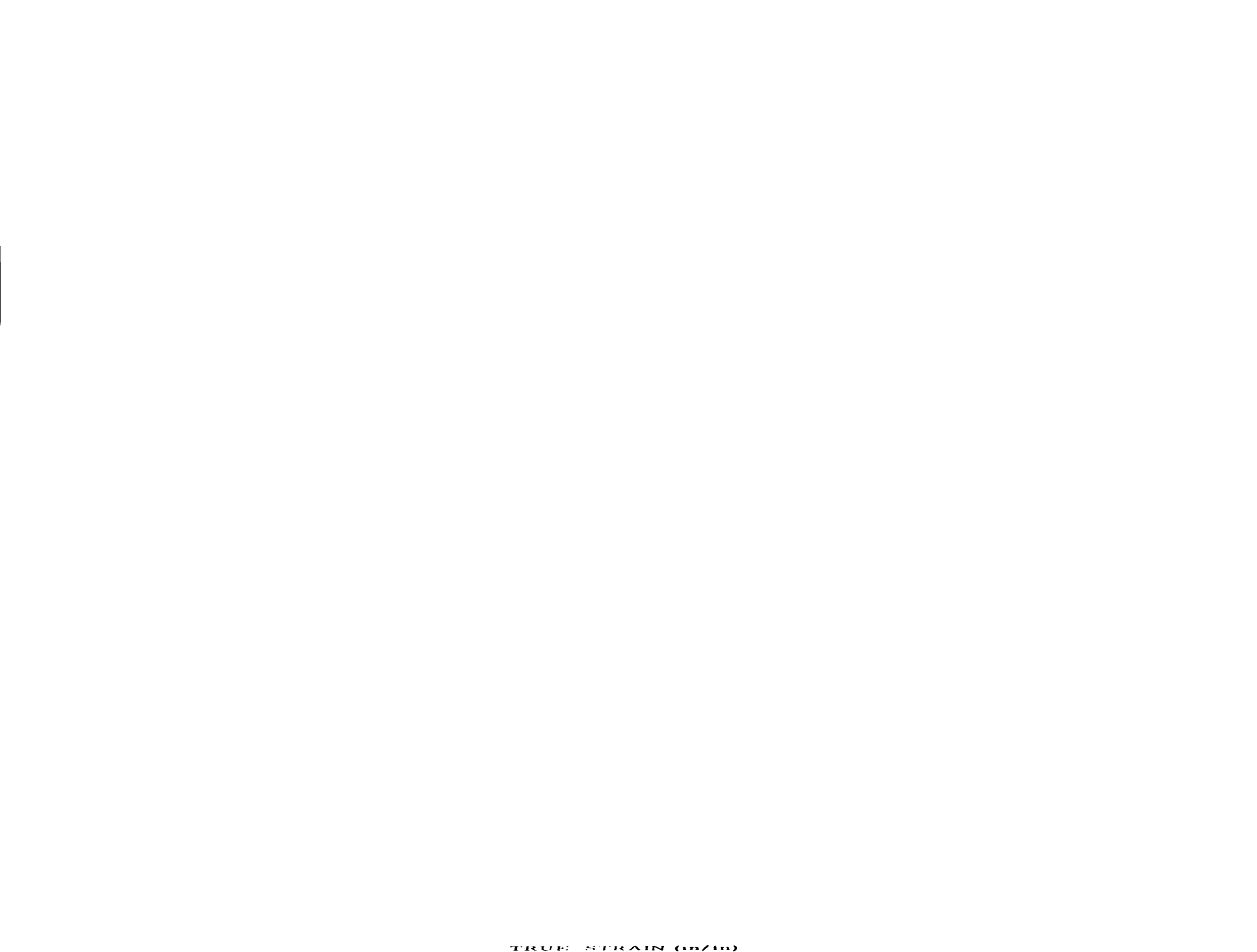
TRUE STRAIN (dr/r)

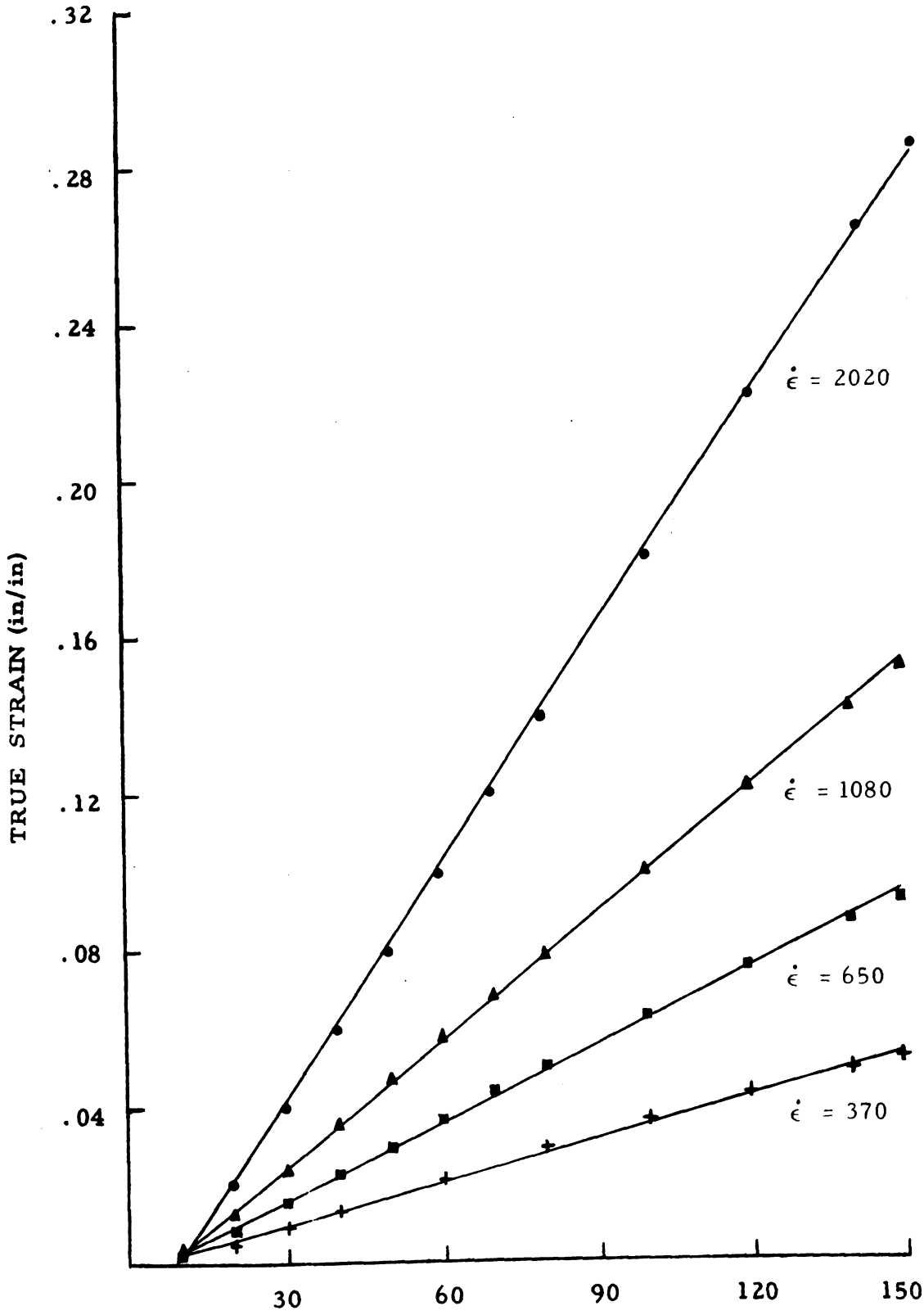

Figure 22. Strain-Time Curves at 30°C

TRUE STRAIN (in/in)

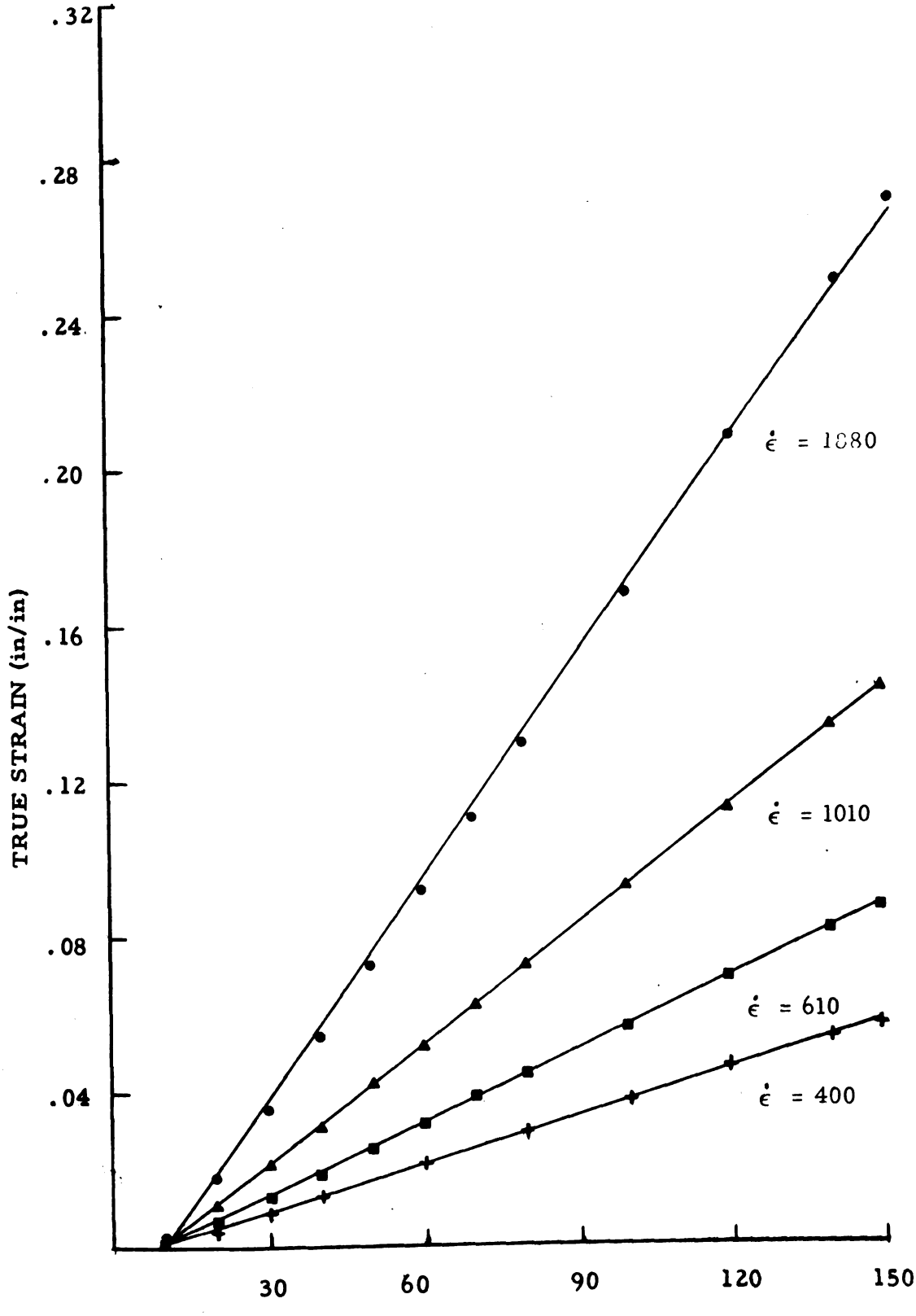

Figure 23. Strain-Time Curves at 550°C

The pressure bar method used in this experiment is seen to produce nearly constant strain rates for aluminum at strains above approximately 0.5 percent. The linearity of the strain-time curves is due to the shape of the transmitted pulse since the specimen strain is calculated from the area under the curve obtained by subtracting the transmitted pulse from the incident pulse. Fortunately, the linearity is quite good at all test temperatures even though the shape of the transmitted pulse changed with temperature. The curves for the intermediate temperature tests are not given because they are similar to the ones shown.

Lindholm (1960) found that the strain-time curves produced for lead and copper by this method were not linear although they could be assumed linear to a fair approximation.

The very low strains during the first 10 microseconds are due to the smaller area under the rise portion of the incident pulse.

The split Hopkinson pressure bar method used produces a limited range of strain rates. Significant extensions beyond the range of 300 to 2000 inches per inch per second obtained in this investigation are not feasible. As discussed earlier, the yield point of the bar material places an upper limit on the strain rate and friction effects prevents the use of a shorter specimen to increase strain rates. In order to obtain lower strain rates at the level of strains used in this experiment, it would be necessary to increase the length of the striker bar and to reduce the impact velocity. If the length of the striker bar is increased it is also necessary to increase the length of the pressure bars in order to avoid reflections of the longer pulse in the strain records, and the apparatus would soon become unwieldy. If the impact velocity is reduced, the force applied to the specimen soon becomes so small that it will produce only elastic

strains. The lower velocities would also produce lower strains in the pressure bars which would require a refinement in measuring technique. Lower specimen strain rates could also be obtained by increasing the length of the specimen but this increases the possibility of errors due to wave propagation effects in the specimen.

4.4 Stress-Strain Curves

Typical stress-strain curves for specimens at all six test temperatures are given in Figure 24. Curves at four strain rates are shown at each temperature. It is seen that increased temperatures have a very pronounced effect on the magnitude of stress and that strain rate has a much greater effect on stress at high temperatures than at room temperature.

Due to the nature of the loading pulse, it was difficult to obtain accurate data for low levels of strain especially at the higher strain rates. The oscillations which appeared on the transmitted pulse at the higher temperatures limited the accuracy at the lower strains, but the accuracy obtained by taking an average curve through the oscillations was quite adequate at strains of 3 percent and above for the highest strain rates and was accurate for strains as low as 0.5 percent at the lower strain rates. The curves were extended to the origin for the sake of appearance.

With the inaccuracy at the lower strains, it was impossible to determine the effects of strain rate and temperature on Young's modulus. However, some work has been done on this problem. The variation of E with temperature as determined statically and dynamically was given for aluminum by Vosteen (1958) (see also Garofalo, 1960).

In Figure 25, a room temperature stress-strain curve from the present experiment is shown along with curves at lower strain rates obtained by Lindholm (1960) using the same type of

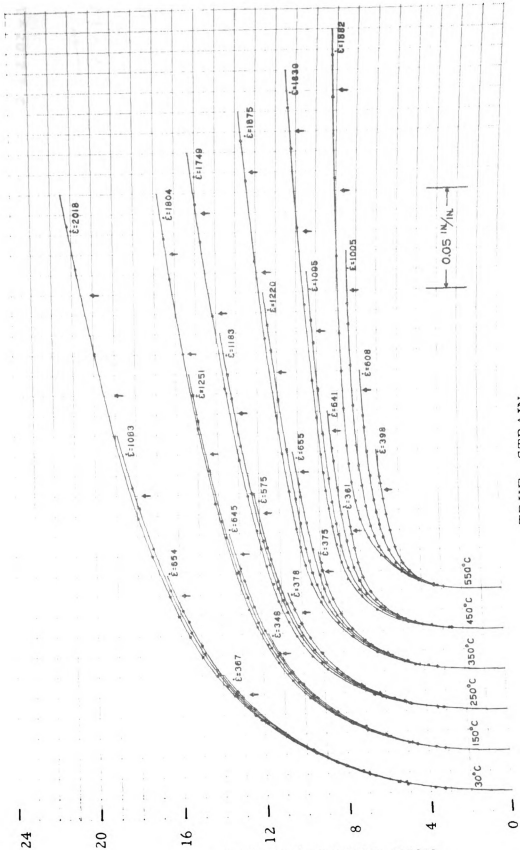

Figure 24. Stress-Strain Curves at Various Test Temperatures

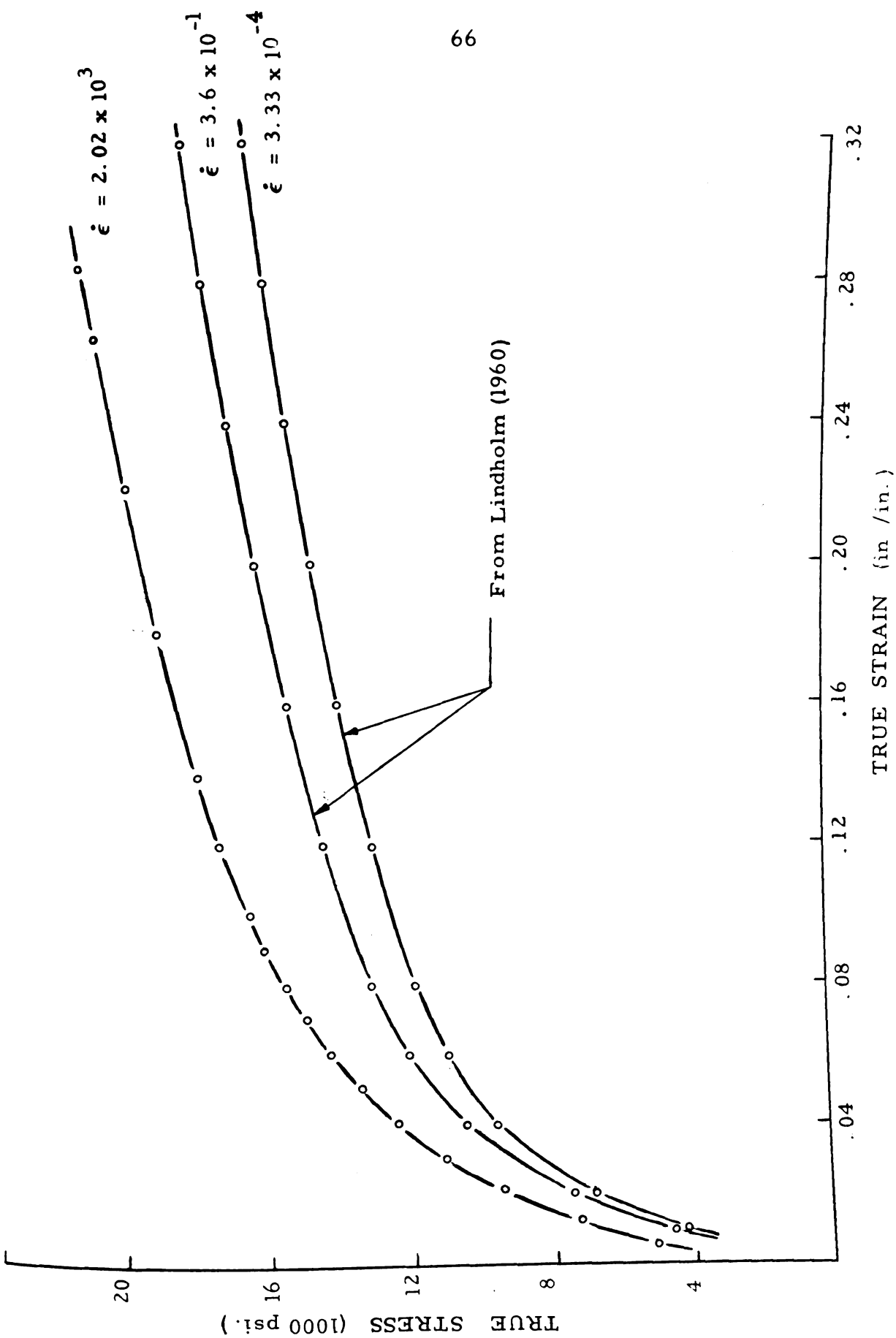

Figure 25. Stress-Strain Curves at Several Strain Rates.

aluminum and the same specimen size as used in the present investigation. These lower strain rate tests were performed on a Model FGT Baldwin-Emery SR-4 Universal Testing Machine. The machine had a constant loading speed which could be changed by means of a variable speed motor. It should be mentioned that stresses obtained by Lindholm in the impact range of strain rates, using an apparatus similar to the one used here, were all approximately 5 percent lower than those obtained in the present study. Part of this difference is believed to be due to a slight difference in the specimen material. Tests performed in this investigation showed that stresses at room temperature varied by as much as 8 percent between different bars of supposedly the same material.

A factor which could influence the shape of the stress-strain curve is the change from isothermal to adiabatic conditions as the strain rate is increased. An approximate calculation based on an adiabatic condition was made for a specimen in the present experiment. For a strain of 25 percent the specimen temperature increases about $12^{o}C$ which would cause the stress to decrease by about 250 pounds per square inch according to temperature curves determined in this study. This stress change would have little effect on the shape of the stress-strain curves.

4.5 Stress-Strain Rate Curves

The stress-strain rate curves at each temperature were plotted on both semi-logarithmic and log-log coordinate systems in order to evaluate the validity of the logarithmic and the power flow laws as given by Equations (1.7) and (1.9) respectively. The semi-logarithmic curves are shown in Figures 26-30 and the log-log curves are shown in Figures 31-34. Each point in these figures represents a separate test with a new specimen where the stress at 0.05 inches

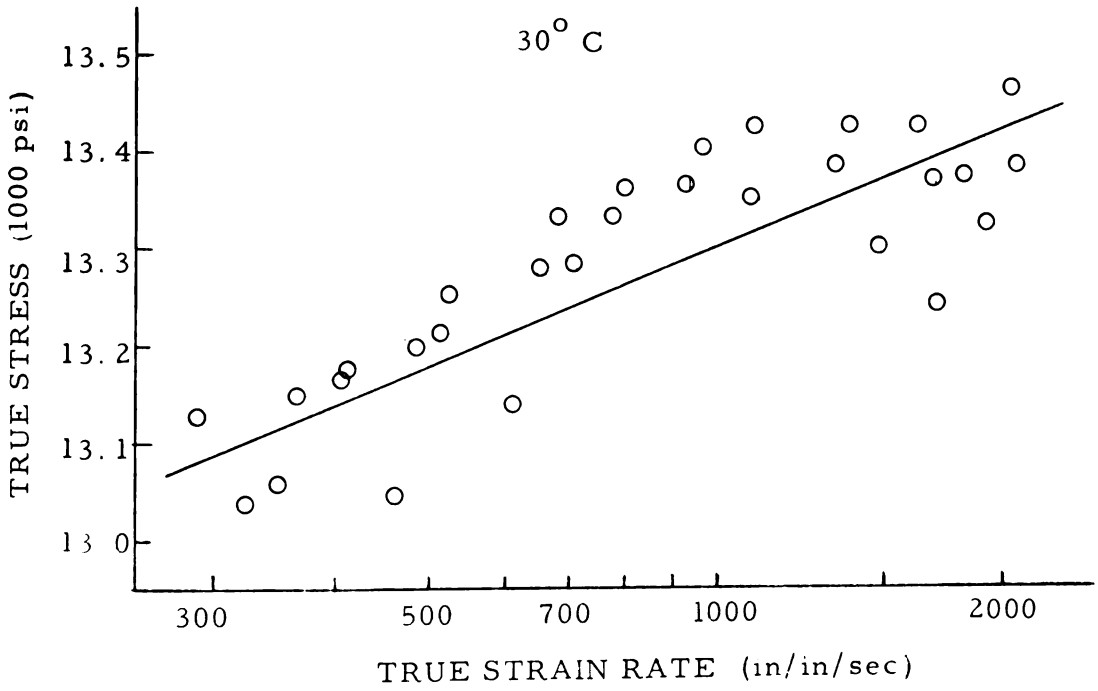

Figure 26. Stress Versus Log Strain Rate at 5 Percent True Strain

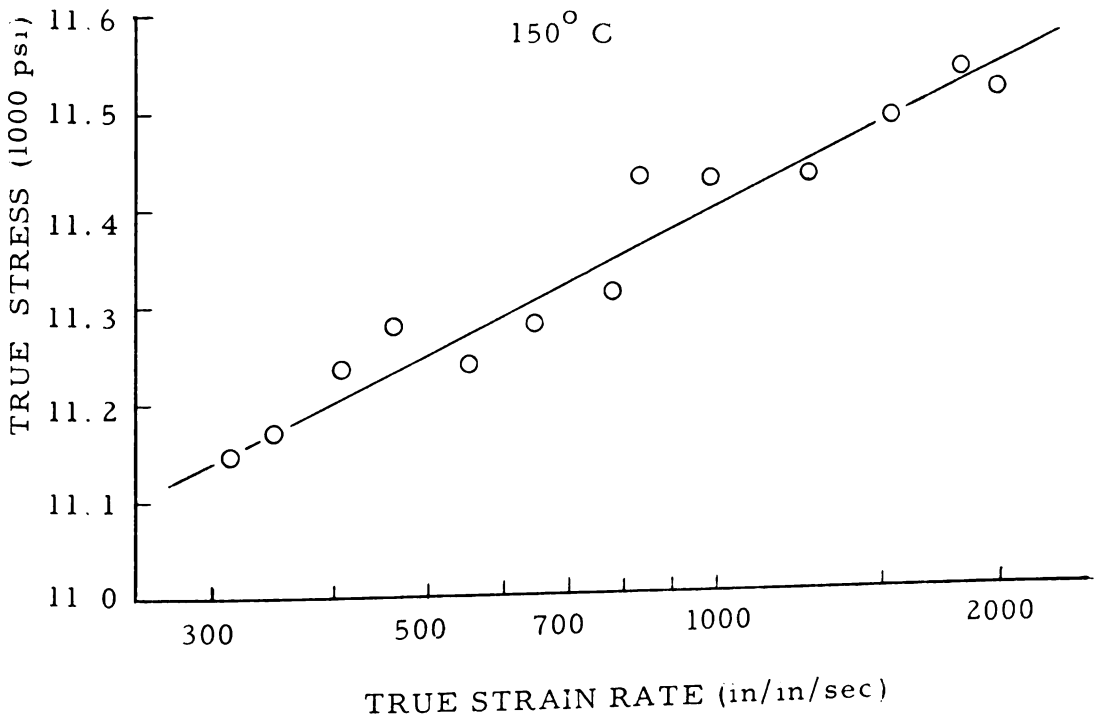

Figure 27. Stress Versus Log Strain Rate at 5 Percent True Strain

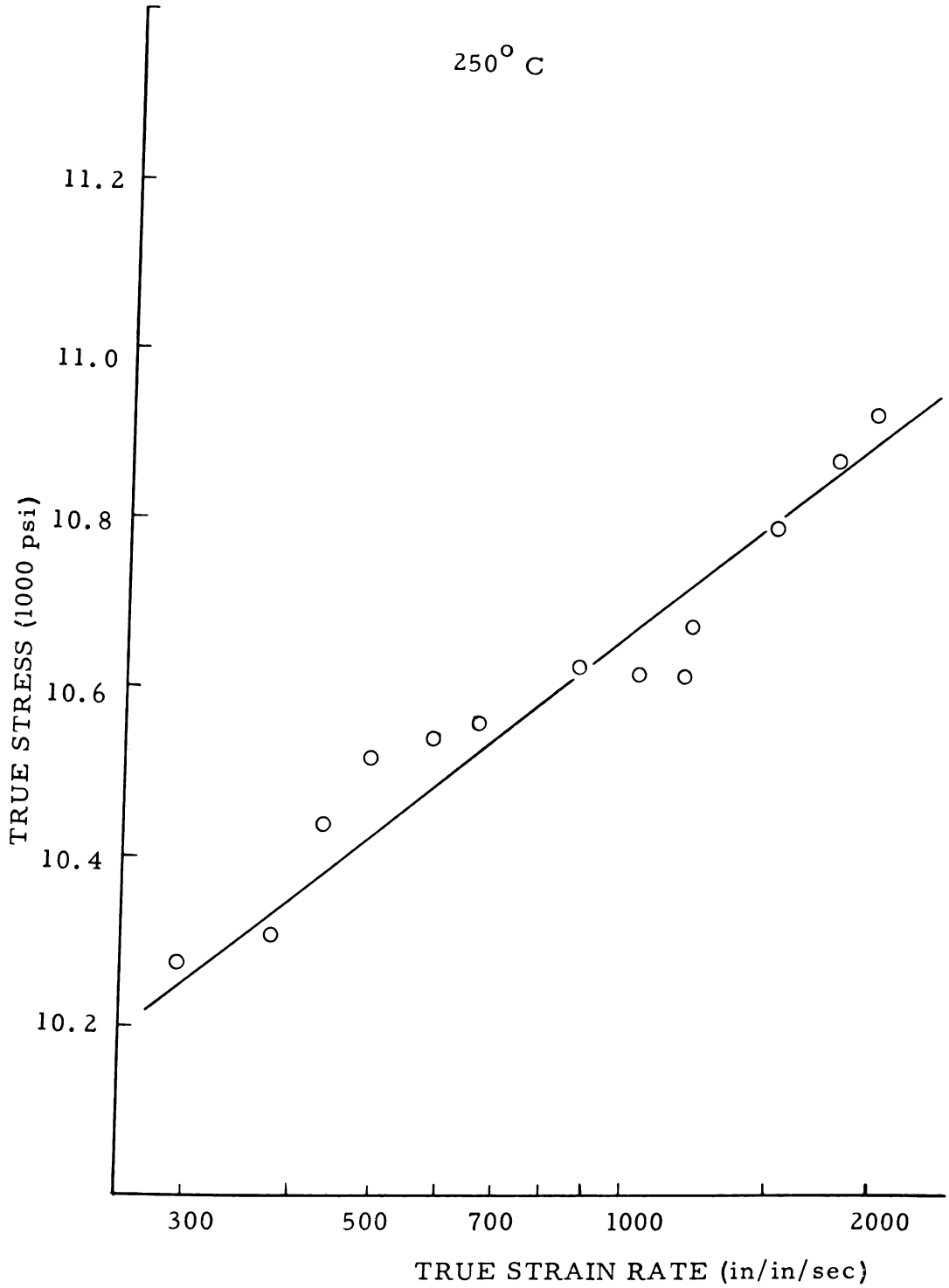

Figure 28. Stress Versus Log Strain Rate at 5 Percent True Strain

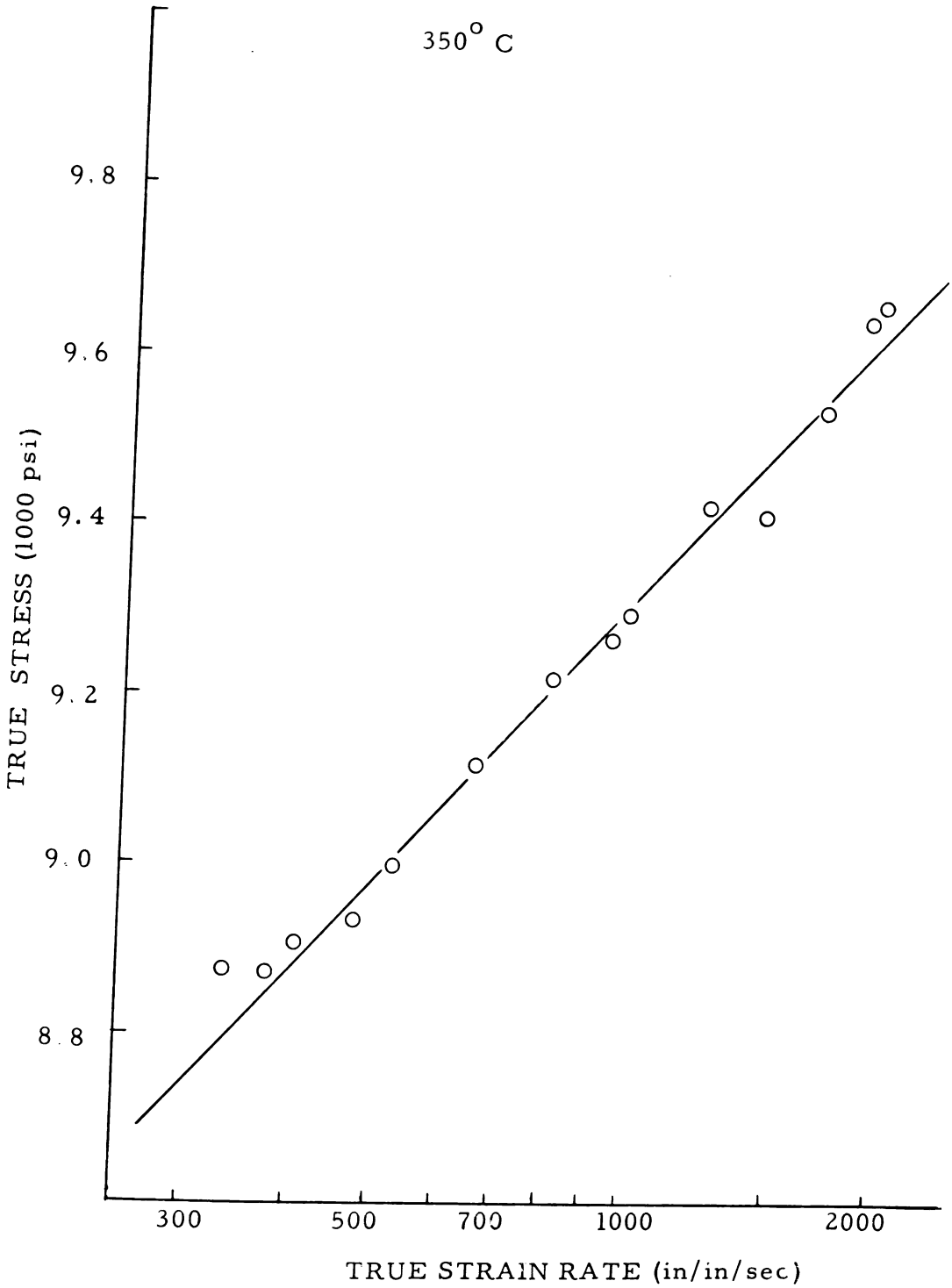

Figure 29. Stress Versus Log Strain Rate at 5 Percent True Strain

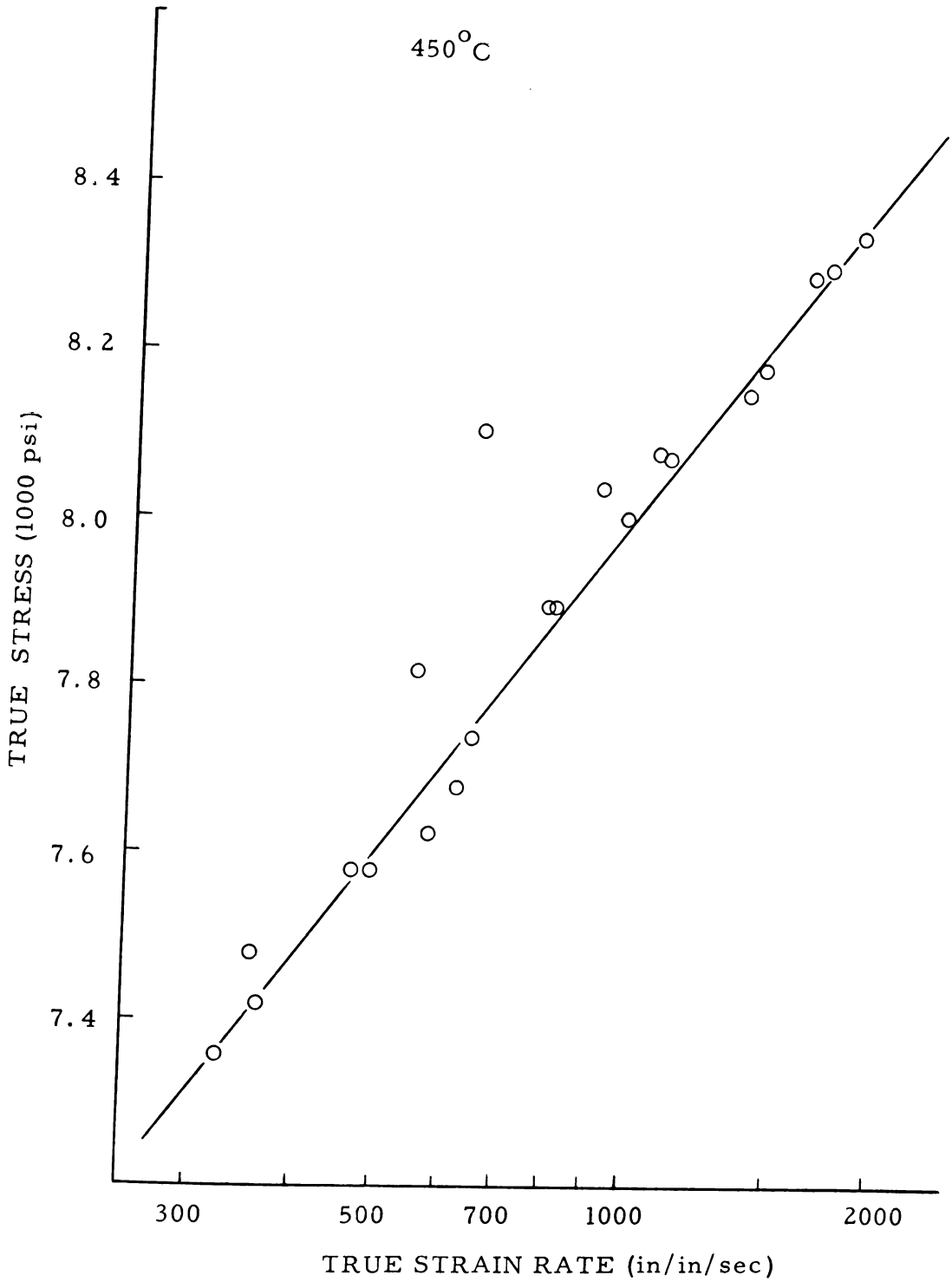

Figure 30. Stress Versus Log Strain Rate at 5 Percent True Strain

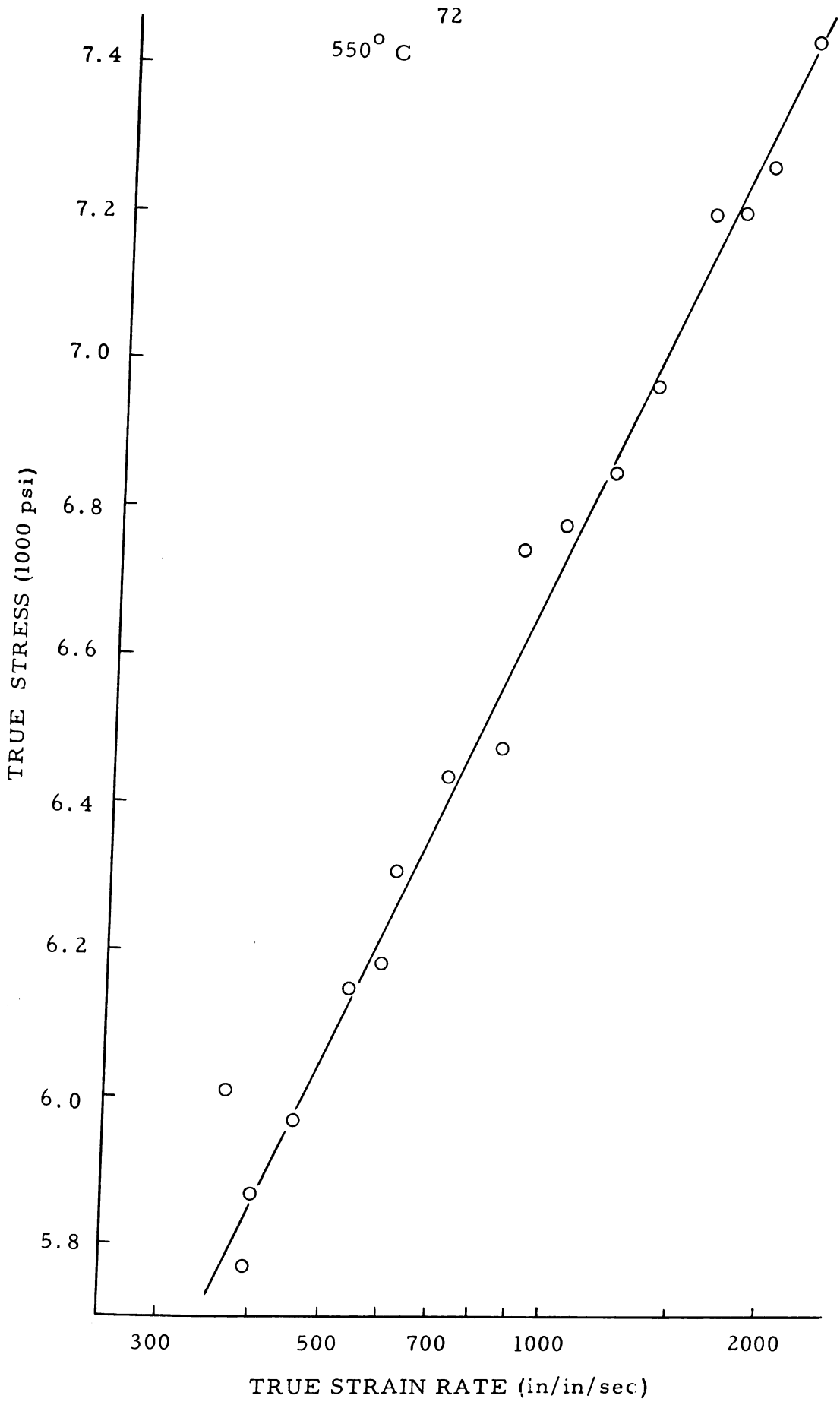

Figure 31. Stress Versus Log Strain Rate at 5 Percent True

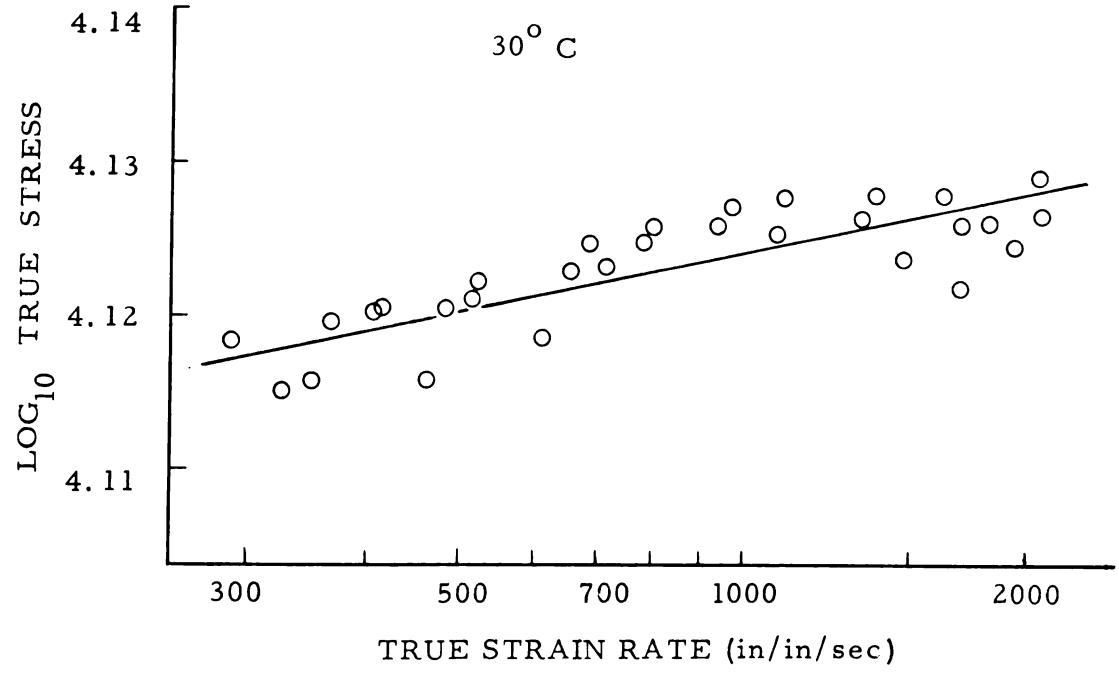

Figure 32. Log Stress Versus Log Strain Rate at 5 Percent True Strain

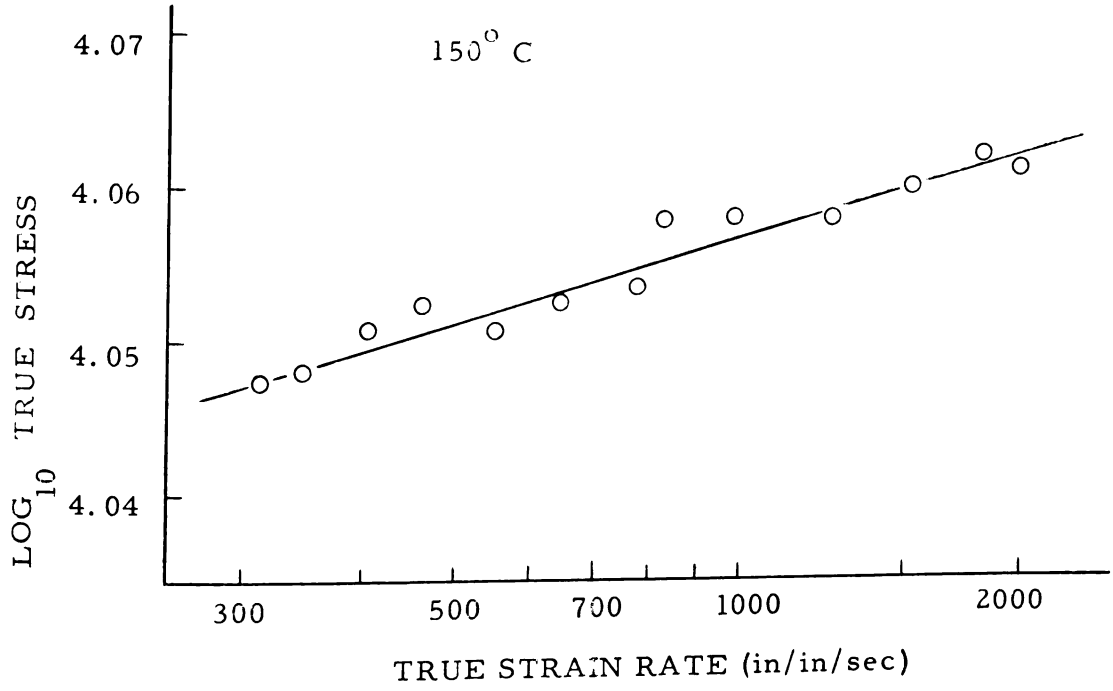

Figure 33. Log Stress Versus Log Strain Rate at 5 Percent True Strain

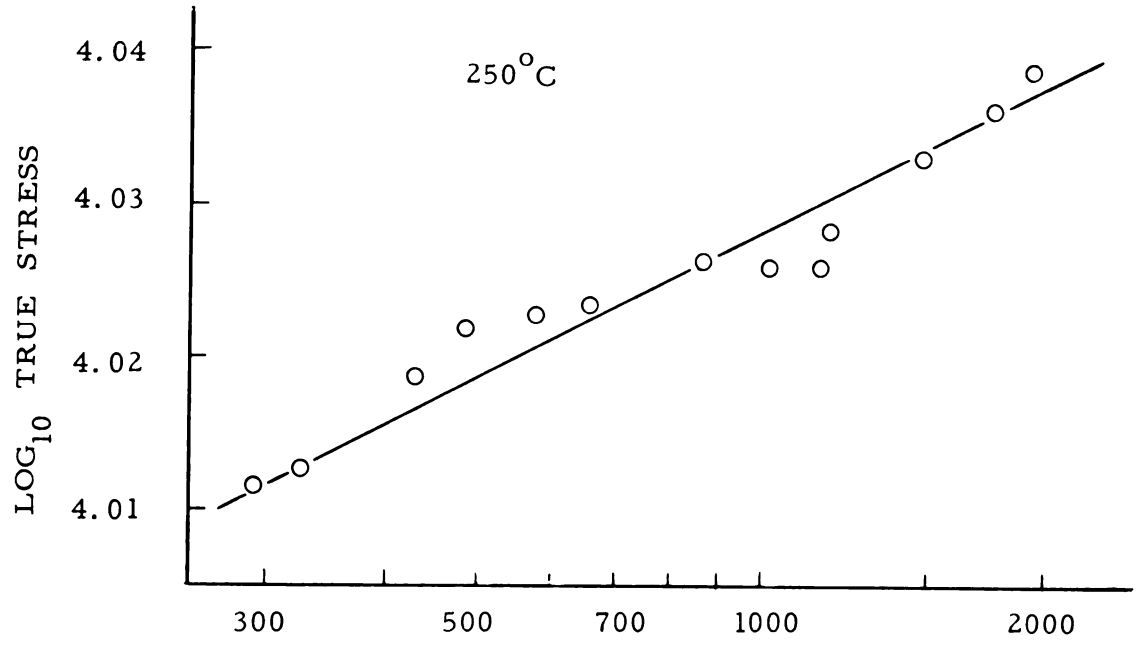

Figure 34. Log Stress Versus Log Strain Rate at 5 Percent True Strain

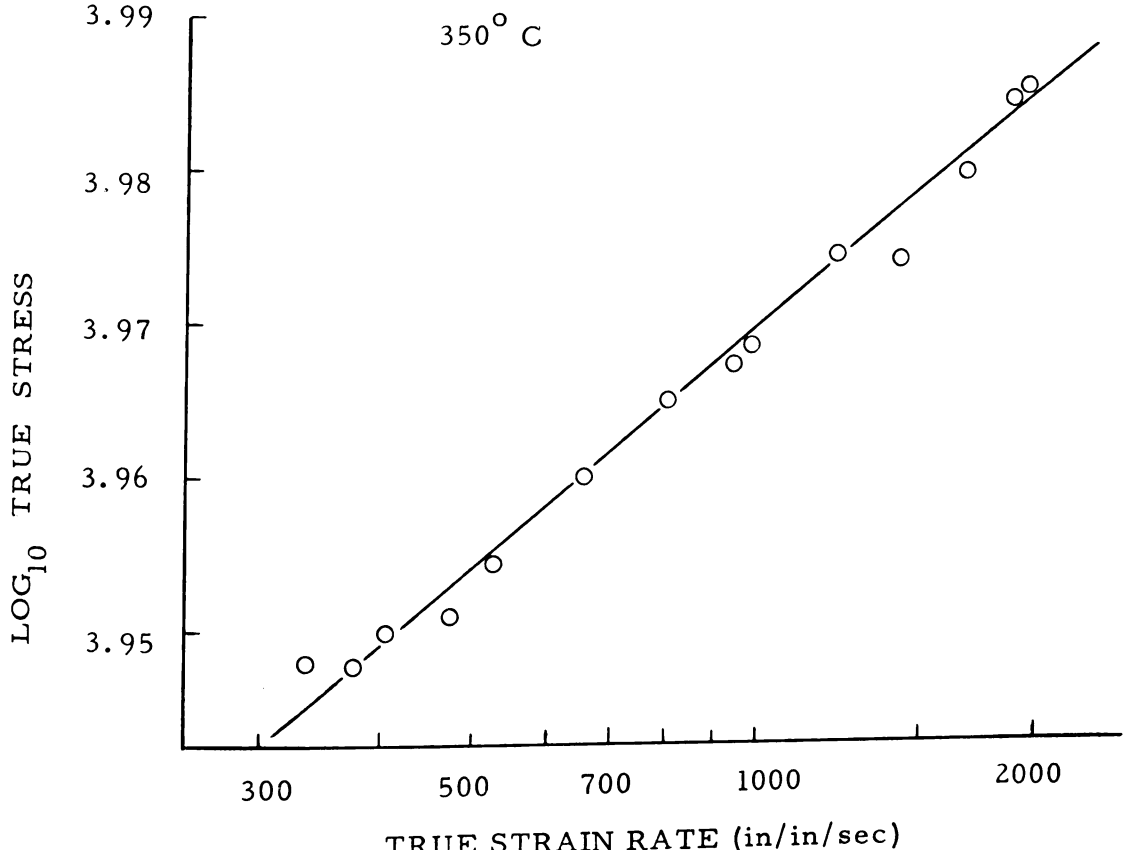

Figure 35. Log Stress Versus Log Strain Rate at 5 Percent True Strain

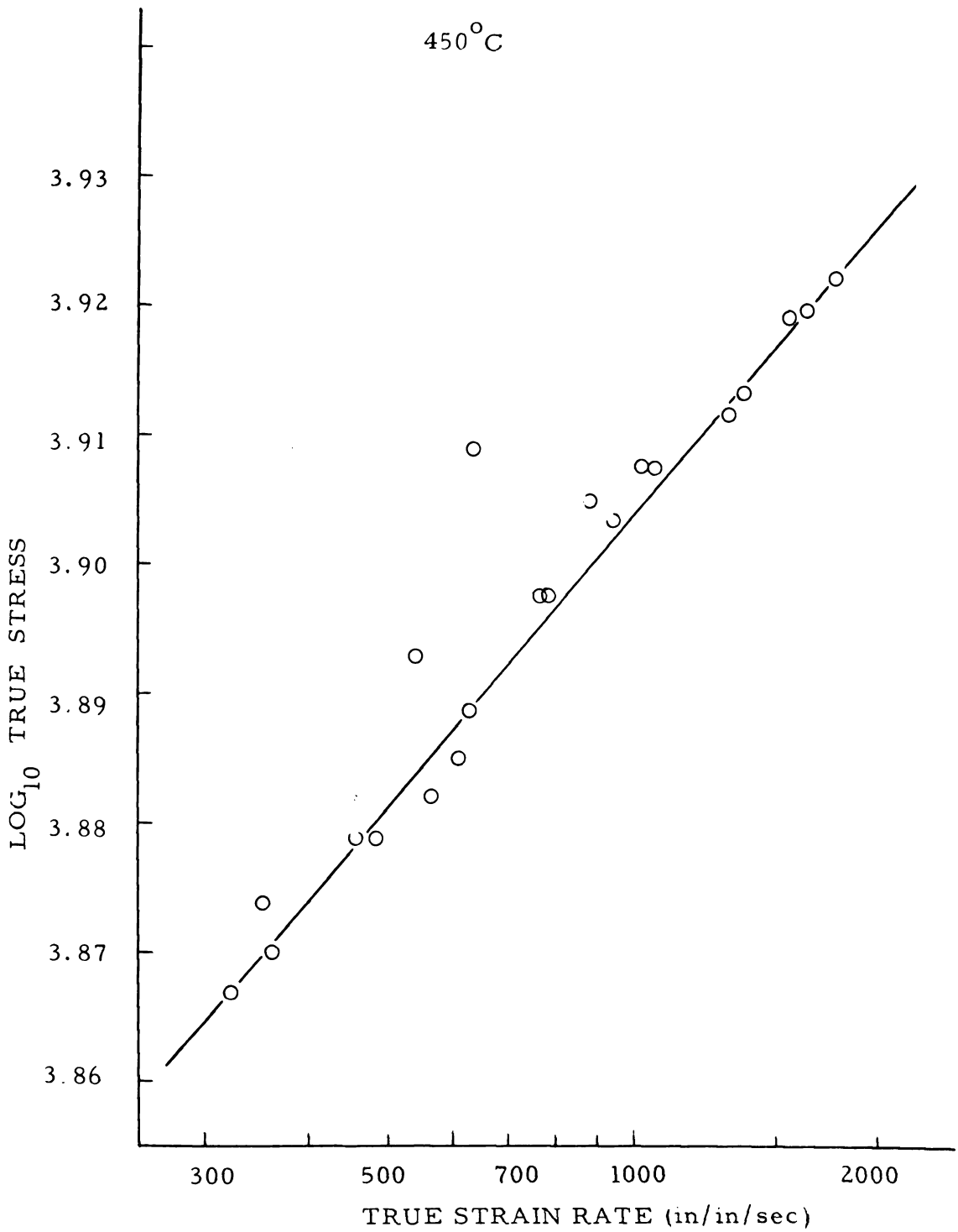

Figure 36. Log Stress Versus Log Strain Rate at 5 Percent True Strain

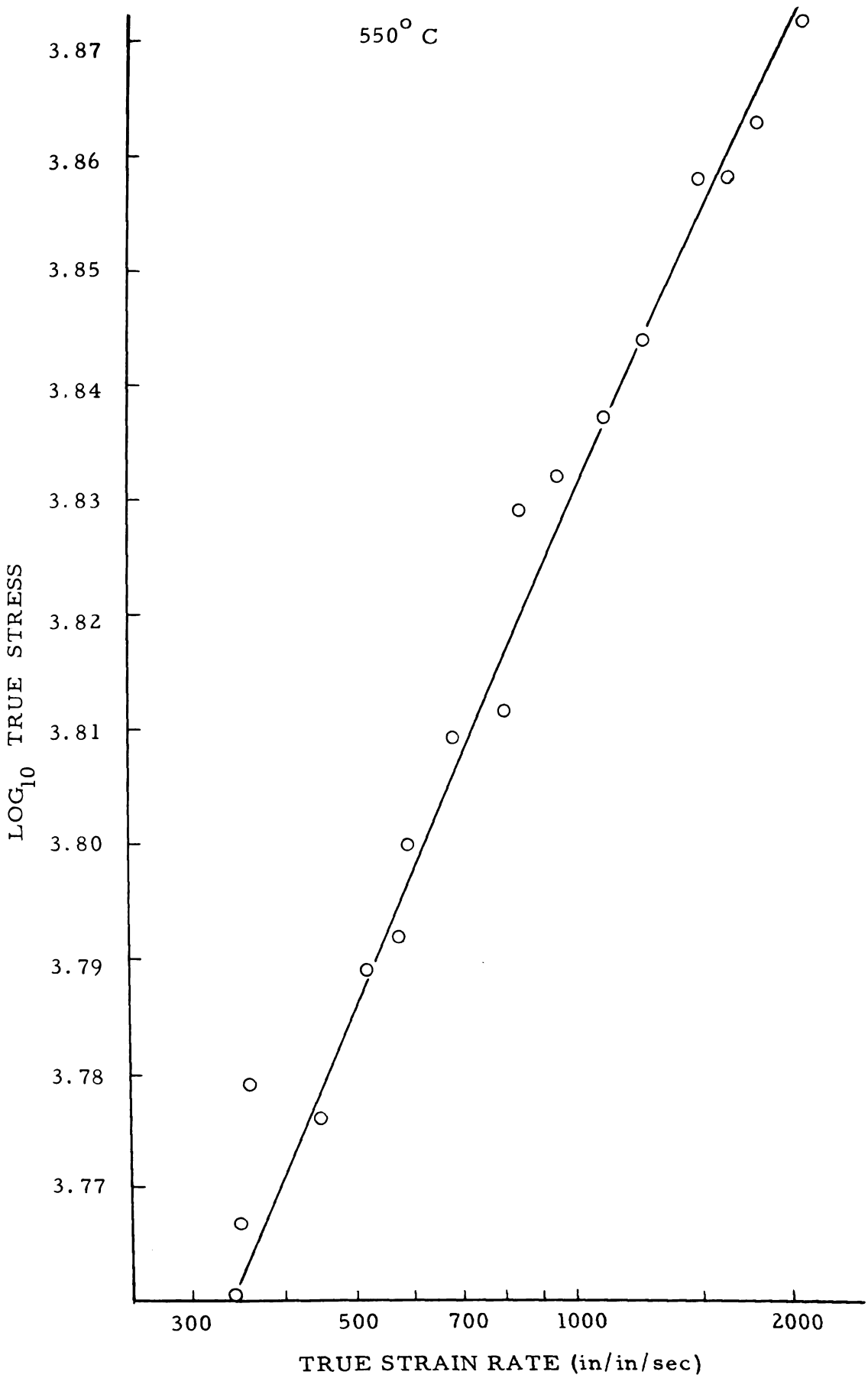

Figure 37. Log Stress Versus Log Strain Rate at 5 Percent True Strain

per inch strain was taken from the plotted stress-strain curve of the specimen. It is seen in Figure 24 that this level of strain makes use of the widest range of strain rates since the lower strain rate curves only extend to approximately 5 percent strain. The difference in the lengths of the stress-strain curves is due to the fact that the duration of the loading pulse is the same for all tests.

Most of the scatter in the data is probably due to variations in the material and the lubrication of the specimen faces, though some of the scatter is of course due to the limitations of the strain measuring equipment and to errors in the measurements taken. The accuracy improved considerably with an increase in temperature, but some improvement was to be expected here since the same percentage error at the lower stresses gives a smaller deviation. There are a few points at the higher temperatures which lie quite far from the curves. This is believed to be due to material and lubrication effects. The specimens were selected in a random fashion in order that the influence of any gradual change in material along the bar would not be systematic.

There is very little difference between the semilogarithmic and the log-log curves. This is probably due to the comparatively small range of strain rates obtained. However, when stress-strain rate curves are plotted on these two coordinate systems for a true strain 0.1054 inches per inch and compared with the results of Alder and Phillips (1954) at the same level of strain, the log-log plot is seen to be more linear. These semilogarithmic and log-log curves are shown in Figures 38 and 39 respectively. Alder and Phillips' data was obtained from compression tests at lower strain rates in which the specimens were machined from extruded aluminum bars and annealed at 400^{o}C for one hour in vacuum.

18

16

14

12

10

8

6

4

2

TRUE STRESS (KSI)

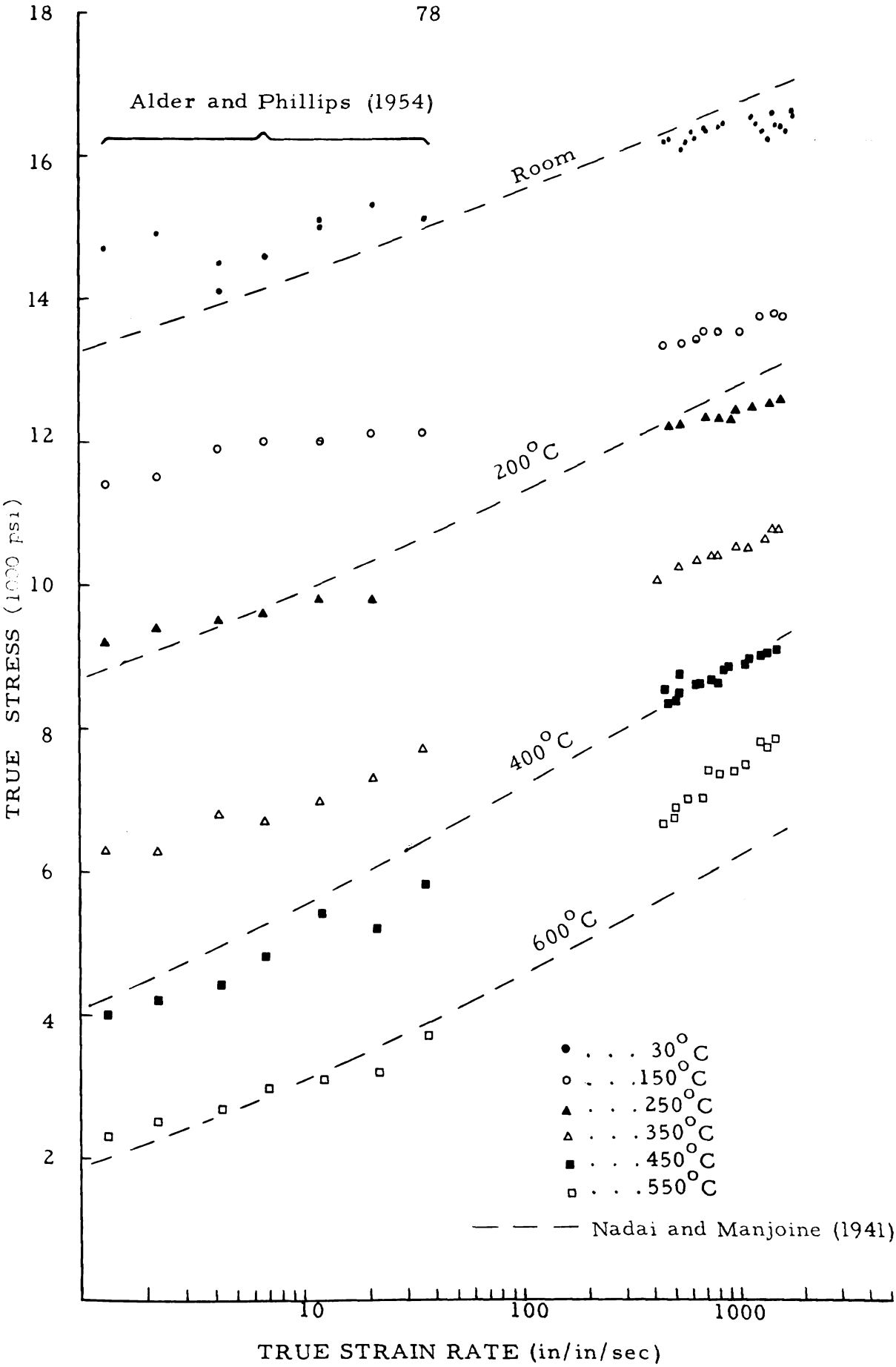

Figure 38. Stress Versus Log Strain Rate at 10.54 Percent True Strain

Fig

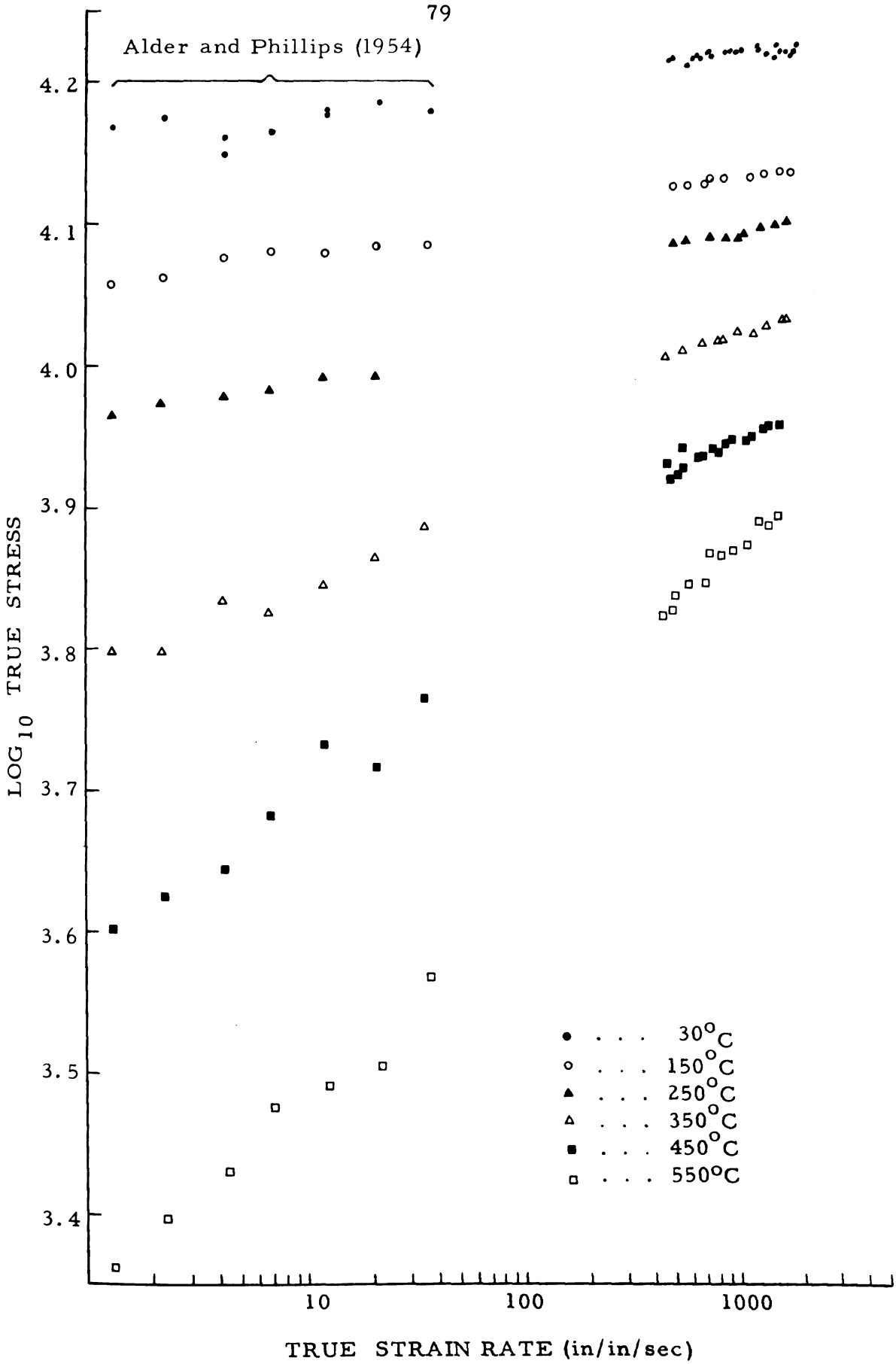

Figure 39. Log Stress Versus Log Strain Rate at 10.54 Percent True Strain

Figure 39 shows that the slopes of Alder and Phillips' data compare well with the present data on a log-log plot, but the magnitudes of stress in their data are lower at nearly every temperature. There are several possible explanations for the differences in stress. First, there may be errors in the measurements from either or both experiments. Second, the stresses in the present experiment may be higher due to specimen lubrication problems. Third, the materials used in the two experiments did not have the same chemical composition. Fourth, it may be that the curves are actually shaped this way. It is likely that the difference in the materials and lubrication effects are to blame for most of the discrepancy. The material used by Alder and Phillips was probably more pure than that used here. It was 99.21 percent aluminum compared to as low as 99.00 percent in the material used here.

The effect of alloying elements on the stresses in aluminum was studied experimentally by Dorn, Pietrokowsky and Tietz (1950). The results of quasi-static tests up to 30 percent true strain at room temperature show for instance, that increasing the copper content of nearly pure aluminum from a level of 0.065 percent to 0.120 percent increases the stresses of the stress-strain curve by approximately 8 percent. Nearly all of Alder and Phillips' specimens contained 0.10 percent copper while the specimens used in the present experiment had a possible maximum of 0.20 percent. The difference between Alder and Phillips' results and the present results at room temperature is approximately 4 percent.

Dorn, Pietrokowsky and Tietz also showed that grain size has a considerable effect on the stress, but this effect is believed to cause a negligible difference in the results since the annealing of the specimens in the present experiment was carried out under nearly

the same conditions as those in Alder and Phillips' experiment.

The interface friction that occurs in the plastic compression of cylindrical specimens was studied by van Rooyen and Backofen (1960). They used primarily Number 1100F aluminum, and the lubricants tested included molybdenum disulfide, the lubricant used for four temperature runs in the present study. The interface shear stress that occurred over the face of their 2 inch diameter by 0.5 inch long specimen using molybdenum disulfide averaged about 10 percent of the normal stress when the specimen was compressed to 10 percent reduction. If this value for interface shear stress is used, an approximate calculation for 10 percent reduction in the present experiment shows that about 4 percent of the energy of compression would be used to overcome interface friction.

The results of tensile impact tests performed on aluminum by Nadai and Manjoine (1941) are shown in the form of dotted lines in Figure 38. Although these curves are not strictly comparable since they represent ultimate stresses for which no correction is made for reduction in area, the slopes of the curves are quite similar to those of the compression test data shown. Since the strain at which ultimate stress is reached may vary with the strain rate, the stress values are not at a constant strain as in the present tests. It is also difficult to determine actual strain rate in the relatively long specimens used in tension. Nadai and Manjoine used an average rate for which it is necessary to assume a uniform strain distribution in the specimen.

Since there is little difference in the linearity between the semi-logarithmic and the log-log plots of the data from the present study, both the logarithmic and the power law will be used to represent the data. These laws as given previously by Equations (1.7) and (1.9) are given here in the slightly different forms

$$\sigma = \sigma_o (\epsilon, T) + k(\epsilon, T) \log \dot{\epsilon} \qquad (4.1)$$

and

$$\sigma = \sigma_o'(\epsilon, T)\dot{\epsilon}^{n(\epsilon, T)} \tag{4.2}$$

where σ_o, σ_o', k and n are shown as functions of strain and temperature and not a function of the material since the data is for aluminum only. In these equations σ_o and σ_o' are stresses at unit strain rate, k represents the slope of a semi-logarithmic plot of stress versus strain rate at a particular level of strain and temperature, and n is the slope of a log-log plot of σ/σ_o versus strain rate at particular values of strain and temperature. If Equation (4.1) is divided by σ_o we have

$$\frac{\sigma}{\sigma_o} = 1 + \frac{k}{\sigma_o} \log \dot{\epsilon} \tag{4.3}$$

where k/σ_o represents the slope of a plot of σ/σ_o versus the logarithm of strain rate. This shows that k/σ_o is a measure of the rate sensitivity of the material. The exponent n is also a rate sensitivity parameter as may be seen more readily if Equation (4.2) is written in the form

$$\log \frac{\sigma}{\sigma_o'} = n \log \dot{\epsilon} \tag{4.4}$$

No significant change in the slope of the stress-strain rate curves was observed between strain levels of 0.05 inches per inch and 0.1054 inches per inch, and the stress-strain curves obtained at low strain rates did not extend far enough to obtain reliable stress-strain rate data for strains higher than about 10 percent. Therefore, the dependence of k and n on level of strain was not determined. The change in k and n with temperature was determined at 5 percent strain from the curves shown in Figures 26-37. The values of k and n at the various test temperatures are given in Table 1. The values of σ_o and σ_o' which were obtained by extrapolating back to the unit strain rate abscissa are also given. The values of σ_o are lower than

TABLE 1. Values of k, σ_o, k/σ_o n and σ_o' in the Logarithmic and Power Laws at 5 Percent Strain

Temp. °C	k(psi)	σ_o(psi)	$\frac{k}{\sigma_o}$	n	σ_o'(psi)
30	413	12,600	0.034	0.017	12,140
150	498	9,910	0.050	0.022	10,020
250	795	8,290	0.096	0.028	8,550
350	1110	5,990	0.185	0.040	6,520
450	1310	4,070	0.322	0.073	4,820
550	2100	130		0.141	2,510

TABLE 2. Values of n Obtained by Alder and Phillips (strains are nominal).

Temp. °C	Values of n for a strain of:				
	10%	20%	30%	40%	50%
18	0.013	0.018	0.018	0.018	0.020
150	0.022	0.022	0.021	0.024	0.026
250	0.026	0.031	0.035	0.041	0.041
350	0.055	0.061	0.073	0.084	0.088
450	0.100	0.098	0.100	0.116	0.130
550	0.130	0.130	0.141	0.156	0.155

those of σ_o' and the magnitude of the difference increases with temperature. The value of σ_o at 550°C is no doubt too small to be an actual stress value at this strain rate and temperature. Therefore, this value was not used to calculate a value for the rate sensitivity coefficient k/σ_o. This shows that the power law gives a better overall fit to the data.

Lindholm found that k for aluminum at room temperature varied from 367 psi. at 0.03 inches per inch strain to 661 psi. at 0.24 inches per inch strain and k/σ_o varied only slightly over this range of strains. These were much smaller variations than either the lead or copper showed. Alder and Phillips also found that the variation of the strain rate effect exponent n with level of strain was comparatively small in aluminum at room temperature but the variation with strain increased markedly with temperature. This is seen in Table 2 where the values of n as determined by Alder and Phillips are given for comparison with the present data.

The values of k/σ_o and n from Table 1 are plotted versus temperature in Figures 40 and 41. These curves cannot be represented with accuracy by either a logarithmic or a power function.

4.6 Stress-Temperature Curves

Stress versus temperature plots at true strains of 0.05 and 0.1054 inches per inch and at several strain rates are given in Figures 42 and 43. These figures show that the data may be represented to a fair approximation by straight-line plots, although the points for 150°C consistently fall below the lines while those for 250° are consistently above it. It is possible that the actual specimen stresses are those given by the data, although there are several other possible explanations for the apparent deviations of the given stress values. For instance, the effectiveness of the molybdenum disulfide

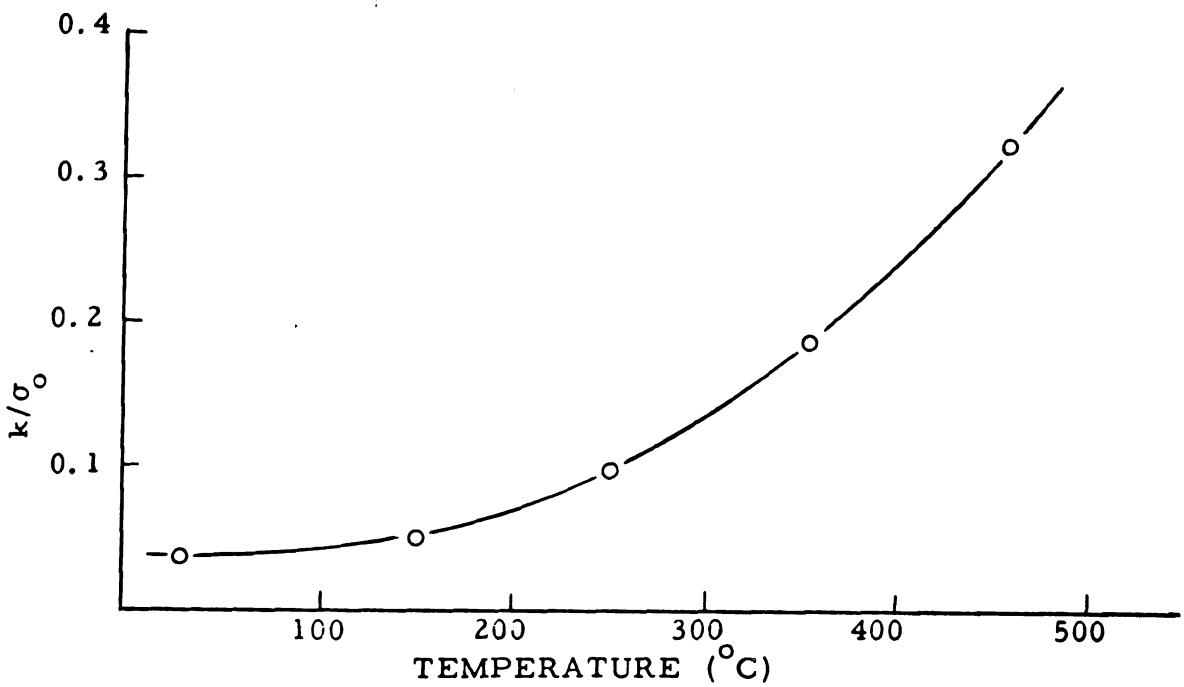

Figure 40. Dependence of Strain Rate Effect Coefficient k/σ_o on Temperature at 5 Percent True Strain

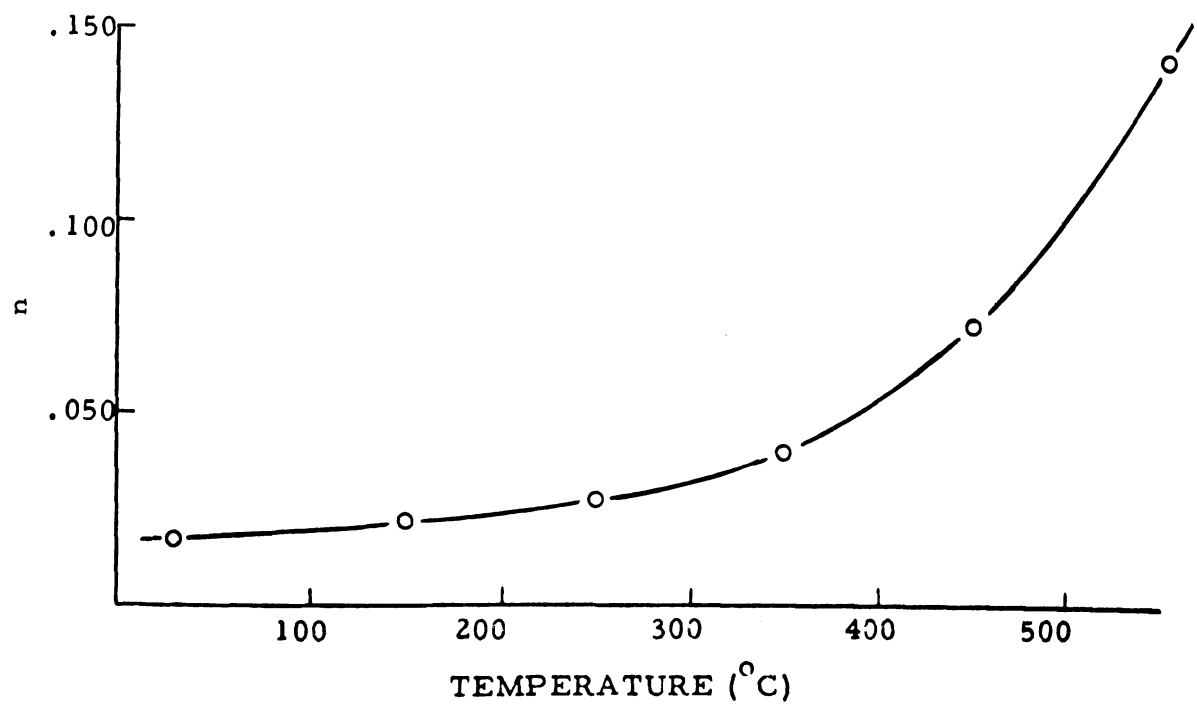

Figure 41. Dependence of Strain Rate Effect Exponent n on Temperature at 5 Percent Strain

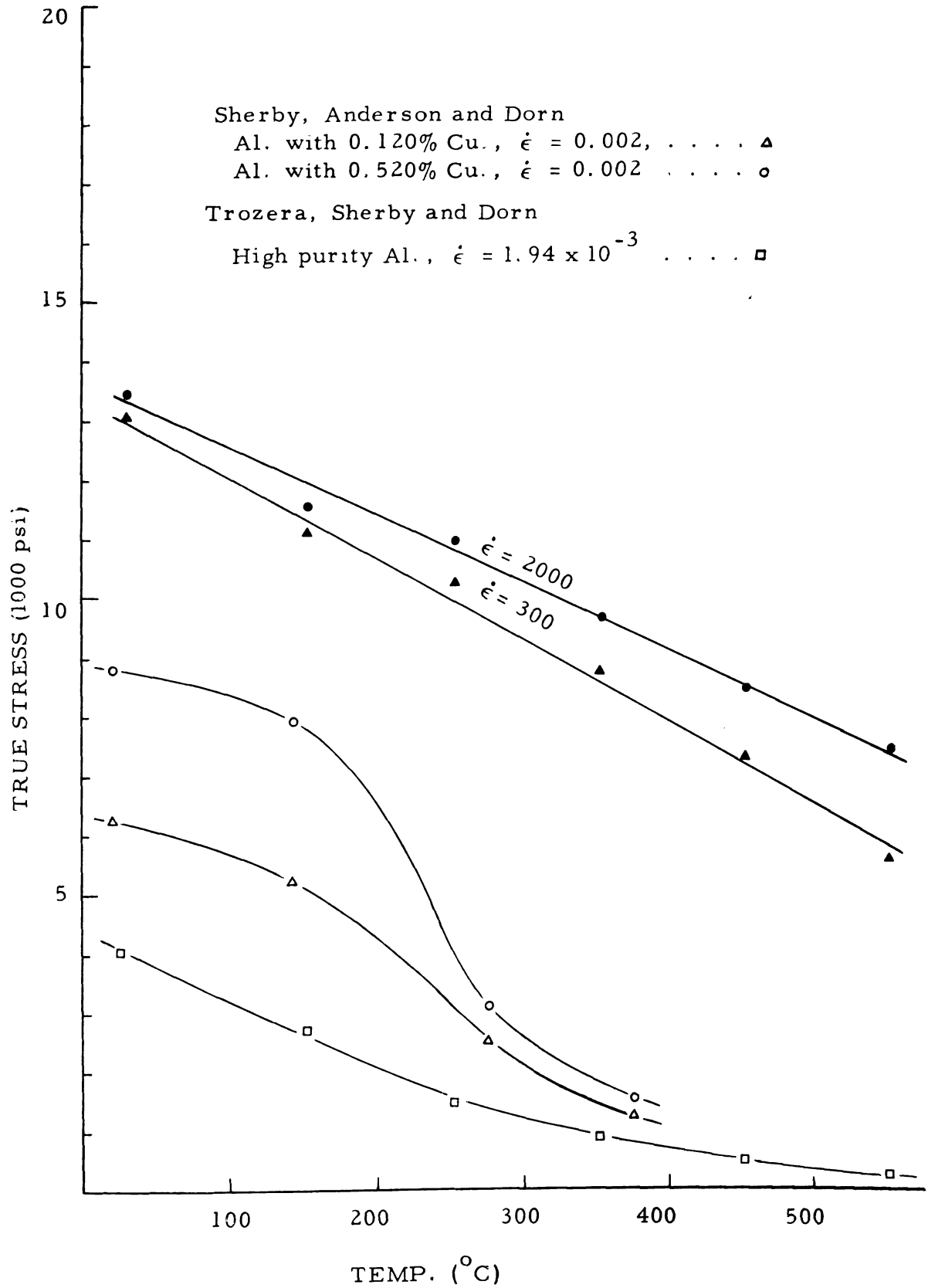

Figure 42. Stress Versus Temperature at 0.05 Inches Per Inch True Strain

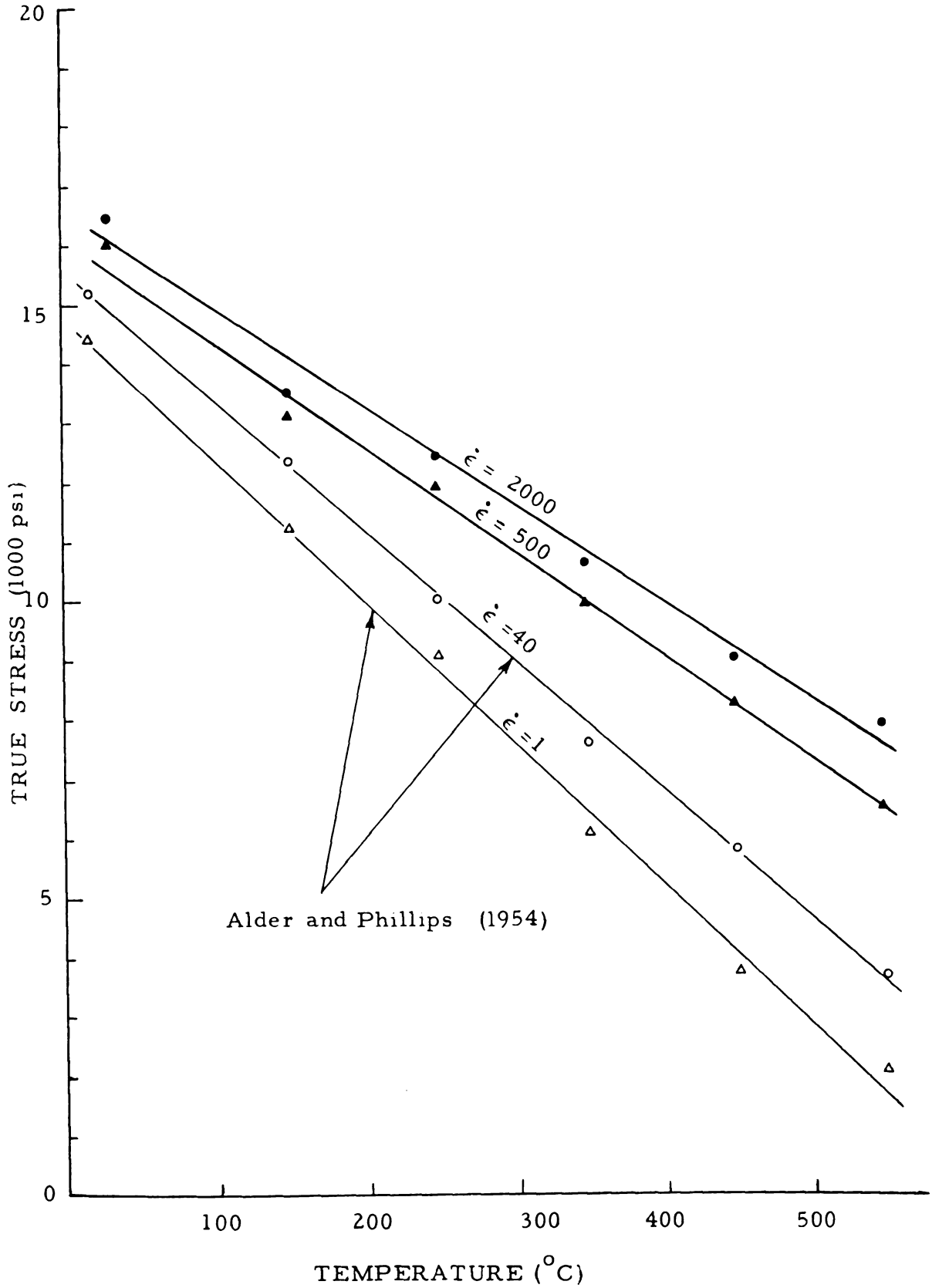

Figure 43. Stress Versus Temperature at 0.1054 Inches Per Inch True Strain

lubricant no doubt changed with temperature. The powdered graphite may have caused the apparently high measured stresses that occurred at 250°C. Also, the viscosity of the glass lubricant used at 550°C may have caused an apparent increase in stress with an increase in strain rate. This would also influence the values of k and n given in the previous section.

Sherby, Anderson and Dorn (1951) have shown that alloying elements and the amounts of them present in aluminum also have a considerable effect on the shape of the stress-temperature curve. Two curves from the data of Sherby, Anderson and Dorn which are for aluminum with different amounts of copper are shown in Figure 42. A third curve for high purity aluminum which was taken from Trozera, Sherby and Dorn (1957) is also shown in Figure 42. Trozera, Sherby and Dorn obtained stress-strain curves from tensile tests on high purity aluminum at temperatures from - 195 to 545°C and at strain rates from 9.63×10^{-7} to 0.167 inches per inch per second.

It is also possible that the apparent deviations in the stress values were caused by a change in the measuring equipment between temperature runs. There was approximately one week between temperatures runs.

The data from Alder and Phillips as shown in Figure 43 are represented quite well by straight lines. The points for these curves were obtained from straight lines drawn through stress-strain rate points plotted from their tabulated data.

Stress versus temperature curves for several levels of strain at a strain rate of 2000 per second are given in Figure 44.

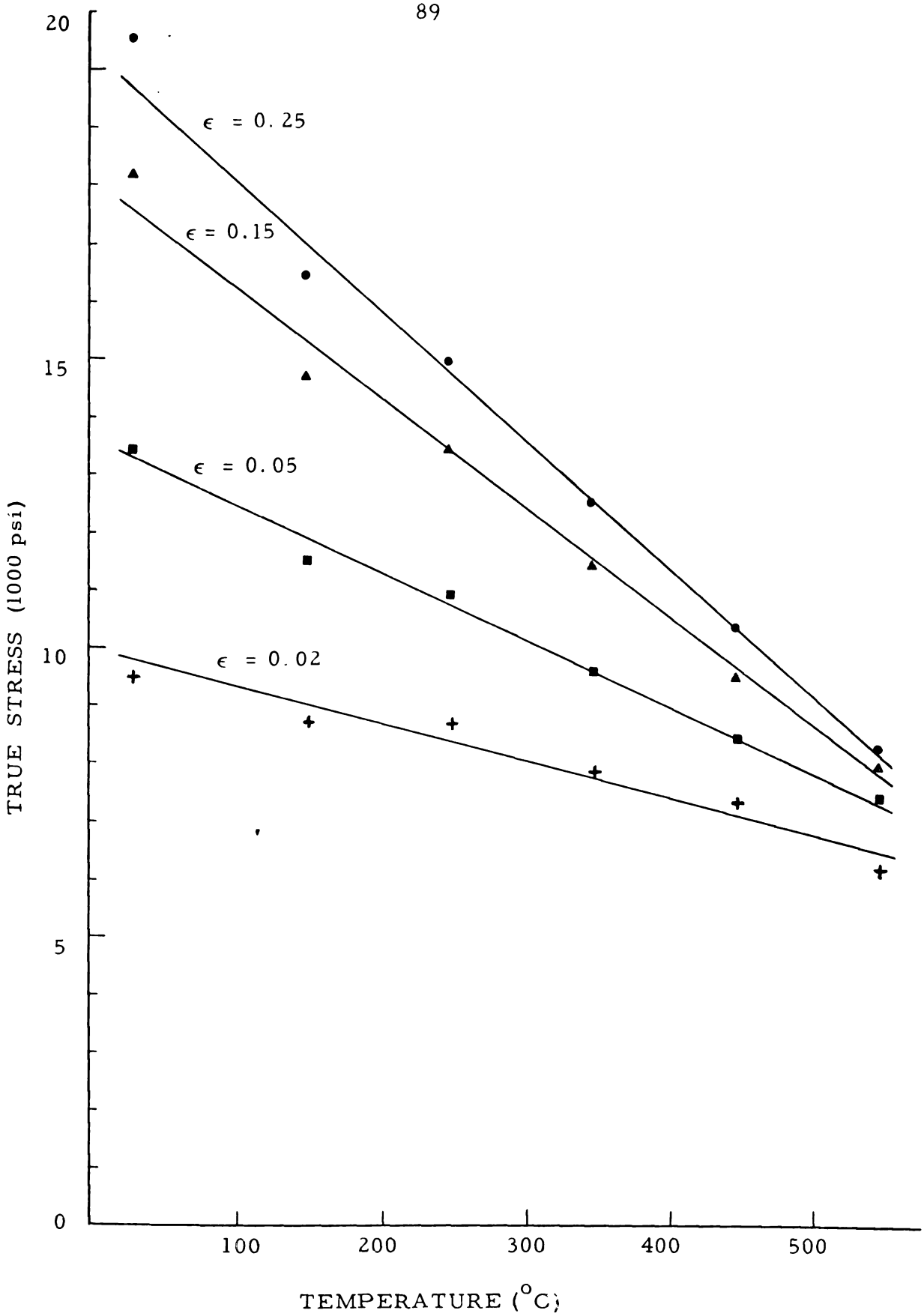

Figure 44. Stress Versus Temperature at a Strain Rate of 2000 Inches Per Inch Per Second

CHAPTER V

SUMMARY AND CONCLUSIONS

An experiment was performed in which short cylindrical specimens (1/2 inch in diameter by 1/4 inch long) of commercially pure aluminum were subjected to impact loads at room temperature and at elevated temperatures by means of a split Hopkinson pressure bar apparatus in which resistance strain gages were mounted on the pressure bars to obtain records of the impact pulses. An electric resistance type furnace surrounded the area of the specimen. Nearly constant strain rates, over the entire range of plastic strains reached in the experiment, were obtained for a range of rates from 300 to 2000 inches per inch per second. True strains of approximately 5 percent were obtained at the lower strain rates and strains of over 25 percent were attained at the highest strain rates. Six test temperatures from 30 to 550°C were used. True stress-strain curves were plotted for each of the 108 specimens and points were taken from these curves to plot true stress-true strain rate and true stress-temperature curves at strain levels of 0.05 and 0.1054 inches per inch. The accuracy of the stress-strain curves for strains below 0.5 percent was not sufficient for determining Young's modulus.

The stress-strain rate curves could be represented quite well with either the logarithmic law

$$\sigma = \sigma_o + k \log \dot{\epsilon} \tag{5.1}$$

or the power law

$$\sigma = \sigma_o' \dot{\epsilon}^n \tag{5.2}$$

where σ_o, σ_o', k and n are functions of strain and temperature. The ratio k/σ_o and the exponent n are the slopes of the linear

semi-logarithmic and the log-log plots of σ/σ_o and σ/σ_o' versus strain rate, and are therefore measures of the rate sensitivity of the material. The rate sensitivity was found to increase with temperature but stress-strain rate curves were not obtained over a sufficiently large range of strains to determine the dependency of rate sensitivity on the level of strain. Values of k, k/σ_o and n were tabulated for all test temperatures at a level of 5 percent strain.

When the results were correlated with the data of Alder and Phillips obtained from compression tests at lower strain rates, the power law was found to give a better fit to the plotted points.

Further studies are suggested along several lines: (a) increase the range of constant strain rates to cover both lower and higher rates, (b) perform impact tests at very low temperatures as well as elevated temperatures over a wide range of strain rates, (c) perform tests with a high purity aluminum in order to minimize the stress increasing effects of alloys, (d) find lubricants which have similar properties at various test temperatures and (e) obtain accurate stress-strain curves over the range of strains which includes the elastic region and extends well into the plastic region for all temperatures and strain rates.

BIBLIOGRAPHY

1. Alder, J.F. and Phillips, V.A., "The Effect of Strain Rate and Temperature on the Resistance of Aluminum, Copper and Steel to Compression," J. Inst. of Metals, vol. 83, 1954-55, p. 80.

2. Alter, B.E.K., and Curtis, C.W., "Effect of Strain Rate on the Propagation of a Plastic Strain Pulse Along a Lead Bar," J. Appl. Phys., vol. 27, 1956, pp. 1079-1085.

3. Austin, A.L., and Steidel, Jr., R.F., "A Method for Determining the Tensile Properties of Metals at High Rates of Strain," Proc. Soc. Exp. Stress Anal., vol. 17, no. 1, 1959, pp. 99-114.

4. Becker, R., "Uber Plastizitat, Verfestigung and Rekristallisation," Zeitschrift fur technische Physik, vol. 7, 1926, pp. 547-555.

5. Bell, J.F., "Propagation of Large Amplitude Waves in Annealed Aluminum," J. Appl. Phys., vol. 31, no. 2, 1960, pp. 277-282.

6. Bell, J.F., "Propagation of Plastic Waves in Solids," J. Appl. Phys., vol. 30, no. 2, 1959, pp. 196-201.

7. Brosius, G.F. and Hartley, D., "Evaluation of High Temperature Strain Gages," Proc. Soc. Exper. Stress Anal., vol 17, no. 1, 1959, pp. 67-84.

8. Campbell, W.R., "The Determination of Dynamic Stress-Strain Curves from Strain Waves in Long Bars," Proc. Soc. Exp. Stress. Anal., vol. 10, no. 1, 1952, p. 113.

9. Chree, C., "The Equations of an Isotropic Elastic Solid in Polar and Cylindrical Coordinates, their Solution and Application," Trans. Camb. Phil. Soc., vol. 14, 1889, p. 250.

10. Clark, D.S. and Duwez, P.W., "Discussion of the Forces Acting in Tension Impact Tests of Materials," J. Appl. Mech., vol. 15, 1948, pp. 243-247.

11. Clark, D.S. and Duwez, P.E., "The Influence of Strain Rate on Some Tensile Properties of Steel," Proc. Am. Soc. Test. Mat., vol. 50, no. 3, 1950, pp. 560-576.

12. Cottrell, A.H., Dislocations and Plastic Flow in Crystals, Clarendon Press, Oxford, 1953, pp. 99-215.

13. Cunningham, D.M. and Goldsmith, W., "Short-Time Impulses Produced by Longitudinal Impact," Proc. Soc. Exp. Stress Anal., vol. 16, no. 2, 1958, pp. 153-162.

14. Curtis, C.W., "Propagation of an Elastic Strain Pulse in a Semi-Infinite Bar," International Symposium on Stress Wave Propagation in Materials, edited by Norman Davids, Interscience Publishers, Inc., New York, 1960, pp. 15-43.

15. Davies, R.M., "A Critical Study of the Hopkinson Pressure Bar," Phil. Trans. Roy. Soc. Lond., Ser. A, vol. 240, 1948, pp. 375-457.

16. Deutler, H., "Experimentelle Untersuchen uber die Abhangigkeit der Zugspannungen von Verformungsgeschwindigkeit," Physikalische Zeitschrift, vol. 33, 1932, pp. 247-259.

17. Donnell, L. H., "Longitudinal Wave Transmission and Impact," Trans. Am. Soc. Mech. Engrs., vol. 52, 1930, pp. 153-167.

18. Dorn, J.E., Pietrokowsky, P. and Tietz, T.E., "The Effect of Alloying Elements on the Plastic Properties of Aluminum Alloys," Trans. Am. Inst. Mining Met. Engrs., vol. 188, 1950, pp. 933-943.

19. Duwez, P.E. and Clark, D.S., "An Experimental Study of the Propagation of Plastic Deformation under Conditions of Longitudinal Impact," Proc. Am. Soc. Test. Mat., vol. 47, 1947, pp. 502-532.

20. Eyring, H., " Viscosity, Plasticity, and Diffusion as Examples of Absolute Reaction Rates," J. Chemical Physics, vol. 4, 1936, pp. 283-291.

21. Flynn, P.D. and Frocht, M.M., "On Saint Venant's Principle Under Dynamic Conditions," J. Experimental Mechanics,

published by Soc. Exp. Stress Anal., Phila., Pa., Jan., 1961, pp. 16-20.

22. Freudenthal, A.M., The Inelastic Behavior of Engineering Materials and Structures, John Wiley and Sons, Inc., New York, 1950, pp. 135-140.

23. Garofalo, F., "Survey of Various Special Tests Used to Determine Elastic, Plastic, and Rupture Properties of Metals at Elevated Temperatures," J. Basic Engineering, published by Am. Soc. Mech. Engrs., Dec., 1960, pp. 867-881.

24. Goldsmith, W., "Impact," Edward Arnold Ltd., London, 1960, p. 338.

25. Guyton, W.L., "Stress-Strain Characteristics of Materials at High Strain Rates, Part VII - Further Studies of Dynamic Compressive Yield Stress," Report issued by Structural Mechanics Research Laboratory, University of Texas, Austin, June, 1961; on research sponsored by Sandia Corp., Albuquerque, N.M.

26. Habib, E.T., "A Method of Making High-Speed Compression Tests on Small Copper Cylinders," J. Appl. Mech., vol. 15, no. 3, 1948, p. 248.

27. Hopkins, H.G., "Dynamic Anelastic Deformations of Metals," Appl. Mech. Reviews, vol. 14, no. 6, June, 1961, pp. 417-431.

28. Hopkinson, B., "A Method of Measuring the Pressure Produced in the Detonation of High Explosives or by the Impact of Bullets," Phil. Trans. Roy. Soc. Lond., Ser. A, vol. 213, 1914, pp. 437-456.

29. Hollomon, J.H. and Jaffe, L.D., Ferrous Metallurgical Design, John Wiley and Sons, Inc., New York, 1947, p. 112.

30. Johnson, J.E., Wood, D.S. and Clark, D.S., "Dynamic Stress-Strain Relations for Annealed 2S Aluminum under Compression Impact," J. Appl. Mech., vol. 20, 1953, p. 523.

31. von Karman, T. and Duwez, P., "The Propagation of Plastic

Deformation in Solids," J. Appl. Phys., vol. 21, 1950, pp. 987-994.

32. Karnes, C.H., "Stress-Strain Characteristics of Materials at High Strain Rates, Part IV - Experimental and Theoretical Analysis of Plastic Impacts on Short Cylinders," Report issued by Structural Mechanics Research Laboratory, University of Texas, Austin, 1960; sponsored by Sandia Corp., Albuquerque, N.M.

33. Kolsky, H., "An Investigation of the Mechanical Properties of Materials at Very High Rates of Loading," Proc. Phys. Soc. Lond. vol. 62B, 1949, pp. 676-700.

34. Krafft, J.M., "Elimination of the Transient Strain Fluctuations which Result from Longitudinal Impact of Bars," Proc. Soc. Exp. Stress Anal., vol. 12, no. 2, 1955, pp. 173-180.

35. Krafft, J.M., Sullivan, A.M. and Tipper, C.F., "The Effect of Static and Dynamic Loading and Temperature on the Yield Stress of Iron and Mild Steel in Compression," Proc. Roy. Soc. Lond., Ser. A, vol. 221, 1954, pp. 114-127.

36. Lee, E.H. and Wolf, H., "Plastic-Wave Propagation Effects in High-Speed Testing," Trans. Am. Soc. Mech. Engrs., vol. 73, 1951, pp. 379-386.

37. Lindholm, U.S., "An Experimental Determination of the Stress-Strain Strain Rate Relations of Several Metals," Thesis, Division of Engineering Research, Michigan State Univ., 1960.

38. Lubahn, J.D., "Derivation of Stress, Strain, Temperature, Strain-Rate Relation for Plastic Deformation," J. Appl. Mech., vol. 14, Trans. Am. Soc. Mech. Engrs., vol. 69, 1947, pp. A229-A230.

39. Ludwik, P., "Uber den Einfluss der Deformationgeschwindigkeit bei Bleibenden Deformationen mit Besonderer Berucksichtigung der Nachwirkungserscheinungen," Physikalische Zeitschrift, vol. 10, 1909, pp. 411-417.

40. MacGregor, G.W. and Fisher, J.C., "A Velocity-Modified Temperature for Plastic Flow of Metals," J. Appl. Mech., vol. 13, Trans. Am. Soc. Mech. Engrs., vol. 68, 1946, pp. A11-A16.

41. Malvern, L.E., "Plastic Wave Propagation in a Bar of Material Exhibiting a Strain Rate Effect," Quart. Appl. Math., vol. 8, 1950, pp. 405-411.

42. Malvern, L.E., "The Propagation of Longitudinal Waves of Plastic Deformation in a Bar of Material Exhibiting a Strain-Rate Effect," J. Appl. Mech., vol. 18, 1951, pp. 203-208.

43. Manjoine, M.J., "Influence of Rate of Strain and Temperature on Yield Stresses of Mild Steel," J. Appl. Mech., vol. 11, no. 4, 1944, pp. A211-A218.

44. Manjoine, M.J. and Nadai, A., "High-Speed Tension Tests at Elevated Temperatures," Proc. Am. Soc. Test. Mat., vol. 40, 1940, pp. 822-839.

45. Mann, H.C., "High Velocity Tension Impact Tests," Proc. Am. Soc. Test. Mat., vol. 36, part II, 1936, p. 85.

46. Nadai, A. and Manjoine. M., "High-Speed Tension Tests at Elevated Temperatures - Parts II and III," Trans. Am. Soc. Mech.Engrs., vol. 63, 1941, pp. A77-A91.

47. Nadai, A. and McVetty, P.G., "Hyperbolic Sine Chart for Estimating Working Stresses of Alloys at Elevated Temperatures," Proc. Am. Soc. Test. Mat., vol. 43, 1943, pp. 735-748.

48. Orowan, E., "Zur Kristallplastizitat," Zeitscrhrift fur Physik, vol. 89, 1934, pp. 605-659.

49. Plass, Jr., H.J., "Current Research on Plastic Wave Propagation at the University of Texas, Part I-A Theory of Longitudinal Plastic Waves in Rods of Strain-Rate Dependent Material, Including Effects of Lateral Inertia and Shear," Plasticity, edited by E.H. Lee and P.S. Symonds, Pergamon Press, New York, 1960, pp. 453-474.

50. Pochhammer, L., "Uber Fortpflanzungsgeschwindigkeiten kleiner Schwingungen in einem unbegrenzten isotropen Kreiszylinder," J. reine angew. Math. (Crelle), vol. 81, 1876, p. 324.

51. Prandtl, L., "Ein Gedankenmodell zur Kinetischen Theorie der Festen Korper," Zeitschrift fur Angewandte Mathematic und Mechanik, vol. 8, 1928, pp. 85-106.

52. Rakhmatulin, K. A., "Propagation of a Wave of Unloading," Prikl. Mat. i Mek., vol. 9, 1945, pp. 91-100, (in Russian). Translation All-T2/15, Brown Univ., (1948).

53. Rayleigh, J.W.S., The Theory of Sound, vol. 2, Dover Publications, New York, 1945, p. 427.

54. Riparbelli, C., "On the Relation Among Stress, Strain and Strain-Rate in Copper Wires Submitted to Longitudinal Impact," Proc. Soc. Exper. Stress Anal., vol. 14, no. 1, 1956, pp. 55-70.

55. Ripperger, E.A., "Current Research on Plastic Wave Propagation at the University of Texas, Part II - Experimental Studies of Plastic Wave Propagation in Bars," Plasticity, edited by E.H. Lee and P.S. Symonds, Pergamon Press, New York, Oxford, London, and Paris, 1960.

56. Ripperger, E.A., "Stress-Strain Characteristics of Materials at High Strain Rates, Part V - Dynamic Compressive Yield Stresses," Report issued by Structural Mechanics Research Laboratory, University of Texas, 1960; on research sponsored by Sandia Corp., Albuquerque, N.M.

57. Rooyen, G.T. van and Backofen, W.A., "A Study of Interface Friction in Plastic Compression," Inter. J. Mech. Sci., vol. 1, no.1, January, 1960, pp. 1-27.

58. Seeger, A., " Theorie der Kristallplastizitat, Part I - Grundzuge der Theorie, Part II - Die Grundstruktur der dichtest gepackten Metalle und ihr Einfluss auf die plastische Verformung, Part III - Die Temperatur - und Geschwindigkeitsabhangigkeit der Kristallplastizitat," Zeit. Naturf., vol. 9, 1954, pp. 758-881.

59. Seeger, A., "The Temperature Dependence of the Critical Shear Stress and of Work-hardening of Metal Crystals," Philosophical Magazine, Ser. 7, vol. 45, 1954, pp. 771-773.

60. Sherby, O. D., Anderson, R.A. and Dorn, J.E., "Effect of Alloying Elements on the Elevated Temperature Plastic Properties of Alpha Solid Solutions of Aluminum," Trans. Am. Inst. Mining and Met. Engrs., vol. 191, pp. 643-652.

61. Sokolov, L.D., "Influence of Velocity on the Resistance of Metals to Deformation," Shurnal Technicheskoi Fiziki, vol. 16, 1946, pp. 437-442 (in Russian).

62. Sokolov, L.D., "The Investigation of the Relationship between Resistance to Plastic Strain of Metals and Amorphous Bodies and the Strain Rate and Temperature of Experiment," Zhurn. Tekhn. Fiziki, vol. 17, 1947, pp. 543-548 (in Russian).

63. Sokolov, L.D., "The Influence of Degree of Deformation on the Dependence of Rate of Strain," Zhurn. Tekhn. Fiziki, vol. 18, 1948, pp. 93-97 (in Russian)

64. Sokolov, L.D., "On the Problem of Calculation of the Resistance of Metals to Plastic Deformation in Connection with Strain and Temperature," Akademiia Nauk S.S.S.R. Doklady, vol. 67, 1949, pp. 459-462 (in Russian).

65. Sokolov, L.D., "A Systematic Study of the Dependence of the Resistance to Deformation on Rate of Deformation and Temperature in Single Phase Metals," Akademiia Nauk S.S.S.R. Doklady, vol. 70, 1950, pp. 839-841 (in Russian).

66. Sternglass, E.J. and Stuart, D.A., "An Experimental Study of the Propagation of Transient Longitudinal Deformations in Elastoplastic Media," J. Appl. Mech., vol. 20, 1953, pp. 427-434.

67. Tapley, B.D., "Stress-Strain Characteristics of Materials at High Strain Rates, Part VI - The Propagation of Plastic Waves in Finite Cylinders of Strain-Rate-Dependent Material," Report issued by Structural Mechanics Research Laboratory, University of Texas, Austin, 1960; on research sponsored by Sandia Corp., Albuquerque, N.M.

68. Taylor, G.I., " The Plastic Wave in a Wire Extended by an Impact Load," The Scientific Papers of Sir Geoffrey Taylor, Cambridge University Press, 1958, pp. 467-479.

69. Trozera, T.A., Sherby, D.D. and Dorn, J.E., "Effect of Strain Rate and Temperature on the Plastic Deformation of High-Purity Aluminum," Trans. Am. Soc. Metals, vol. 49, 1957, pp. 173-188.

70. Vitovec, F.H., "On Dynamic Creep with Special Consideration of Strain Rate Effects," Proc. Am. Soc. Test. Mat., vol. 57, 1957, pp. 977-986.

71. Vosteen, L.F., "The Effect of Temperature on Dynamic Modulus of Elasticity of Some Structural Alloys," NACA Tech. Note 4348, August, 1958.

72. White, M.P. and Griffis, L., "The Propagation of Plasticity in Uniaxial Compression," J. Appl. Mech., vol. 15, 1948, pp. 256-260.

73. Witman, F.F. and Stepanoff, V.A., "Influence of Deformation Speed on Cold Embrittlement of Steel," Zhurnal Tekhnicheskoi Fiziki, vol. 9, 1939, p. 1070. (in Russian)

74. Work, C.E. and Dolan, T.J., "The Influence of Strain Rate and Temperature on the Strength and Ductility of Mild Steel in Torsion," Proc. Am. Soc. Test. Mat., vol. 53, 1953, pp. 611-626.

75. Zener, C. and Holloman, J.H., "Effect of Strain Rate on the Plastic Flow of Steel," J. Appl. Phys., vol. 15, 1944, pp. 22-32.

APPENDIX A
CALCULATION OF WAVE REFLECTIONS DUE TO TEMPERATURE CHANGES

In this appendix the equations giving the amplitude of the transmitted and reflected strain waves when a strain pulse encounters a discontinuous change in Young's modulus will be derived and experimental evidence of the validity of these equations for continuous changes in Young's modulus will be presented. These Equations were given in Chapter II as Equations (2.3) and (2.4).

Consider the fictitious case of a long metallic bar of uniform cross-section in which the temperatures on opposite sides of a particular cross-section are different, say T_1 and T_2. Since the modulus of elasticity is a function of temperature, we have a bar like the one shown in Figure 45 where Young's modulus suddenly changes from E_1 to E_2 where the subscripts correspond to the temperatures in the two sections. If a stress wave approaches the abrupt change from the left as the arrow indicates, part of the wave will be reflected and part of it will be transmitted through the cross-section. From a summation of forces at the cross-section of temperature change we have

$$\sigma_I + \sigma_R = \sigma_T \tag{A.1}$$

where the subscripts I, R and T correspond to the incident, reflected and transmitted pulses respectively. Now if ϵ_I, ϵ_R and ϵ_T represent the strains corresponding to the stresses of Equation (A.1) then using Hooke's law we have

$$E_1(\epsilon_I + \epsilon_R) = E_2 \epsilon_T \tag{A.2}$$

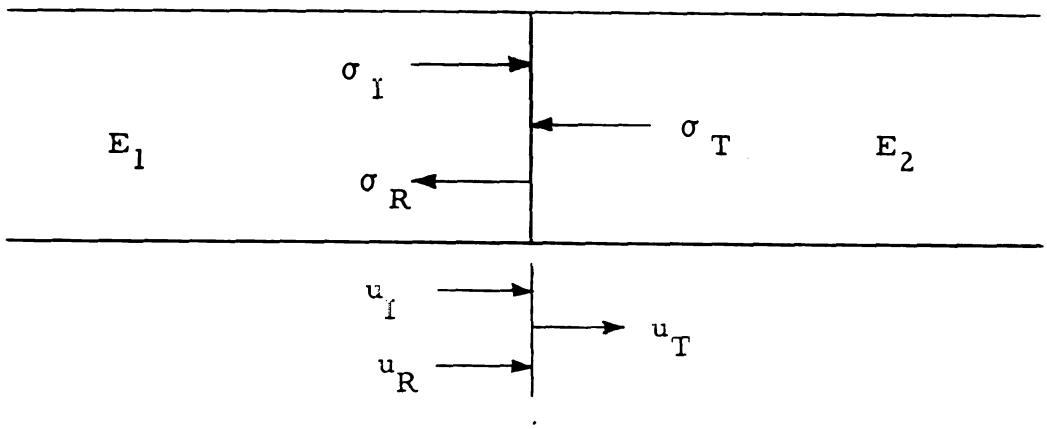

Figure 45. Bar with a Discontinuous Change in E.

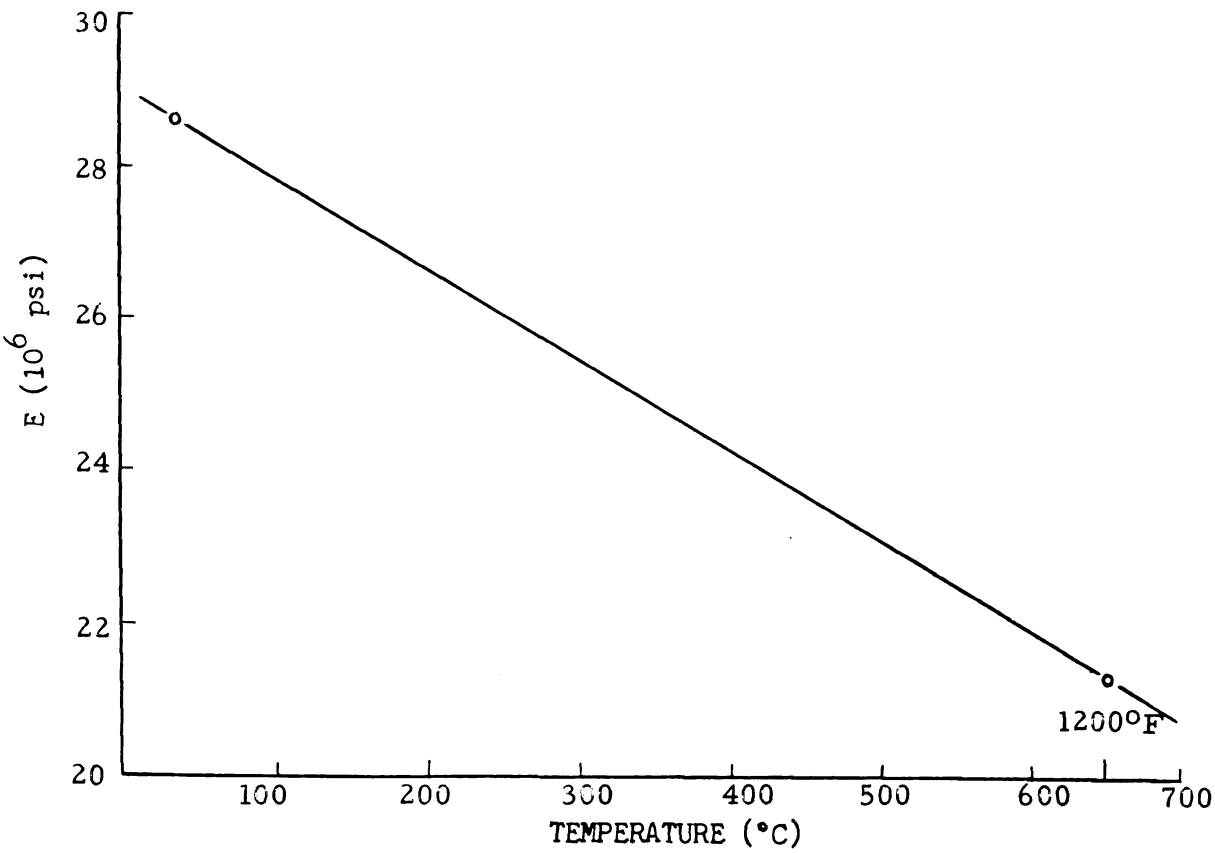

Figure 46. Modulus of Elasticity Versus Temperature for 18-8 Stainless Steel Pressure Bars.

If the bar material remains continuous at the cross-section we must also have

$$u_I + u_R = u_T \tag{A.3}$$

where u_I, u_R and u_T represent the displacements at the cross-section which are due to the incident, reflected and transmitted stress waves respectively. If we take the derivative of both sides of Equation (A.3) with respect to time and substitute from the elastic wave propagation relation

$$\epsilon = \frac{1}{c} \frac{du}{dt} \tag{A.4}$$

we have

$$c_1 (\epsilon_I - \epsilon_R) = c_2 \epsilon_T \tag{A.5}$$

where c_1 and c_2 represent the wave velocities in the first and second sections of the bar respectively and the negative sign represents a negative velocity. It is easily shown by consideration of the temperature coefficient of expansion of steel that the change in density ρ in the bar is insignificant when compared to the change in E so that c_1 may be taken proportional to $\sqrt{E_1}$ and c_2 may be taken proportional to $\sqrt{E_2}$. This is from the elastic wave velocity equation $c = \sqrt{E / \rho}$. Using these proportionalities in Equation (A.5) we have

$$\sqrt{E_1} (\epsilon_I - \epsilon_R) = \sqrt{E_2} \epsilon_T \tag{A.6}$$

From Equations (A.2) and (A.6) we can solve for the ratio of transmitted pulse to incident pulse and the ratio of reflected pulse to incident pulse, that is

$$\frac{\epsilon_T}{\epsilon_I} = \frac{2E_1}{E_2 + \sqrt{E_1 E_2}} \tag{A.7}$$

and

$$\frac{\epsilon_R}{\epsilon_I} = \frac{\sqrt{E_2} - \sqrt{E_1}}{\sqrt{E_2} + \sqrt{E_1}} \tag{A.8}$$

Equations similar to these were derived by Rayleigh (1945) for the determination of transmitted and reflected sinusoidal waves at a point of sudden change in material.

Two separate experiments were performed in order to determine the usefulness of these equations in the present investigation. The first involved the mounting of two high temperature Nichrome V foil strain gages at the center of the furnace on a long pressure bar. A photograph of the gage installation is given in Figure 47. These gages were used to determine the amplitude of a strain pulse after it passed through the temperature distribution on the incident side of the furnace. This amplitude was compared with the amplitude of the incident pulse obtained from a standard incident gage station approximately at room temperature. The high temperature gages had a one-inch gage length and a resistance of 138.4 ± 0.2 ohms at room temperature. The room-temperature gage factor was 2.3 ± 0.1. These gages were mounted with Tatnall H ceramic cement (for use at temperatures up to $1500^{\circ}F$), and the short lead wires were welded to copper wires which were insulated in ceramic tubing.

Typical oscilloscope records of the strain pulse obtained from the high temperature gage station are shown in Figure 48. Figure 48a is at room temperature and Figure 48b is at $1200^{\circ}F$. It is seen that the reflection of the pulse from the transmitter bar side of the temperature distribution is superposed onto the rear portion of the pulse, increasing the amplitude. The strain calculations were based on measurements taken at a point immediately following

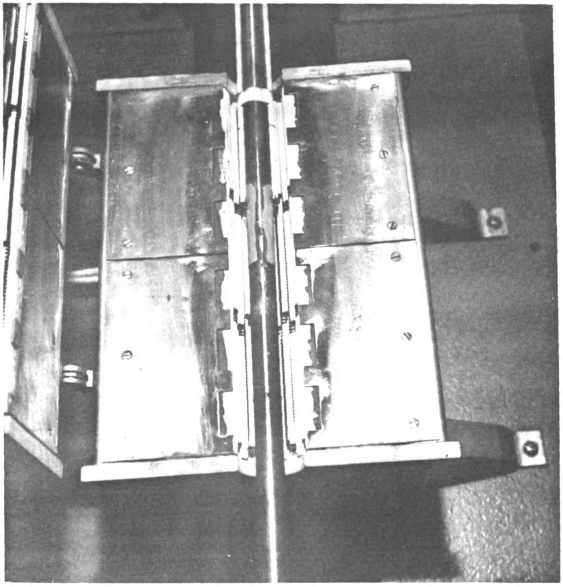

Figure 47. Close-up of High Temperature Gage Installation

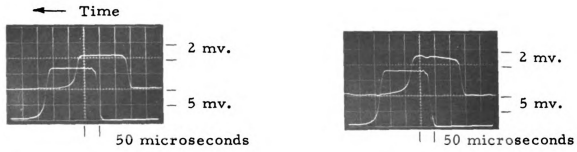

(a) Room Temperature (b) 1200°F

Figure 48. Pulse Records at Center of Furnace in a Long Pressure Bar

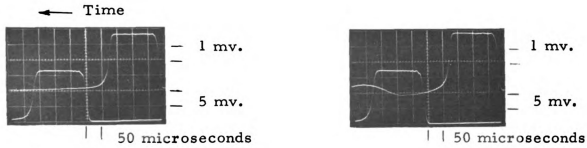

(a) Room Temperature (b) 1200°F

Figure 49. Records used for Measuring Temperatures Reflections in a Long Pressure Bar

the rise portion of the pulse. In order to calculate the strain in the bar from these measurements it was necessary to use a linear variation of gage factor with temperature from the data of Brosius and Hartley (1959) who tested Nichrome V foil gages up to 1100° F. The linear variation was assumed to extend to 1200°F for the present experiment. The variation in gage resistance with temperature was also included in the calculations.

The calculation of transmitted strain amplitude from Equation (A. 7) included values of E taken from the E versus temperature curve given in Figure 46. The slope of the curve in this figure was taken from Garofalo (1960). Pulse records were obtained at 300, 600, 900 and 1200°F and the difference between calculated and experimental values was less than one percent for the temperatures used below 1200°F, and the difference at 1200°F was less than 3 percent.

The second experiment was performed in order to verify Equation (A. 8) and to check a method devised to calculate reflected waves. In this second experiment, the reflected portion of an incident pulse was measured directly from photographs which were obtained from a gage station mounted 28 inches from the center of the furnace and 12 inches from the impact end of the long bar. These photographs are shown in Figure 49. The pulse reflected from the temperature gradients appears immediately after the incident pulse on the upper channel in Figure 49b. The strain gages used at this first gage station were SR-4 Type A-8 wire gages with a nominal resistance of 120. 5 ohms and a gage factor of 1. 81 $\pm$ 2 percent. It should be mentioned here that the small peak which appears just after the rise of the upper channel pulses seems to be a characteristic of the A-8 gages. This peak also appeared in Lindholm's (1960) data, which was obtained with A-8 gages. The temperature at the center of the

furnace for Figure 49b was 1200°F. The reflection pulse was determined from the difference of the upper channel traces shown in Figure 49.

The calculated reflection pulse was obtained by assuming step functions for the temperature distributions on both sides of the furnace and using Equation (A.8) to calculate the increments of reflection at the discontinuous jumps in temperature. The increments were superposed onto one another to obtain the reflected strain pulse shown in Figure 50 as the solid line curve. The incident pulse was assumed to have a trapezoidal shape to make the graphical construction simpler. Time in Figure 50 is measured from the instant the incident pulse reached the gage station and the increments of reflection are shifted to the right by an amount equal to their time of travel from the gage station to their corresponding points of reflection and return. The discontinuous jumps in temperature were spaced according to equal time intervals of wave travel. This meant that the points of reflection had to be spaced closer together at the hot section of the bar since the wave velocity was lower there. This method of determining temperature gradient reflections was used for all elevated temperature tests in the present investigation.

The temperature distribution which was used for the above calculations is shown as the dotted step function in Figure 51. Actual temperature distributions were measured by means of ten thermocouples which were spaced at two inch intervals measuring from the center of the furnace. The regularly used thermocouple located 3/8 inch from the center of the furnace was used to determine the first point on the graph.

The pulses transmitted through the solid bar in the furnace, as shown on the lower traces of the photographs in Figure 49, were

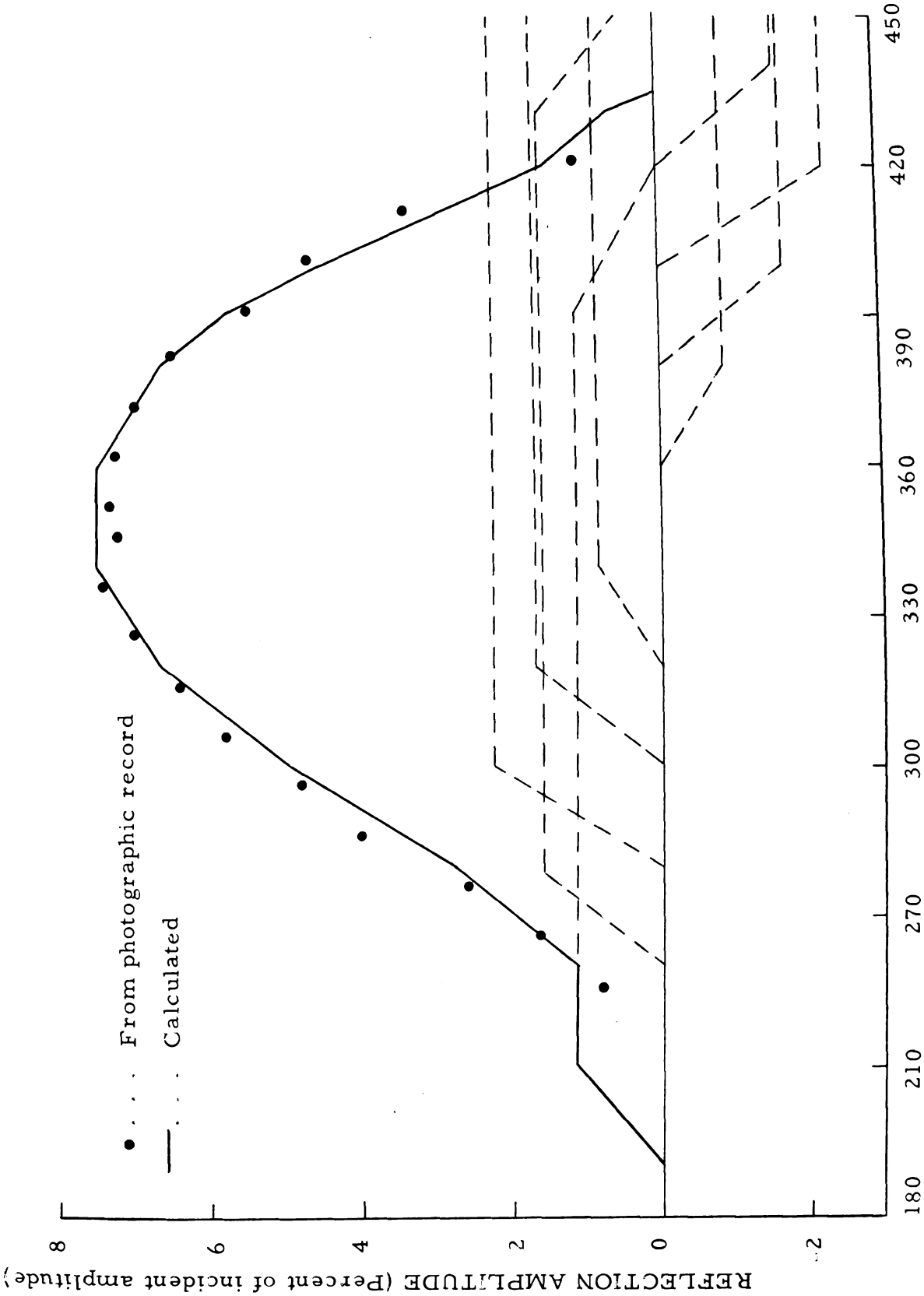

Figure 50. Strain Waves Reflected from a Heated Section of a Stainless Steel Bar. The Maximum Temperature in the Bar was 1200°F

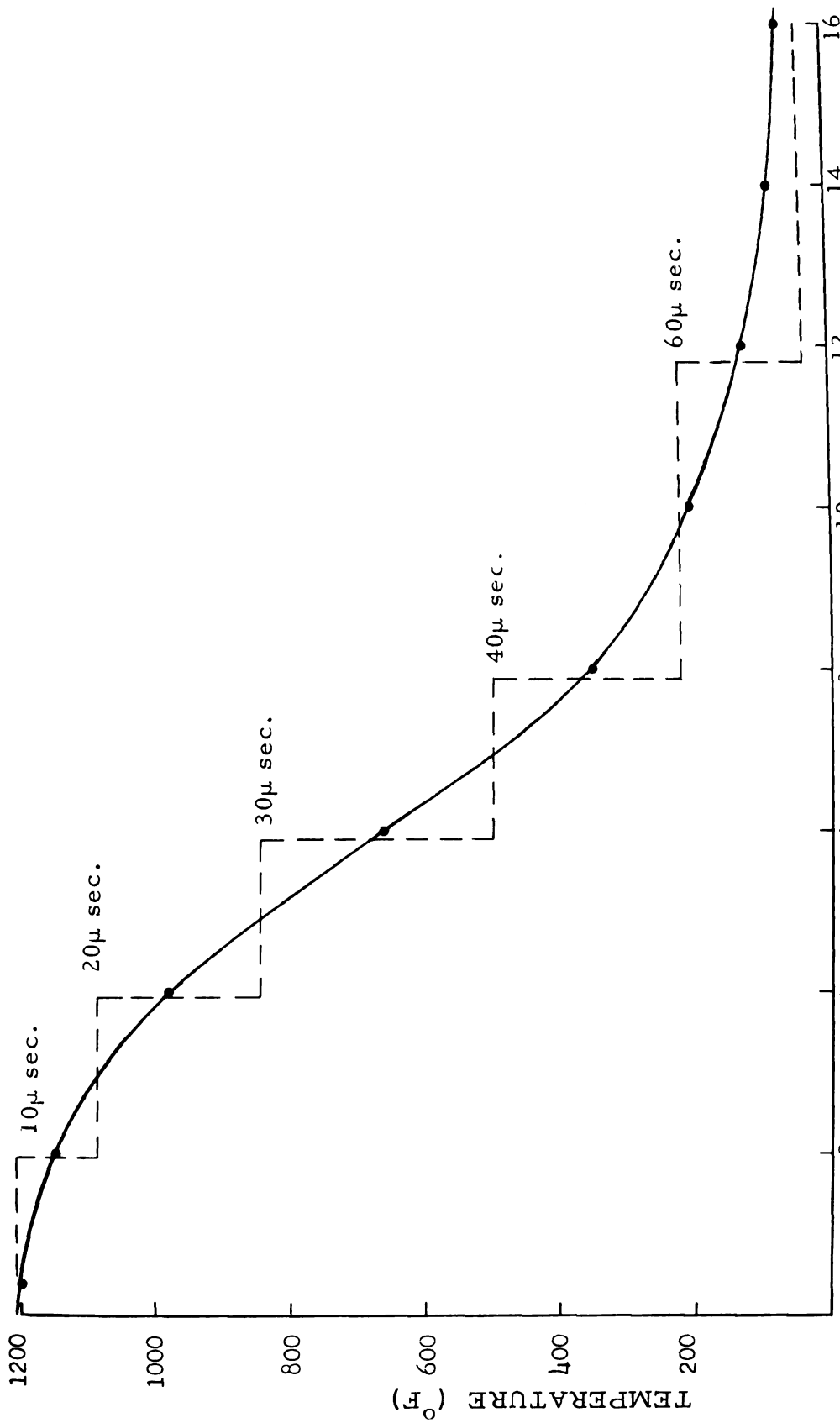

Figure 51. Temperature Distribution in Pressure Bar Measuring from Center of Furnace

obtained from a standard transmitter gage station using foil gages. The transmitted pulse in Figure 49b appears to be unchanged in amplitude and shape after passing through the hot section of the bar. Calculations from Equation (A. 7) predict a decrease in amplitude of 0. 5 percent. A decrease in amplitude of approximately this magnitude was detected by taking measurements.

APPENDIX B
EXPERIMENTAL SUPPORT FOR THE METHOD USED IN CALCULATING SPECIMEN STRAIN

B.1 Verification of the Relation $\epsilon_I - \epsilon_R = \epsilon_T$

The relation $\epsilon_I - \epsilon_R = \epsilon_T$ is obtained from Equation (2.11) when the pressure bars are at room temperature. Equation (2.11) was a necessary part of the derivation of Equation (2.14) used for calculating specimen strains Therefore, an experimental verification of the relation $\epsilon_I - \epsilon_R = \epsilon_T$ will provide support for the intergration method of calculating specimen strains. The accuracy of the assumption that the stress is equal on both sides of the specimen, which is the basis of the above relation, is also important in determining stress in the specimen since the stress measurements are calculated from the transmitter bar strain at the interface with the specimen.

The relation was checked by comparing actual strain records of the incident, reflected and transmitted pulses which were all recorded at the same time for a specimen at room temperature. The oscilloscope record of the three pulses is shown in Figure 52. The pulse reflected from the specimen is the inverted pulse, which follows immediately after the incident pulse on the upper channel. These traces were obtained from the regular transmitter gage station and a station on the incident bar mounted 18 inches from the specimen. A plot of all three pulses on the same time axis is shown in Figure 54. The error between the reflected pulse as measured from the photograph and the pulse obtained by taking the difference of the incident and transmitted pulses is approximately 2 percent. Some of this difference may be due to oscilloscope and photographic distortions.

It is seen that the transmitted pulse is a little longer than

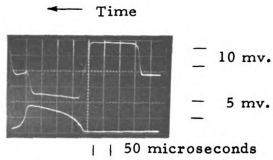

Figure 52. Record of Incident, Reflected and Transmitted Pulses

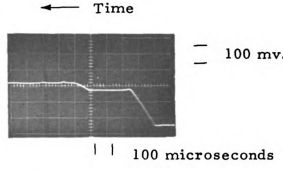

Figure 53. Record from Strain Gage Mounted on Specimen

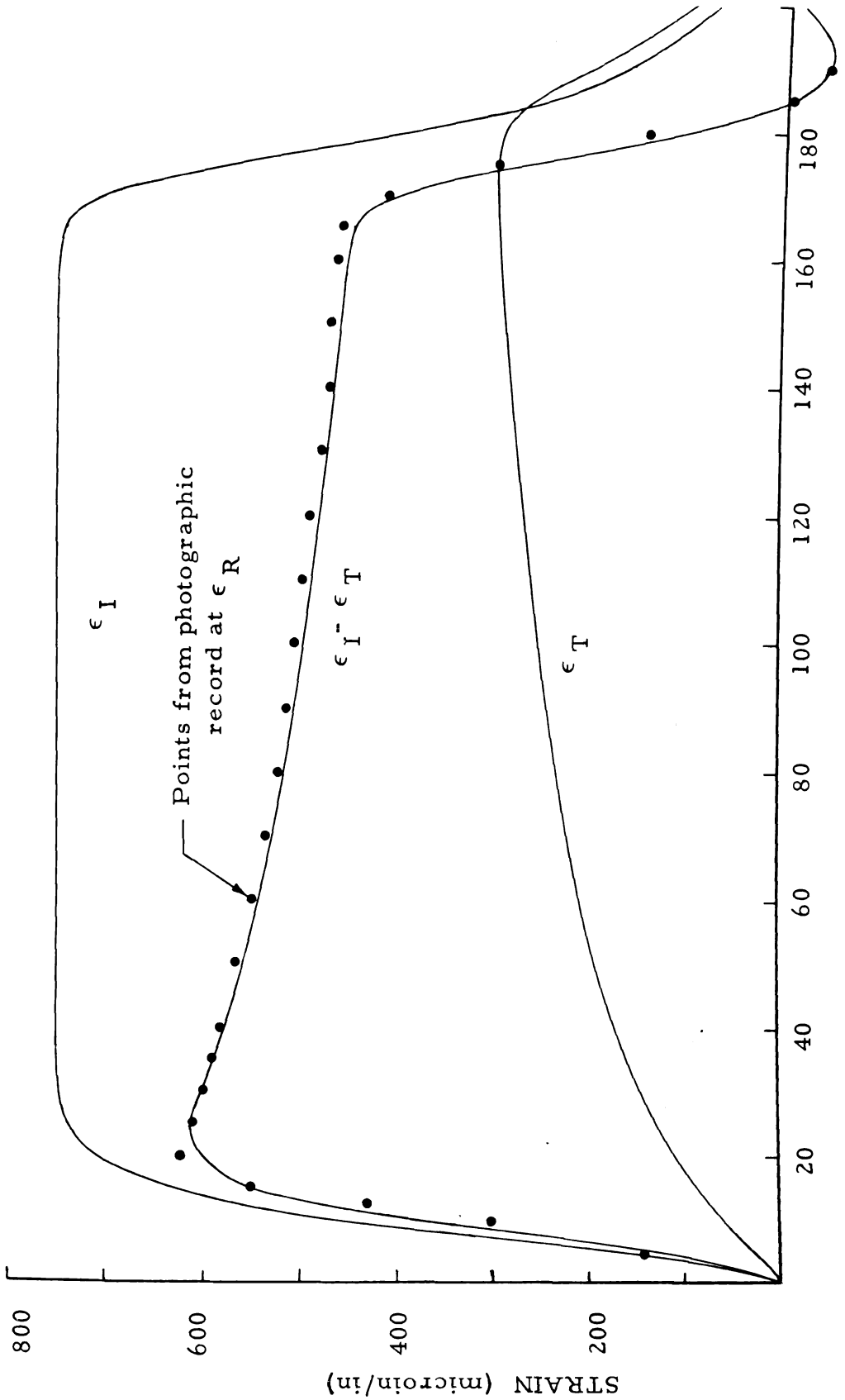

Figure 54. Comparison of $\epsilon_I - \epsilon_R$ and ϵ_T

the incident pulse. This is a result of taking the difference between the incident and reflected pulses. The amplitude of the reflected pulse naturally starts to decrease at the same time that the amplitude of the incident pulse begins to decrease and the difference between the two curves, that is the transmitted pulse, remains approximately the same for an additional 10 microseconds.

The experimental results given in the next section provide additional support for the use of $\epsilon_I - \epsilon_R = \epsilon_T$ in the derivation of specimen strain.

B.2 Comparison of Calculated and Measured Specimen Strains

An experimental verification of the integration method used to calculate specimen strains was carried out by mounting strain gages directly onto several standard specimens. One SR-4 Type FAP-12-12 120 ohm foil gage with a gage length of 1/8 inch was mounted longitudinally on each specimen. A close up of the specimen and gage installation is shown in Figure 55. The gage was connected to one arm of a Wheatstone bridge in which the other three arms were 120 ohm precision resistors. The signal from the bridge was amplified and fed into a Tektronix Type 532 single-beam oscilloscope, and a record of the strain was obtained with an oscilloscope camera as in the regular tests.

The dual beam oscilloscope was also used in this experiment so that records of the strains at the incident and transmitted gage stations could be obtained simultaneously with the specimen strain record. The scopes were triggered with the same signal produced by a piezoelectric element mounted ahead of the incident gage station. The records for three specimens at room temperature and at true strain rates of 485, 710 and 1010 per second were obtained. The photographically recorded specimen strain-time curve obtained

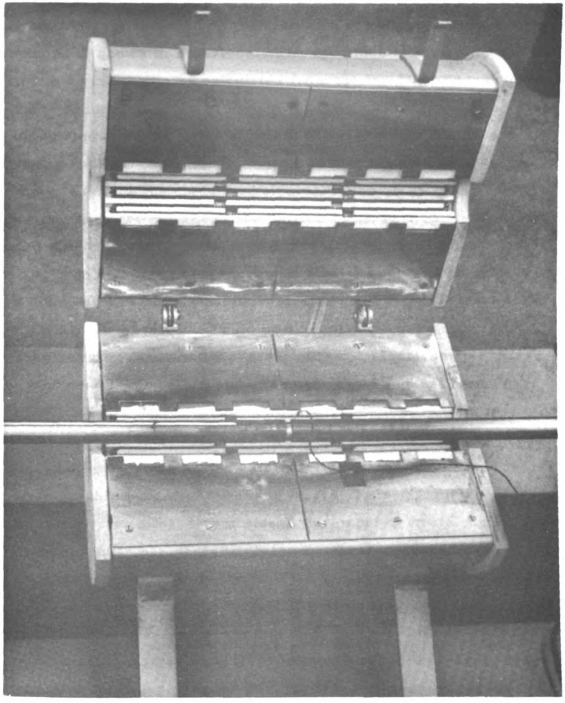

Figure 55. Close-up of Specimen with Gage Mounted on it.

from the gage mounted on the specimen at a strain rate of 710 per second is shown in Figure 53. The specimen true strain-time record for this strain rate as calculated from the incident and transmitted pulse records is given in Figure 56 along with a true strain record calculated from the nominal strain of the photographic record. This figure shows that the strain measured by the gage on the specimen is much less than the calculated strain. In the order of increasing strain rates the measured specimen strains were low by 8.1, 16.6 and 23.9 percent. Therefore, a direct comparison of calculated specimen strains versus measured strains could not be made. But a comparison of total specimen strains could be made since total strain in the specimens could be determined from the three photographic records from the pressure bars, and micrometer measurements of the specimens before and after each test could be made for a direct calculation of total specimen strain.

The total specimen strain was obtained from the pressure bar photographic records in an indirect manner. It is seen in the photographic record of specimen strain obtained from the gage mounted on the specimen that an additional increment of strain occurs after the main pulse has passed. This increment of strain is due to the reflected strain pulse in the incident pressure bar, which returns to the specimen after another reflection from the striker end of the incident bar, which is now a free end. This additional increment of specimen strain was calculated as a percentage increase over the strain occurring during the passing of the incident pulse, and this percentage increase was then applied to the specimen strain determined by the integration method to obtain the total specimen strain.

This indirect method of calculating the total strain from the integration method data by using a correction factor based on the

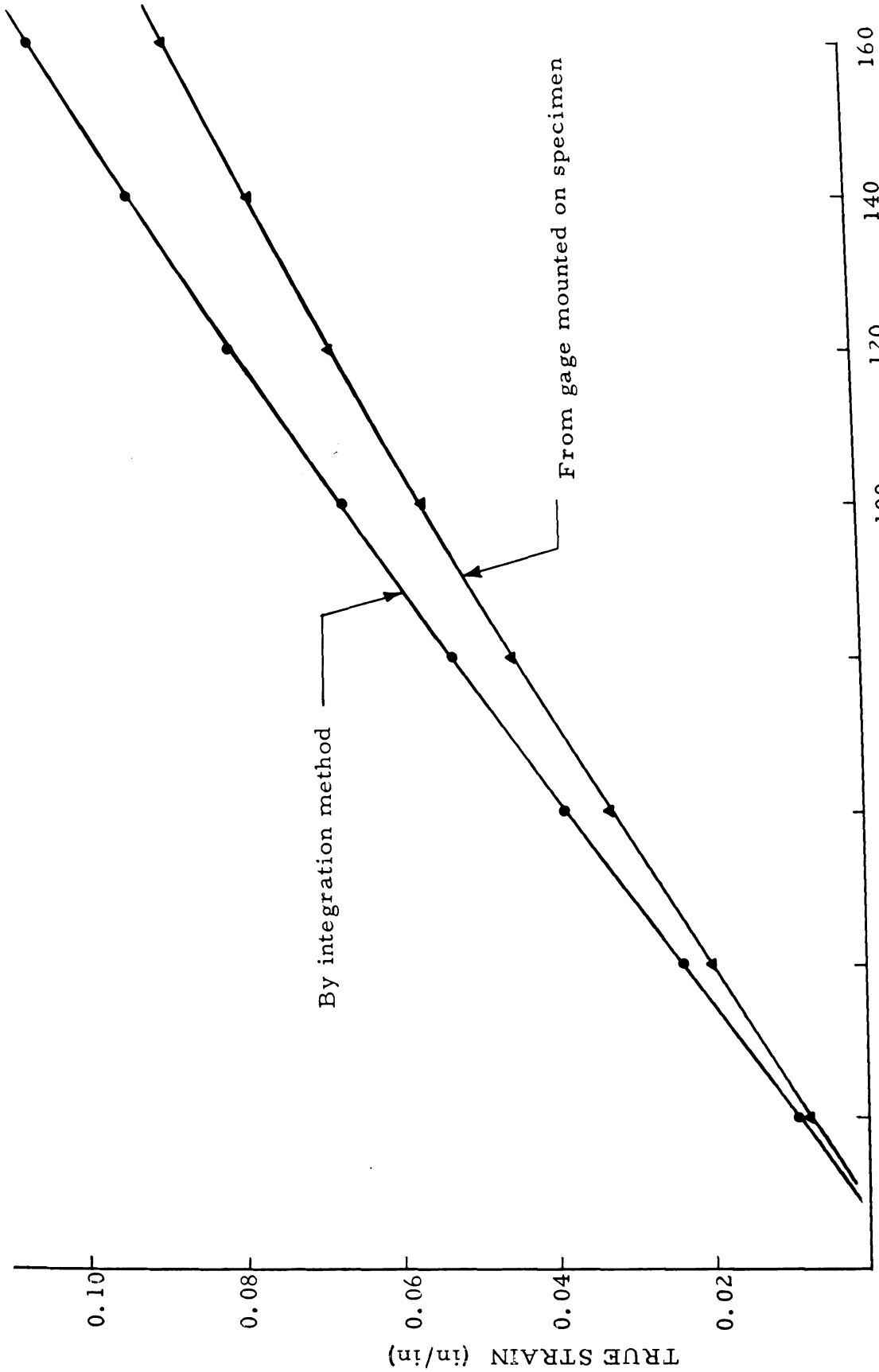

Figure 56. Specimen Strain Versus Time

specimen gage data was used because the pressure bar records do not show the additional increment of strain caused by the pulse reflected from the striker end of the incident bar. The correction factor will be valid if the percentage error of the strain gage mounted on the specimen is constant over the total range of specimen strain. The error appears to be constant at least for the strains due to the incident pulse, as is seen in Figure 56. The total strains determined in this manner for the three specimens were compared with strains calculated from micrometermeasurements before and after impact; the error at a strain rate of 485 per second is 0.8 percent, at a rate of 710 per second it is 1.4 percent and at 1010 per second it is 8.9 percent. It is believed that the two specimens tested at the lower strain rates provide a valid check on the integration method. The larger error with the third specimen is believed to be due to a faulty measurement from the gage mounted on the specimen. It was difficult to establish a zero level of strain on the photographic record for this specimen because the initial part of the trace was slightly obscured.

The second pulse, not shown by the pressure bar records, does not affect the data presented in the results of the main investigation reported in Chapter 5, since we are there concerned only with the transient behavior during the first pulse. The correction factor was used only for the purpose of checking the integration method specimen strains against the micrometer measurements of length in order to establish the validity of the integration measurements.

Strain gage errors at high strain rates for resistance gages mounted on aluminum have also been encountered by other investigators. Bell (see discussion at the close of the paper by Ripperger, 1960a) found that wire resistance strain gages mounted

on aluminum gave measurements which were 26 percent low at a strain rate of 1000 per second when compared with strains measured by a diffraction grating technique. The level of strain in his experiments was 2.5 percent. This is in fair agreement with the 8.1, 16.6 and 23.9 percent errors at corresponding rates of 485, 710 and 1010 inches per inch per second found in the present investigation. Cunningham and Goldsmith (1958) found an error of approximately 8 percent when the measured change in momentum of a 1/2 inch diameter steel ball impacting on the end of a 1/2 inch square aluminum bar was compared with the momentum calculated from a record of the strain pulse obtained by means of wire resistance strain gages mounted on the bar. The impact velocity of the ball was approximately 170 feet per second. This error did not occur when the gages were mounted on a steel bar.

ROOM USE ONLY

ROOM USE ONLY

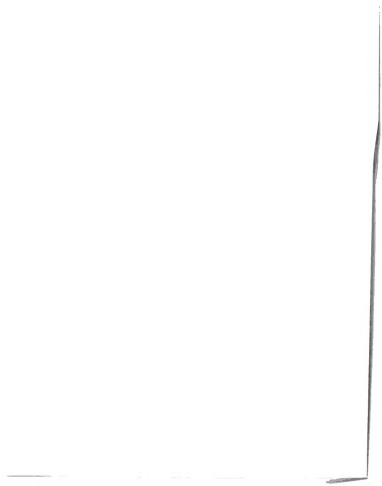

MICHIGAN STATE UNIVERSITY LIBRARIES
3 1293 03046 3172